LASER TISSUE INTERACTION AND WAVE PROPAGATION IN RANDOM MEDIA: MUELLER MATRIX POLARIMETRY

Shamaraz Firdous

Department of Physics & Applied Mathematics
Pakistan Institute of Engineering & Applied Sciences,
Islamabad, Pakistan.

2007

This work is submitted as thesis in partial fulfillment for the award of the degree of Doctor of Philosophy in Laser Physics, Department of Physics and Applied mathematics, Pakistan Institute of Engineering & Applied Sciences, Islamabad, Pakistan.

LASER TISSUE INTERACTION AND WAVE PROPAGATION IN RANDOM MEDIA: MUELLER MATRIX POLARIMETRY

CERTIFICATE

Certified that the work contained in this thesis is carried out by Shamaraz Firdous under my supervision from Department of Physics & Applied Mathematics, Pakistan Institute of Engineering & Applied Sciences, Islamabad, Pakistan, and approved as to style and content.

Dr. Masroor Ikram
Supervisor,
Department of Physics & Applied Mathematics,
Pakistan Institute of Engineering & Applied Sciences,
Islamabad, Pakistan

Dr. Nasir M. Mirza
Head of Department,
Department of Physics & Applied Mathematics,
Pakistan Institute of Engineering & Applied Sciences, Islamabad, Pakistan.

DEDICATION

This thesis is dedicated to Professor Dr. Atta-ur-Rehman, TI, SI, HI, NI, Chairman, Higher Education Commission (HEC), Pakistan. The research and development (R&D) in our country was suffering due to paucity of funds for the higher education as well as due to lack of priority and interest. However, presently plenty of funds have been made available by President of Pakistan and Dr. Atta-ur-Rehman through HEC. He took numerous initiatives in indigenous scholarship schemes, human resources development, expertise and foreign faculty hiring, quality assurance, etc.

He sponsored a number of research proposals and projects by various universities and research institutes of Pakistan. The contribution of Dr. Atta-ur-Rehman will always be remembered for promoting higher education and research activities in Pakistan.

This study has been sponsored by Higher Education Commission (HEC), Pakistan, under the merit PhD scholarship scheme 2002.

ACKNOWLEDGEMENTS

There are many people that deserve recognition for their contribution to my thesis project. I would like to thank numerous people for their support and for making this work a reality. First, I would like to thank my advisor Dr. Masroor Ikram who has been a friend, a colleague, and a mentor; I could not have asked for better. Then I would like to acknowledge the contributions of Dr. Nasir M. Mirza, Dr. Sikandar M. Mirza, Dr. M. Tufail, Dr. S. A. Bhatti, Dr. M. Nawaz, Dr. Shahid Qamar, and Dr. Matiullah for helping in PhD courses and giving encouragement to this research. Secondly, I would like to thank my colleague Mr. Khalid Hassan, who helped me in research early on when I joined the laser laboratory.

In addition, I would like to thank my colleagues Mudassar, Nameeqa Firdous, Afshan Irshad, Bakht and Raghib for their help and all other APD and PIEAS personals for their contribution in one form or the other. Thirdly, I would like to thank my family, friends, and sister families for their constant prayers and support. I would not have made it without them. The authors acknowledge the enabling role of the Higher Education Commission Islamabad, Pakistan and appreciate its financial support through "Merit Scholarship Scheme for PhD Studies in Science & technology". Finally, I would like to thank Prof. Dr. Irene Georgakoudi, Dept. of Biomedical Engineering, Tufts University, USA, and USDOS, Government of USA for providing me opportunity of research at BME, Tufts University, USA in 2006.

List of Publications

The work presented in this thesis is based on the following publications

Refereed Journals

1. S. Firdous and M. Ikram, Mueller matrix imaging polarimetry for the characterization of turbid medium, Annals of Bio-med. Res. Education, 5, 55-60 (2005).
2. S. Firdous, K. Hassan, and M. Ikram, Formulation of Mueller Matrix and modeling of depolarizing and scattering of nitrobenzene in a Kerr Cell, Applied. Optics. 44(7), 1171-1177 (2005).
3. S. Firdous and M. Ikram, Polarized Laser Beam Scattering through Turbid Medium for Application in Tissue Imaging, Science Asia, 31,167-172 (2005).
4. S. Firdous and M. Ikram, Polarized Mueller Matrix Analytical Model for Glucose Measurement in Vitro, Turk. J. Med. Sci., 35, 145-159 (2005).
5. S. Firdous and M. Ikram, and M. Faisal, Measurements of the optical properties of Breast tissues in vitro using Mueller matrix polarimetry, Int. J. Cancer Res. 1, 29-35(2005).

Refereed Proceedings

1. S. Firdous and M. Ikram, Transmission and scattering matrix of polarization imaging for biological turbid medium, Proc. SPIE, 5867, 25-35(2005).

2. S. Firdous and M. Ikram, Imaging of biological tissues with optical coherence tomography system using Jones-Mueller calculus, Proc. SPIE, 5861, 237-244 (2005).
3. S. Firdous and M. Ikram, Characterization of turbid medium through diffusely scattering polarized light and matrix calculus-II, Proc. IEEE, pp 115-123, International Networking and Communications Conference, 11-13 June, Lahore University of Management Sciences, 2004.
4. S. Firdous K. Hassan, and M. Ikram, Modeling of electro-optic devices for scattering and absorption of polarized light with Muller Matrix, Proceeding of International Symposium on Photonics in Measurement, pp 285-306, Institute of Optics Technology, 23-24 June, Frankfurt, Germany, 2004.
5. S. Firdous and M. Ikram, Characterization of turbid medium through polarized laser beam using optics calculus, Proceeding of World Conference on 21st Century Mathematics, pp 52-67, March 17-20, School of Mathematical Sciences, G. C. University, Lahore, 2004.

Research work presented in seminars, conferences

1. International Thematic Workshop on "the use of stem cell in human regenerative medicine" 10-18 Jan 2007, COMSTECH, Islamabad, Pakistan.
2. 6th Biennial International Conference of Pakistan Society of Cardiovascular & Thorasic Surgeons, 14-18 December 2006, Karachi, Pakistan.
3. Third International Oncology and Nuclear Medicine Conference & First International Conference on Pediatric Oncology, 8-10 July 2005, Karachi, Pakistan.
4. International Conference on Biotechnology and Informatics, Baluchistan University of IT and Management Sciences, 7-15 April 2004, Quetta, Pakistan.
5. International science conference, 07-09 May 2004, AJK, University, Muzafarabad, Azad Kashmir.

ABSTRACT

In this research work we have characterized the bio-materials with Mueller matrix optical polarimetry. The images and matrix elements with Mueller calculus provides a comprehensive information of samples due to which it is possible to combine all the necessary parameters for describing a beam of light into a single image. The resultant describing the light beam is simply the four-parameter Stokes vector and determined by measuring a flux transmitted through a set of polarization optics, polarization generating optics provide linear and circular polarized light to sample and polarization analyzing optics collect polarized output light from sample to detecting devices. The characteristic Mueller matrix in all experiments contains 16 elements, having total 49 intensity measurements at different polarization states. In practice, all 16 elements may not be independent. Only seven out of sixteen Mueller matrix elements are independent and others depending on the symmetry and certain properties of the optical medium.

The potential of the developed polarimetric system for the detection of normal and malignant tissues lesions lies in its ability to reject deeply scattered light at different depths, based on the incident and scattered polarizations within the tissue. In addition, the ability to fully characterize the polarization properties of the sample under investigation can provide useful information in terms of the morphological structure differences present between normal and cancerous tissue. These changes help to characterize and distinguish between tissue types.

The Stokes Mueller polarization images of transmitted intensity along with degree of polarization provides fingerprint of the turbid medium. Careful analysis of images and degree of polarization, differentiation of scatterer in term of its concentration, size, shape and orientation is possible. The linear polarization preservation is dominant over circular

due to scatterer density rather then size of the particle in medium. We have seen that linearly and circularly polarized light propagates differently for turbid samples. we have indicated the structural features in turbid medium that influence the degree of polarization and the importance of these structures on polarized light propagation. Using the experimental data we have compared the intensities of the two orthogonal polarized components and have found that the average difference is negligibly small. Therefore within a less than 5% average error we can use the semi-isotropic scattering to simplify our Mueller matrix and have only five unknown coefficients. We applied our characterization study for simulation of biomaterial and found useful results.

In addition, the ability to fully characterize the polarization properties of the sample under investigation, the information of the morphological structure differences of normal and cancerous tissue is achieved. These changes can be used to help characterize and distinguish between tissue types. Furthermore, the ability to acquire such measurements in a minimal time frame gives promise for the future application of such a system to differentiate between normal, benign, and cancerous tissue. In this study different tissue-like materials (water, vegetable oil, milk, and other intralipid phantoms), different types of animal tissue in vitro have been investigated with the aim of correlating the dominant spectral features. Tissues that contain water are clearly distinguishable from fatty tissue on account of the absorption bands for water. The transmission differences are sufficiently clear to permit characterization of turbid medium and biological tissues.

The Stokes –Mueller matrix polarimetric system, due to its simplicity and versatility, this may prove to be an ideal system for structural analysis of turbid sample and soft tissues. The Stokes- Mueller matrix polarimetry is a major step forward towards bio-material characterization, especially malignant tissues and turbid medium.

Table of Contents

Chapter-4

Chapter-5

LIST OF FIGURES

LIST OF TABLES

discovery is said to be an accident meeting a prepared mind (Albert von Szent-Gyorgyi)

INTRODUCTION

Imaging through turbid media and biological tissues is an important field of research for biomaterial characterization. The work described in this thesis is aimed at improving the imaging algorithm. The approach taken comprised two steps, (1) Development of Mueller matrix polarimetric system, and (2) Investigation of the turbid medium and biological tissues with Mueller matrix polarimeter.

Motivation

The widespread availability of suitable laser sources and detectors has aided the rapid development of new optical technologies for the monitoring and diagnosis, as well as treatment, of malignant diseases. Currently emphasis has mostly been laid on medical applications using infrared or visible light instead of others daily used modalities. Clinical studies have shown that the absorption and scattering characteristics at some wavelength by normal tissues differ significantly from some tumors and this behavior has been adapted for discriminating or locating tumors in the human body.

For accurate diagnostic and treatment modalities of biomaterials, one should have a clear understanding of the mechanism of interaction of the laser light with the tissue. Laser tissue interactions can loosely be classified into photo thermal, photomechanical, or photochemical interactions, however, most interactions do not fall clearly into one of these categories, and often multiple processes are competing with each other. Hence, it is extremely difficult to unravel the mechanism of interaction. To date, many studies have been carried out for investigating the effects of irradiation on biological tissues, but the

results of these studies have not presented a clear picture of the mechanism involved, and in many cases, connect with each other. Mueller matrix polarimetry can be used in a clinical setting to test the feasibility of its use for malignant diseases in human tissues and ophthalmic procedures.

Organization of the thesis

We have used the optics calculus (Stokes, Jones, and Mueller matrix) for imaging and characterization of biological medium. Starting with introduction of my PhD topic, the 1st chapter contains the essential background material related to polarization optics and light absorption, transmission, scattering and a review of the field of optical imaging that is needed to understand the latter chapters. The 2nd chapter provides a introduction to Stokes, Jones and Mueller matrix optical calculus. The review mainly concentrates on the analysis methods adopted in Mueller matrix imaging polarimetric setup. The 3rd chapter describes the material and methods adopted during the research, the polarimetric characteristics, experimental setup, error analysis and precaution needed for accurate results through Mueller matrix polarimeter. In 4th chapter, the polarization properties of light scattered from a scattering medium have been investigated. It has been shown that the degree of polarization is sensitive to the optical properties of the turbid medium and this offers a potential tool for characterizing the medium. In this chapter different stokes polarimetric applications have been investigated. The experimental results for turbid and bio-materials with the help of Stokes polarimetry are quoted. The absorption, scattering and transmitted images are explained through Stokes polarimetry and the material is characterized through these images.

In 5th chapter the theoretical calculations of optics calculus have been described and resultant seven independent elements of Mueller matrix are derived, and other nine out of total 16 can be attain through these seven independent elements. We formulated that only five element of Mueller matrix can provide complete description of electro-optical material under some symmetry conditions. In 6th chapter Mueller matrix error analysis and 2nd and 3rd order images of turbid sample are discussed in detail, which provide a finger print of material, determination of size, shape, orientation and optical activity, as well as the difference between normal and maligned tissues. In 7th chapter the useful results for turbid

phantom characterization, skin tissues, breast tissues and glucose monitoring in vitro through Stokes-Mueller polarimetric system are presented. The 8th chapter summarizes the results and targets achieved through this research work and future recommendations for further study.

Background of thesis

Over the past decade the area of applied research known as biomedical optics has flourished. The principal goal of biomedical optics, and arguably its most ambitious, is the development of a diagnostic imaging modality based on optical illuminating radiations. Optical imaging presents several potential advantages over existing radiological techniques [1, 2]. First, the radiation is non-ionizing, and therefore reasonable doses can be repeatedly employed without harm to the patient. Second, optical methods offer the potential to differentiate between soft tissues, due to their different absorption or scatter at different wavelengths, which are indistinguishable using other modalities. Third, specific absorption and scattering by natural chromophores (such as oxy-hemoglobin) allows functional information to be obtained. Optical imaging research has focused on a variety of possible clinical applications [3-5].

The widespread availability of suitable laser sources and detectors has aided the rapid development of new optical technologies for the monitoring and diagnosis, as well as treatment, of malignant diseases. Furthermore, new polarimetric base optical techniques are helping to advance fundamental biomedical research [6, 7]. Imaging is the creation of a visual representation of some measurable property of a person, object, or a phenomenon. Thus, `Imaging Science' becomes the pursuit of scientific understanding of imaging or an imaging technique. This inter-disciplinary branch strives to view phenomena normally invisible to the human eye by translating them through some means, to a visually perceptible form [8, 9].

In general, researchers have approached the task of improving the performance of transillumination in two ways. The so-called direct approach is based on a reasonable assumption that photons which are least scattered provide inherently better spatial resolution and contrast since they propagate closest to a straight line through the tissue.

Imaging therefore involves appropriate filtering, or gating, to isolate this transmitted component from the majority of the multiply scattered light [10, 11]. A broad variety of gating techniques have been proposed and tested experimentally. Some methods rely on a fraction of photons being able to propagate without scatter or loss of initial coherence or polarization state, while other methods gate according to the lengths of the photon path length [12]. The second, indirect approach is based on the assumption that, given a set of measurements of transmitted light between pairs of points on the surface of an object, there exists a unique three-dimensional distribution of internal scatterers and absorbers which would yield that set. Thus imaging becomes a task of solving an inverse problem using an appropriate model of photon transport. In principle, the measurements could be of any type, even total transmitted intensity. However, the measurement of one or more characteristics of the temporal distribution of transmitted light, or an equivalent in the frequency domain, is considered more suitable. Where mean photon flight time is found to be less dependent on surface interactions and scattering than total transmitted intensity. [13, 14].

Polarization optical imaging is attractive in the biomedical field because it is a non-invasive, non-ionizing, and functional imaging modality [15, 16]. Compared with X-ray imaging which uses ionizing radiation, optical imaging is safe because it uses low energy photon [17]. It is inexpensive compared with magnetic resonance imaging (MRI) [18], and compared with ultrasound imaging [19], optical imaging provides better soft-tissue contrast, which is based on optical properties (i.e., absorption and scattering) [20, 21]. Because the absorption and scattering of biological tissues in the visible and near infrared region are related to the molecular constituents of tissues and electronic and vibration structures at the molecular level, they are intrinsically sensitive indicators of tissue abnormalities and functions [22, 23]. Cancerous tissues manifest significant architectural changes at the cellular and sub-cellular levels, which are revealed in the optical scattering properties. Angiogenesis and hyper-metabolism, which are hallmarks of cancers, are intrinsic to the optical absorption properties. Optical imaging holds promise for early cancer diagnosis [24, 25].

Optical information can also be used to deduce physiological parameters such as the oxygen saturation of hemoglobin [26]. This makes optical functional imaging possible. Oxygen saturation is closely related to the metabolic state of lesions and is an important diagnostic parameter. However, optical imaging faces the challenge: strong optical scattering in biological tissues, which leads to poor image resolution. Because biological tissues are optically turbid media, light is strongly scattered inside tissues. A typical scattering coefficient for visible light in biological tissues is 100 cm^{-1}, compared to 0.2 cm^{-1} for X-ray used in medical diagnosis. Scattering causes light to change its direction and multiple scattering causes light to lose its original direction. Light transmitted through tissues can be classified as: ballistic light, quasi-ballistic light and diffuse light. Ballistic light experiences no scattering and carries direct imaging information. Quasi-ballistic light experiences minimal scattering and carries some imaging information. Diffuse light follows tortuous paths and carries little direct imaging information. Correspondingly, optical imaging techniques are classified as: ballistic light imaging and diffuse light imaging. In the ballistic imaging, diffuse light is rejected and ballistic or quasi-ballistic light is collected. The imaging is suitable for thin tissue samples but suffers loss of signal and resolution for thick tissues because of the strong scattering of light by the tissue [27]. The diffuse imaging is developed for thick-tissue samples, which includes frequency domain optical imaging and diffuse tomography. In this kind of imaging, sophisticated image reconstruction algorithms based on diffuse equation or transport equation are applied. The image quality however is usually algorithm dependent and the image resolution is not good enough [28]. Another imaging technique is Mueller matrix calculus was developed by H. Mueller in the early nineteen- forties to describe the propagation of optical beams represented by Stokes parameters. It appears that Mueller was the first to determine the matrices that now bear his name for the polarizer, wave plate, and rotator. The use of matrices to deal with complex polarization problems was a significant breakthrough with respect to carrying out the difficult calculations. At the same time that Mueller was developing his calculus using the Stokes parameters another calculus was being developed by R. C. Jones, based on amplitude formulation. The Mueller matrix provides the full characterization of a polarization element. The characteristic Mueller

matrix for any optical device or scattering medium contains 16 elements, based on 49 experimental optical intensity measurements. The set of these 16 elements contains all the necessary information about the material under investigation [29].

The concept of combining polarized light images in matrix form was introduced in 1997 by Andreas Hielscher and collaborators at Los Alamos National Laboratory [30]. Because Mueller matrices give the complete description of the effect, objects have on polarized light, they were the best choice for representing complex media such as human tissue or other biological matter [31]. Stokes-Mueller calculus is also preferable to other options such as Jones calculus because it can show circular polarization without involving imaginary numbers. In many cases biological materials behave as scattering medium and can cause elliptically or circularly polarized light to be created [32].

The technology needed to these Mueller matrix images has steadily improved over the last few years. Modern CCD elements allow even invisible frequencies of light (near infrared) to be measured with high spatial resolution and an accurate response to light level. Finally, computer technology is now so advanced that even a modest personal computer is more than adequate for manipulating images with millions of pixels. The use of modern CCD cameras and imaging software has allowed Mueller matrices of highly scattering media to be created quickly and efficiently. Through careful analysis of Mueller matrix images, we can characterize the cancerous and normal tissues with change in image pattern [33, 34]. The technique of imaging scattered light is currently being used in all areas of scientific study and would likely one day lead to many advances in our knowledge and the world around us [35].

Man is so made that he can only find relaxation from one kind of labor by taking up another (Anatole France)

Chapter 1

POLARIZED LIGHT AND OPTICAL IMAGING

1.1 Light mater interaction

The duality of light, the fact that it exhibits both wave and particle nature, it explains light interactions at the macroscopic level, using geometric or ray optics, and accounts for phenomena such as shadow formation while the wave nature of light explains light interactions at the micro and sub-micro level and accounts for photon interference and diffraction phenomena. In general, for the propagation of light we use Maxwell's equation, and for the interaction of light with matter, where the absorption and emission of light involves, we use the quantum theory [36]. In order to have a clear understanding on the use of polarized light for biomedical applications, it will be essential to investigate both the wave and particle nature of light. The knowledge of this theory pertains to the measurements that will be necessary to enable the discrimination of the properties of matter that we are interested in.

The interaction of light with matter has been shown schematically in Fig 1.1. The quantity, arrangement, and interactions of electrons, nuclei, atoms, molecules, and other elementary particle constituents of matter determine these properties. In order to be able to extract all of the available information about the optical dielectric properties of matter, polarized light inputs are necessary. The reason for this is that the polarization of light has the measurable effect of increasing the discrimination ability of light interrogation of matter. This increased specificity is a direct consequence of the ordered and quantized behavior of the constituent elements of matter and is best investigated using quantum mechanics.

However, even a macroscopic level investigation of the effects of polarized light on matter can reveal the average information about structural bonds, electronic states, and electronic alignments, which determine the measurable optical dielectric properties of matter [37].

The biological materials and other random inhomogeneous media render imaging difficult due to the random multiple scattering of light. Inhomogeneities in the media cause scattering which may alter the direction of propagation, polarization and phase of light. While the propagation of light through such media may be analyzed either by means of the wave picture or the photon picture, the latter is more appealing. Photons travel in straight line paths until they encounter an inhomogeneity, when they are scattered in random directions. The scattering is said to be in the Rayleigh regime when the radius, a of the scatterer, is less than the wavelength of light. In this case, the intensity of scattered light is equal in both the forward and backward directions. As the size of the particle increases, the scattering is more peaked in the forward direction. The case of $a > 1$, known as the Mie regime, shows peaking in some angles [38].

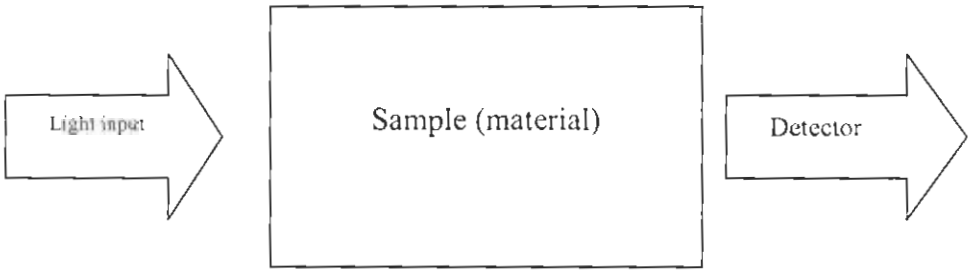

Figure 1.1 Schematic diagram for the use of polarized light to determining the properties of matter.

In a turbid medium made up of a random aggregate of scatterers, the photons undergo repeated scattering. The turbid medium is characterized by the scattering mean free path, l_s, which is the mean distance the photons travel before getting scattered, and the transport mean free path " l^*" which is the mean distance photons travel before the direction of propagation is randomized. Since it is quite possible that photons are forward scattered (and continue to travel in the same direction), $l^* > l_s$. The transport mean free path depends

upon the number density of scatterers, refractive index contrast between the medium and the scatterers, and the anisotropy factor, i.e. a factor quantifying the directional distribution of scattering. Typical values of l^* for infrared light in tissues are 1–2 mm. The light emerging from a turbid medium consists of three components [39], the ballistic, the diffusive and the snake photons (Fig 1.2). These differ in their paths through the medium, and consequently in their imaging properties. The un-scattered or forward scattered photons travel un-deviated and emerge the first, having traveled the shortest distance through the medium. These preserve the characteristics of the incident light, namely direction of propagation, polarization and are hence best for imaging. However, they are few in number, their intensity falling off as $I = I_0 \exp(\frac{-x}{l^*})$ where I_0 is the input intensity, and x is the distance traveled.

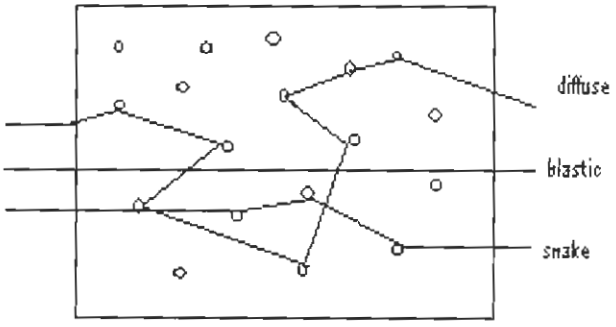

Figure 1.2 Trajectories of photons in a random medium, showing the ballistic, diffusive and snake components.

The diffuse component, which forms the bulk of the emergent light in turbid media is made up of photons that have undergone random multiple scattering, and these emerge later than the ballistic photons because of their increased path lengths. Their polarization, direction of propagation and phase are completely randomized. Snake photons are those that travel in near-forward paths, having undergone few scattering events, all of which are in the forward or near-forward direction. Consequently, they retain the image bearing

characteristics to some extent. Due to the scattering a pulse of light incident on a turbid medium emerges elongated. Typically, a femtosecond pulse is stretched to a picoseconds or a nanosecond pulse on traveling through a turbid medium [40].

1.2 Polarization

1.2.1 Polarized light

Since the thesis deals with imaging using polarized light, we begin with the most basic notion of polarization of light, its representation and measurement. Polarization is a property which arises out of the transverse nature of the electromagnetic (EM) radiation, and is related to the orientation of the plane of vibration of its electric field. The magnetic field associated with the radiation is not taken into account to denote polarization.

The compelling need to study the vectorial nature of light is encountered when one tries to understand light propagation in restricted media like optical turbid medium or in the presence of surfaces with discontinuous refractive indices (biological tissues), where the boundary conditions need to be taken into account. In the case of a plane surface, it can be shown that the electric field can be decomposed in to components parallel and perpendicular to the plane of incidence, and their behavior during reflection and refraction phenomena are independent. So, it looks as though the EM field can be treated as a superposition of two plane-polarized waves, which can form a basis for generating any other polarization state. Since the monochromatic plane wave is the fundamental entity in the description of polarized light, we examine it in greater detail.

The humans are actually at a disadvantage to lower creatures like spiders and squids when dealing with light. Unlike humans, these creatures and several others are aware of the polarization of light. One species of spider can actually navigate through its detection of polarization orientation [41]. As easily as we locate the origin of a sound using two ears, these simple bugs can determine the difference in polarization of scattered sunlight between their eyes, using this information to locate the position of the sun overhead. This one characteristic of light escapes our eyes detection but can still reveal so much information about the world around us [42].

1.2.2 Types of polarization

All light waves are composed of electric (E) and magnetic (B) field vectors and are mutually orthogonal to each other and the direction of propagation. We take only electric field. In the electric field the polarization states (i.e. vertical or horizontal) refer to the orientation of E. it is assumed that the direction of propagation, k , is in the ˆz direction. Polarization states arise from relationships between the magnitude and phase of the orthogonal components of E (i.e. E_x and E_y).

The most general form of polarized light is elliptical polarization. Linear and circular polarizations are simply special degenerate cases of elliptical polarization. The type of polarization is determined by the relative magnitude and phase difference between the two orthogonal components of E. In general, E can be described mathematically by [43]:

$$E = E_x(z,t) + E_y(z,t) \tag{1}$$

where E_x and E_y are given by

$$E_x(z,t) = E_{0x}\cos(\tau + \delta_x) \tag{2}$$

$$E_y(z,t) = E_{0y}\cos(\tau + \delta_y) \tag{3}$$

where $\tau = \omega t - kz$ is the propagation term and " ω " is the angular frequency i.e.

$$\omega = 2\pi f \tag{4}$$

where f is the temporal frequency and " k " is the wave number i.e.

$$k = \frac{2\pi}{\lambda} \tag{5}$$

and t is time, δx and δy are the phase angles of Ex and Ey respectively, and E_{0x} and E_{0y} are the peak magnitudes in the ˆx and ˆy directions.

Randomly polarized light refers to light whose polarization is completely symmetric about the direction of propagation. The terms unpolarized and naturally polarized are often used to refer to randomly polarized light. The simplest form of polarized light is linear polarization. Light is said to be linearly polarized, or plane-polarized, when the electric field remains in a fixed plain that contains both E and k. For light to be linearly polarized, the following has to hold true in equations (2) & (3).

$$\delta = \delta x - \delta y = 0 \tag{6}$$

Substituting equation (6) into equations (2) and (3) results in identical cosine terms for E_x and E_y and equation (1) becomes

$$E = (E_{0x} + E_{0y})\cos(\tau + \delta)) \tag{7}$$

The next simplest case is circular polarization which arises under the following conditions:

$$E_{0x} = E_{0y} = E_0$$

$$\delta = \frac{\pi}{2} + 2m\pi \text{ where } (m = 0, \pm 1, \pm 2, \ldots) \tag{8}$$

For circularly polarized light, equations (2) and (3) become

$$E_x(z,t) = E_0 \cos(\tau)$$

$$E_y(z,t) = E_0 \sin(\tau) \tag{9}$$

where δx has been arbitrarily set to zero without loss of generality. Combining equation (9) gives the following for equation (1)

$$E = E_0(\cos(\tau) + \sin(\tau)) \tag{10}$$

Notice that in the case of circular polarization, the magnitude of E remains constant while the direction of E is time varying. This is the exact opposite of the case of linear polarization.

In fact, linear and circular polarizations are simply special cases of elliptical polarization. In the case of elliptical polarization, both the magnitude and direction of E are time varying. The equation for the polarization ellipse has the following form [44, 45].

$$\frac{E^2_x}{E^2_{0x}} + \frac{E^2_y}{E^2_{0y}} - \frac{2E_x E_y \cos\delta}{E_{0x} E_{0y}} = \sin^2\delta \tag{11}$$

which shows that the polarization can be characterized in terms of the parameters E_{0x}, E_{0y}, and δ. Collett derives the following relationship between ψ and the parameters E_{0x}, E_{0y}, and δ. [45],

$$\tan 2\psi = \frac{2E_x E_y \cos\delta^2}{E^2_{0x} - E^2_{0y}} \tag{12}$$

He also derives the relationship between ψ, α, and δ

$$\tan 2\psi = (\tan 2\alpha)\cos\delta \tag{13}$$

In the case of linear polarization ($\delta = 0$ or π) equation (13) reduces to

$$\psi = \pm\alpha \tag{16}$$

In the case of circular polarization ($\delta = \pi$ or 3π) equation (13) reduces to

$\psi = 0$ indicating that there is no rotation. This makes sense since a circle is rotationally symmetric. Finally, the angle of ellipticity, χ, is defined as:

$$\tan\chi = \frac{\pm b}{a}, \qquad \frac{\pi}{4} \le \chi \ge \frac{\pi}{4} \tag{14}$$

where a and b, the major and minor axis, are given by

$$a = \sqrt{E^2_{0x}\cos\psi + E^2_{0y}\sin^2\psi + 2E_{0x}E_{0y}\cos\psi\sin\psi\cos\delta}$$

$$b = \sqrt{E^2_{0x}\sin\psi + E^2_{0y}\cos^2\psi - 2E_{0x}E_{0y}\cos\psi\sin\psi\cos\delta} \tag{15}$$

1.2.3 Polarization properties

Depolarization Property: Physically, depolarization of light by a sample of matter can be a result of multiple scattering of photons, or a rapid or random change in the phase or wavelength of the emitted photons that result in a scrambling of the output polarization of the emitted light beam such that it does not favor any polarization state over the others. Practically, all matter depolarizes light to a degree established by its asymmetric and inhomogeneous makeup.

Dichroism: Dichroism is the selective absorption of one of the two orthogonal polarization components (x, y) of an incident light wave. A dichroic polarizer is physically anisotropic; producing a preferential absorption of one field component while being essentially transparent to the other. The simplest form of a dichroic polarizer is a grid of parallel conducting wires. There are also certain materials which are inherently dichroic due to the anisotropy which exists in their crystal structure. One of the best known naturally occurring examples is the mineral tourmaline. Certainly the most famous dichroic material is the polaroid sheet.

Birefringence: Many crystalline substances are optically anisotropic. We know that the light excites the electrons within the medium. The electrons are driven by the electric field, they re-radiate secondary wavelets, which then recombine and the resultant wave continues on. The speed of the wave, and thus the index of refraction, is determined by the difference between the frequency of the electric field and the natural, or characteristic, frequency of the electrons. An anisotropy in the binding force will therefore be manifest in an

anisotropy in the index of refraction. A material of this sort, which displays two different indices of refraction, is said to be birefringent [46].

Polarizance Property: For a sample to exhibit polarizance, it has to have a structural arrangement that enables it to reflect, absorb and re-emit, light at oblique angles, or one that results in either the differentially absorption of orthogonal polarization components of light or in the differentially absorption of linear versus circularly polarized light [47].

1.3 Optical properties of matter and biological tissues

Light propagation in turbid medium might be envisioned as a stream of particles, photons, each with a localized quantum of energy. The statistical average transport of photons and their energy through turbid medium, such as tissue, can mathematically be expressed by the different optical models. We can adopt the classical approach and imagine light propagation as a continuous transfer of energy by electromagnetic waves. The light propagation is mathematically represented by vector waves, being scattered and absorbed in the medium

1.3.1 Fundamentals of tissue optics

Light traveling through tissue experiences two main types of interaction: absorption and scattering. Other forms of radiation are also absorbed by tissue. Indeed it is the absorption of x-rays that enables an image to be created. Scatter, however, is a property that is far more dominant for light and so cannot be ignored as it is for other imaging modalities [48]. The principal optical properties to be discussed are:

1. Absorption.
2. Scattering.
3. Anisotropy
4. Refractive index

All of these properties are dependent on the wavelength of the light probing the tissue. Additional optical characteristics of tissues include their fluorescence and inelastic scatter properties

1.3.2 Absorption

Absorption is the transfer of energy from incident radiation to the surrounding tissue. If a non-scattering medium is illuminated with a collimated beam of light with intensity I_0 and wavelength λ, the intensity of the emerging light is given by [48],

$$I = I_0 e^{-\mu_a d} \qquad (16)$$

where $\mu_a(\lambda)$ is the absorption coefficient of the medium and d is the thickness of the sample.

The absorption coefficient is the number of absorption events per unit length (mm^{-1} or cm^{-1}). It follows that its reciprocal $1/\mu a$, often called the absorption mean free path, is the distance required for the intensity to fall to $1/e$ of the original value. If we define the particle density (or volume density), ρ, of an absorber as the number of absorbing particles per unit volume, and the absorption cross section, σ_a, as the cross section area that a perfect absorber would have to cause the equivalent attenuation to a collimated light beam, then we can also express the absorption coefficient as the cross-sectional area of absorption per unit volume of medium.

$$\mu_a = \rho\sigma_a \qquad (17)$$

Thus by substituting equation (17) into equation (16) we obtain:

$$I = I_0 e^{-\rho\sigma_a d} \qquad (18)$$

Within biological tissue there are various substances that contribute to the absorption of light, known as chromophores. Figure 1.3 shows the absorption spectra of some common chromophores from the UV to the mid infrared region of the electromagnetic spectrum. and Figure 1.4 shows the absorption spectra for water[49].

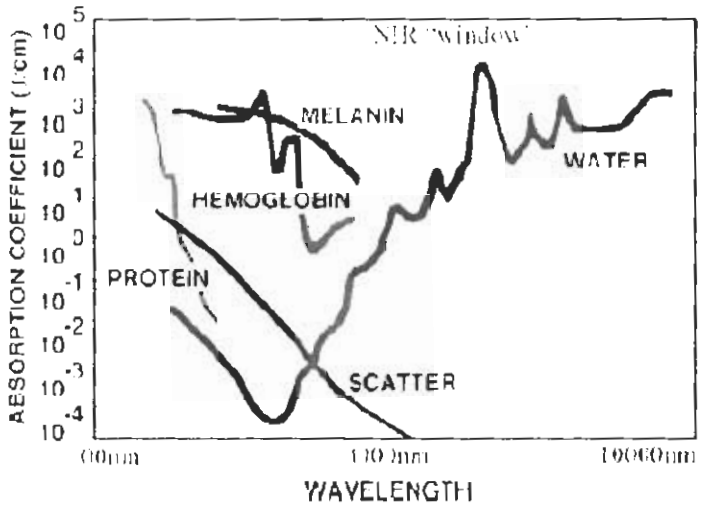

Figure 1.3 The absorption spectra for the main chromophores found within tissue.

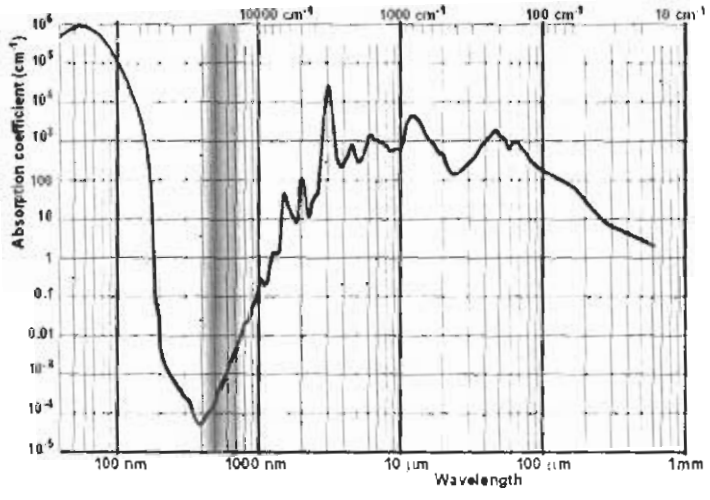

Figure 1.4 The absorption spectra of water in the near infrared region

As can be seen that water has a low absorption over the NIR range. Water can, nevertheless, strongly influence measurements due to the high concentration. In most tissues water is the major constituent with 30 - 60%, this means that the accumulative absorption effect cannot be ignored.

1.3.3 Scattering

When an obstacle is illuminated by an EM wave, electric charges in the obstacle are set into oscillatory motion by the electric field of the incident wave. The accelerated charges re-radiate EM energy in all directions. This secondary radiation is called the radiation scattered by the obstacle. If the frequency of the scattered light is the same as that of the incident light, then the scattering event is called as elastic scattering. If the incident EM energy is transformed into thermal energy, then the process is called as absorption. Scattering and absorption are not mutually independent processes, though, depending on the situation, one may be more prominent than the other.

Optical scattering is caused by in-homogeneity in the refractive index of a medium. The intensity and spatial distribution of the scattering light depends on the size and shape of the in-homogeneity relative to the optical wavelength and disparity of the refractive index. Two cases of scattering are usually considered. Rayleigh scattering relates to scattering particles whose radius a is considerably smaller than the wavelength λ of the incident light. The Mie scattering occurs normally when the size of a particle illuminated by visible or near-infrared light is larger than one micrometer. The effect of scattering can be thought of as a removal of a proportion of the incident intensity from the propagating beam, in much the same way as the effect of absorption [50].

Scatter is the phenomenon that causes the direction of radiation within a medium to be changed. Just as the absorbing properties of a medium can be described by its absorption coefficient μa so the scattering coefficient μs can describe its scattering properties. In the case of a collimated source and single scattering this is given by:

$$I = I_0 e^{-\mu_s d} \tag{19}$$

where I is the non- scattered component of light after traversing a non-absorbing medium of thickness d. The scattering coefficient can also be described in terms of the particle density ρ and the scattering cross section σ_s such that:

$$\mu_s = \rho \sigma_s \tag{20}$$

The scattering coefficient μs represents the probability per unit length of a photon being scattered.

1.3.4 Anisotropy

The scattering properties of bulk media are often described in terms of the reduced scattering coefficient μ_s'.

$$\mu'_s = \mu_s(1-g) \tag{21}$$

Where the anisotropy function "g" is given as:

$$g = \int_{4\pi} \Theta \cos(\theta)\cos(\phi) d\phi \tag{22}$$

The phase function Θ is a function of the angle between the incident and scattered light, It is assumed that Θ is independent of θ, the orientation of the scatterer, such that Θ is dependent only on the scalar product of $\hat{s}$ and $\hat{s}'$.

1.3.5 Refractive index

The speed of light, c, within a specific medium of refractive index n is given by :

$$C = \frac{C_{vacuum}}{n} \tag{23}$$

where C_{vacuum} is the speed of light in a vacuum.

1.4 Optical imaging of turbid and biological materials

1.4.1 Optical imaging

The idea of medical imaging appeared for the first time many years ago and has become one of the most important aspects for the development of medicine. Both in diagnosis and prognosis the contribution of optical imaging has been of catalytic importance. It has helped greatly to the understanding of the function of human organs and has given solutions to problems that used to demand surgical operations in order to assess both the disease and therapy processes [51]. The basic experimental setup consists of the source of radiation, the target and the detector. Since many years optical imaging is a separate scientific field exploiting many physical and computational methods in order to develop techniques suitable for non-invasive imaging. Nowadays the use of on-line imaging systems is possible, which monitor the function of vital organs and blood flow. However, the development of a system that could be used from the patient, such as a monitoring devise for the glucose level in the blood for diabetics, without blood extraction would have been a breakthrough. Even from the 19th century medical doctors together with scientific

groups tried to combine the function of internal organs with external visual symptoms. The goal was the immediate diagnosis without invading the patient's body with an operation.

The most successful method to date is histological analysis, even though it requires the excision of small biopsy tissue samples. The first to attempt an optical biopsy was done with candlelight [52]. Unfortunately the results were disappointing because of the excessive scattering that the light underwent so that any information useful for imaging the interior of the skin was lost. The problem of imaging through light scattering media is also termed as `Imaging through turbid media [53]. Generally, to qualitatively assess the effect of light scattering, researchers resort to the photon picture of light. Scattering can be regarded as consisting of three different components, viz., the ballistic or the un-scattered photons, the diffuse or the multiply scattered photons and the quasi-ballistic photons or weakly scattered photons. Among these components, the ballistic photons which travel straight and un-scattered are the ones which are capable of forming shadow grams of an opaque inclusion. The quasi-ballistic photons, which undergo scattering only through small angles can be imagined to meander about the forward direction like a snake and for this reason are also called as `snake photons'. Though the snake photons also blur the image of the object slightly, they retain their direction to some extent and are hence, useful. The diffuse photons cause most of the blurring and are the ones to be avoided while imaging [54]. In scattered polarized light, the ballistic and snake photons retain their initial polarization state to a greater extent, as compared to the diffuse photons. Hence, polarization of the scattered photons can be used to distinguish the less scattered ones from the rest. Such schemes are called polarization based direct imaging schemes.

There are many other imaging schemes which analyze the diffuse intensity collected, and these are in general called as `Indirect imaging' schemes. In these schemes, imaging is viewed as an inverse source problem and wave equations are used for obtaining the results. In this thesis, we have considered direct & indirect polarization based imaging schemes

1.4.2 Present imaging status

X-rays Imaging

During the recent years however, many techniques have been developed and applied, whereas many more are in experimental stage. They are based on the exploitation of different radiations that can be transmitted through tissue and image the shadow of inner

organs and bones. The most commonly used are X-rays, which are applied to the detection of bone fractions, dental lesions and breast tumor imaging (mammography). X-rays imaging is so clear because of the small wavelength (~ 0.01 nm) of the radiation, which cancels the extensive scattering. The scattering of radiation becomes stronger as the wavelength approaches the dimensions of the components of tissue (typically in the range of nm). Thus, X-rays penetrate deep into the tissue in contrast with highly scattered visible (400 – 800 nm) radiation. The produced image is the 2D projection of the attenuating properties of tissue along the path of the detected X-rays. The principal interactions that cause the attenuation are photoelectric absorption and inelastic scattering. The drawback however of the use of X-rays is introduced by the small wavelength, which is associated with very high energies (~100 KeV for X-rays), which can highly damage the tissue by ionization, breaking of DNA molecules and carcinogenesis. These limits the exposures a patient can undergo during his/her life. Moreover, these energies are much higher than the molecular energy levels, thus making impossible the determination of chemical composition. Finally, X-rays present many difficulties since they cannot be manipulated with conventional optics.

Conventional radiographic imaging provides no depth information, as the 3D body structure is projected onto a 2D image. Another limitation mentioned above is the low soft tissue contrast, which is particularly important in many imaging schemes. X-rays computed tomography imaging is the development that gave the answer to these limitations. It produces thin 2D sections of the body, approximately 1 mm in thickness. Sub-millimeter spatial resolution with good discrimination between tissues (better than 1% attenuation change) can be achieved. The data acquisition is performed with a rotating fan beam X-ray source, which scans along the patient and a series of detectors. The image is then reconstructed from the 2D body slices [55].

Diagnostic Ultrasound imaging

In diagnostic ultrasound imaging, high frequency pulses of acoustic energy are emitted into the patients' body where they experience reflection at boundaries between tissues of different characteristic impedance. From the measurement of time delay and intensity of the reflected pulses (echoes), an image indicating tissue interfaces can be reconstructed. Ultrasound imaging is considered to involve negligible risk, provided that the incident

intensities are sufficiently small. The comparable long wavelengths of ultrasounds minimize scattering and on the same time are harmless for humans. Unfortunately this sets the limit of the resolution to the centimeter range. Moreover as for X-rays they are not absorbed by the molecules, thus giving no information concerning the composition of tissue [18].

Magnetic Resonance Imaging

On the other hand Magnetic Resonance Imaging (MRI) [56]. also referred as Nuclear Magnetic Resonance Imaging (NMR), is utilized to obtain images as a function of proton spin density and relaxation times. The patient is placed inside a strong magnetic field, which is usually generated by large bore super conducting magnets.

The resolution can go below the millimeter scale and many attempts are made to overcome that limit. Further advantages of MRI are the very low risk imposed to the patient and the complete non-invasive nature of the technique. However, some very important features for the diagnosis such as oxygenation of the tissue, are impossible to image. Only recently has it become possible to obtain functional information by using hemoglobin as a paramagnetic tracer. This method called functional MRI is capable of directly measuring the brain activation. The main drawback of MRI however is the extremely high cost of the devise and especially of the super conducting magnets that are necessary for the strong magnetic field, the large size of the equipment and the requirement for the patient to stay still in the magnet for up to about half an hour, as well as the problems associated with the presence of high magnetic fields.

Radioisotope imaging

Radioisotope imaging is fundamentally different from the previously introduced imaging modalities in that the radiation originates from inside the body [56]. Radioisotope tagged compounds in tracer quantities are injected into the patients' body where they decay and produce detectable photons. Hence it is possible to obtain images of the distribution of the radionuclide. Through the suitable choice of a labeled agent its distribution can be made representative of physiological function, such as blood flow, blood volume and various metabolic processes. Radioisotope imaging modalities are single photon emission computed tomography (SPECT) and positron emission tomography (PET).

In SPECT a single ray is emitted per nuclear decay. A gamma camera, fitted with a parallel-hole collimator, rotates around the patient and records 1D projections of the radioactivity. A large number of such data sets allow the reconstruction (using a filtered back-projection similar to X-rays computer tomography) of a 2D cross-sectional image of the radiopharmaceutical distribution inside the body. Combining opposite projections helps to take into account the photon absorption within the body. The question of a relatively cheap and fast imaging technique remains while the need for such a system becomes ever more essential.

1.4.3 Optical imaging methods

Following are the different imaging methods:

Collimated detection, polarization discrimination, coherent gating, holographic gating, heterodyne detection, nonlinear technique, ultra fast shuttering, the Raman amplifier, second harmonic generation, the parametric amplifier, the streak camera, TAC systems, and frequency domain methods.

1.4.4 Creating a polarization image

In the scattering of light, a two dimensional image representing the distribution of intensity of scattered light can be acquired using a CCD camera. Each point in the image directly corresponds to one point on the surface of the scattering medium. If the medium was represented by one matrix of 16 numerical elements, every possible point in the medium would effect the polarization of the laser light in the exact same way. The effect that a given point of the substance has on light depends on how many times the photons were re-radiated by particles before escaping the medium altogether and being collected into the CCD element. Therefore a different matrix must be created for every possible part of the medium. The media used in backscattering experimentation is generally arranged to have a surface area greater then one square centimeter. In this area, slightly smaller than a thumbnail, thousands of individual 4x4 matrices would be needed for the thousands of possible paths the photons from the laser could take. The beauty of images is their ability to represent a huge amount of numerical data in a clean, straight forward manner. Every point in the scattering medium is represented by 16 numerical values in matrix form. All possible numerical values can be translated to a corresponding color value. Thus the matrix

becomes 16 dots of vivid color. But when the thousands of matrices of colored dots are combined to represent the entire surface area of the medium, the dots join to form spatial arrays of color value: pictures. These pictures are easy to interpret distinguishing differing optical properties in a substance [57, 58].

Chapter 2

Optical Calculus and Mueller matrix Polarimetry

The previous sections describe the various types of polarization. The following sections discuss the various mathematical tools developed by Stokes, Jones and Mueller to deal with the propagation and interaction of polarized irradiance. Several calculi have been developed for analyzing polarization, including those based on the Jones matrix, coherency matrix, Mueller matrix, and other matrices of these methods, the Mueller calculus is most generally suited for describing irradiance-measuring instruments, including most polarimeter, radiometers, and spectrometers, and is used exclusively in this thesis [59- 62]. In the Mueller calculus, the Stokes vector S is used to describe the polarization state of a light beam, and the Mueller matrix M to describe the polarization-altering characteristics of a sample. This sample may be a surface, a polarization element, an optical system, turbid medium, biological tissues, and any other light-matter interaction which produces a reflected, refracted, diffracted, absorption, and scattering of light beam.

At present, popular theories of polarized radiation interaction with optical elements or scattering media may be divided into two groups: the Jones calculus, which assumes a coherent addition of waves; and the Stokes-Mueller calculus, which assumes an incoherent addition of waves [63-64]. However, the choices not a matter of taste, in both approaches, one usually starts a theoretical analysis with severely restrictive assumptions. In the Jones calculus, one starts out with Maxwell's equations, whereas in the Mueller calculus, it starts by postulating a linear relation between the input Stokes vector and the output Stokes vector emerging from the optical medium. The development of the Mueller analysis is heuristic and lacks the mathematical rigor of the Jones calculus. However, the Mueller formalism has

an advantage in that it deals with intensities rather than field vectors. If un-polarized light is incident on one or more particles, the Stokes parameters of the scattered light can be shown to be in general, partially polarized. This result shows that scattering is a mechanism for polarizing light. The degree of polarization of the scattered light depends on the scattering direction and some time has been found to be a maximum, when the scattered direction is normal to the incident direction. With this, we come to the conclusion of all the preliminaries needed to deal with studies on scattering of polarized light through turbid medium, which is the main work reported in this thesis.

At nearly the same time that Jones developed his matrix calculus, H. Mueller (1943) working totally independently developed another polarization calculus. Mueller proceeded to express the Stokes parameters developed by Stokes (1852 -1903) as a 1x 4 column matrix and the polarizer, wave plate, and rotator as 4 x4 matrices. Thus, two polarization calculi, the Jones matrix calculus and the Mueller- Stokes calculus, appeared almost simultaneously. The Jones calculus describes the polarization of the optical field in terms of amplitudes and phases, where the Mueller-Stokes matrix calculus describes the polarization in terms of intensities. After the appearance of these two calculi still another calculus appeared. This calculus was developed in the early fifties that grew out of his work on coherence theory. In this calculus, the fields are described in terms of coherence functions and arranged in 2 x 2 matrices [65, 66].

Mueller was the first to determine the matrices that now bear his name for the polarizer, wave plate, and rotator. The use of matrices to deal with complex polarization problems was a significant breakthrough with respect to carrying out the difficult calculations. The Mueller matrix provides the full characterization of a polarization element [67]. Thus, when one is using polarization elements in critical applications such as polarimetry, it is highly desirable that the Mueller matrix of the elements be known. This is analogous to having the interferogram of a lens to ensure that it is of suitable quality for incorporation into a critical imaging system .The optics community has been very slow to adopt Mueller matrices for the testing of optical components and optical systems, delaying a broad understanding of how real polarization elements actually perform. An impediment to the widespread acceptance of Mueller matrices for polarization element qualification has been that the polarization

properties associated with a Mueller matrix (the diattenuation, retardance, and depolarization) are not easily extracted from the Mueller matrix.

The characteristic Mueller matrix for any optical device or scattering medium contains 16 elements, so it requires 16 equations to solve for these elements. Hence, the Mueller matrix is calculable from 49 intensity measurements. The set of these 16 elements contains all the information obtainable from the optical system at this frequency and, in the case of light scattering, at given scattering angle. In practice, all 16 elements may not be independent. Some are zero, and some are identical to others depending on the symmetry and certain properties of the optical medium. For certain ensembles of perfect particles such as spheres, the matrix elements can be exactly predicted.

2.1 Stokes vectors calculus

A major advance to the field came by Sir Georges Gabriel Stokes. Stokes introduced four measurable quantities that now bear the name of Stokes parameters for describing the properties of polarized light. He published the seminal paper, on the composition and resolution of streams of polarized light from different sources [68]. Despite the impressive insight and relatively simple concepts underlying Stokes' original paper, this remarkable study received little attention at that time but would become fully appreciated many decades later. Although his basic motivation for the introduction of these four parameters was to describe mathematically un-polarized light, his parameterization is applicable to any state of polarization, to partially polarized, as well as un-polarized and completely polarized, waves. In a sense the modern description of polarization optics can be said to have started from the time of the publication of papers by Stokes. This was an entirely new and unexplored field. The first Stokes parameter represents the total intensity of the field, and the three others describe the state of polarization. He also formulated a mathematical statement for un-polarized light: the intensity of un-polarized light is unaffected by any rotation of the axes of the reference coordinate system and to any phase change introduced in one of the wave components.

When light in an arbitrary state of polarization propagates through a scattering medium or interacts with some optical element, its polarization properties are modified. Broadly speaking, we may categorize the physical mechanisms that can change the state of

polarization of light into four areas: propagation through anisotropic media, scattering by a system of particles, oblique reflection and refraction at interfaces, and (4) diffraction by apertures. Here we put most of the emphasis on the first two types of interaction. The effect of non-image-forming optical instruments and scattering media on an incident electromagnetic plane wave is to transform the Jones vector and the Stokes vector so that the medium can be represented by a transformation matrix. All these problems involve sets of linear equations, and matrix methods provide an appropriate and compact way to deal with these problems. The polarization of light is fully described by the four elements of the Stokes vector, the measurement of which has become possible because of advances in experimental technology. The statistics of the Stokes parameters is a useful tool for studying scattering media that modify the polarization state of light. Much of the current work on polarization optics utilizes optical techniques that have been developed in the past few decades. Areas of application include characterization of light sources, measurement of the polarization-altering properties of optical systems, and bio-tissues.

The contemporary description of polarized light in terms of Stokes vectors is particularly interesting technique. It provides an extremely effective computational technique in the form of the Mueller matrix methods. A natural starting point for characterizing the turbid media through polarized light is Stokes vectors calculus. It consists of a set of four quantities (called Stokes parameters) that describe the intensity and polarization of incoming beam of light. The beam may be polarized completely, partially, or not at all, it may be monochromatic or polychromatic. The four parameters have the dimensions of intensity, each corresponding not to an instantaneous intensity but to time averaged intensity, the average being taken over a period long enough to permit practical measurement. The vector, though consisting of four physically real parameters, is, of course, a mathematical vector. the four quantities S_0, S_1, S_2, & S_3 comprise a column vector

$$S = \begin{bmatrix} S_0 \\ S_1 \\ S_2 \\ S_3 \end{bmatrix} \tag{24}$$

The vector is often written horizontally, to save space; curly braces are then used, as a reminder that the quantity is indeed a column vector $\{S_0, S_1, S_2, S_3\}$. The first parameter, S_0, is called the intensity. The parameters S_1, S_2, & S_3 may be regarded as the horizontal, +45° and right circular polarized light respectively. When a parameter has a negative value, the preference is for the orthogonal polarization form; thus if the parameter S_3 has the negative sign the polarization is more akin to left-circular polarization than to right-circular polarization.

Operational approach makes use of a set of four filters. Any of several different sets could be used, but to make our account specific we shall assume a set of four filters F_1, F_2, F_3, F_4 that have the following properties, each has a positive transmittance for incident un-polarized light, each is oriented so that its faces are vertical and are perpendicular to the beam, F_1 has the same effect on any incident beam, irrespective of the beam's polarization: in short, it is isotropic, F_2 is opaque to light polarized with its electric vibration direction at 90°, that is, vertical, F_3 is opaque to light polarized at -45°, F_4 is opaque to left-circularly polarized light. Obviously the filters represent non-polarizing, linearly (horizontally) polarizing, linearly (+45°) polarizing and right-circularly polarizing filters respectively, as implied by the polarization forms produced by the four filters used in determining the Stokes parameters of a beam shown in Figure 2.1.

The great appeal of the Stokes parameters is that they can be formulated using directly measurable quantities. Probably the simplest and most appealing definition of the parameters is an operational, Imagine that the four optical filters each of which under natural illumination will transmit half of the incident light [69]. Suppose that the first filter is simply isotropic while the second and third are linear polarizer, whose transmission axes are horizontal and at +45°, respectively. The last filter is a polarizer which is opaque to left circular light each one of these is positioned alone in the path of the beam under study. We are concerned with the radiant flux density transmitted by each of the various filters. Accordingly let, I_0, I_1, I_2, I_3 be the corresponding emergent irradiances (watts per square meter) as measured by a meter insensitive to polarization. The operational definition of the Stokes parameters is then

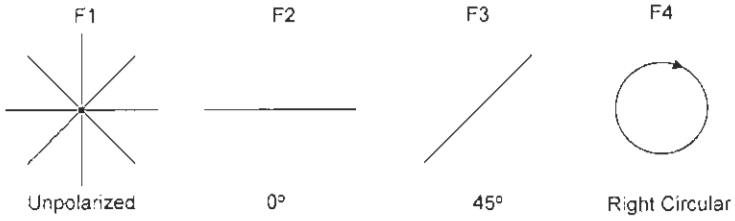

Figure 2.1 Polarization forms determining four Stokes parameters of a laser beam.

$$S_0 = 2I_0$$
$$S_1 = 2I_1 - 2I_0$$
$$S_2 = 2I_2 - 2I_0$$
$$S_3 = 2I_3 - 2I_0 \qquad (25)$$

The quantity S_0 is simply the incident irradiance while S_1, S_2 and S_3 specify the state of polarization. We are indeed dealing only with directly observable quantities. Let's now relate these parameters to the expressions, for the electric field of a quasi-monochromatic light wave propagating in the z direction, viz.

$$E_x(t) = E_{0x}(t)\cos\{(kx - wt) + \delta_x\} \qquad (26)$$

$$E_y(t) = E_{0y}(t)\cos\{(kx - wt) + \delta_y\} \qquad (27)$$

Where $E(t) = E_x(t) + E_y(t)$ and k, w are the mean values of wave traveling in z direction and δ is phase difference. The incident irradiance is given by $I = \varepsilon_0 c\langle E^2(t)\rangle$ or

$$I(t) = \varepsilon_0 c[E_{0x}{}^2(t) + E_{0y}{}^2(t)] \qquad (28)$$

For the natural light $E_{0x}(t), E_{0y}(t), \delta_x$ and δ_y change slowly in comparison to $(kx - wt)$. The irradiance averaged over such a time would then be

$$I(t) = \tfrac{1}{2}(\varepsilon_0 c)[{E_{0x}}^2(t) + {E_{0y}}^2(t)] \tag{29}$$

In contrast, the irradiance, which would actually be measured by a detector, is the average of Eq. (29) over a comparatively long time interval, i.e.,

$$I(t) = 1/2(\varepsilon_0 c)[{E_{0x}}^2 + {E_{0y}}^2] \tag{30}$$

This then corresponds to S_0 or equivalently $2I_0$. The second Stokes parameter, $S_1 = 2I_1 - 2I_0$, is found from the flux density transmitted by a horizontal linear polarizer thus, averaging in the same way as before,

$$I_1 = \tfrac{1}{2}(\varepsilon_0 c)[\langle {E_{0x}}^2\rangle - \langle {E_{0y}}^2\rangle] \tag{31}$$

Clearly then,

$$S_1 = \tfrac{1}{2}(\varepsilon_0 c)[\langle {E_{0x}}^2 - {E_{0y}}^2\rangle] \tag{32}$$

To evaluate S_2 we will need I_2, the irradiance transmitted by a linear polarizer at +45°. The required electric field component, call it E_{45}, is given by

$$E_{45}(t) = (\sqrt{2})^{1/2}(i + j).E(t) \tag{33}$$

Hence, $I_2 = \varepsilon_0 C\langle {E_{45}}^2\rangle$. Substituting Eqs. (26) and (27) into (33), then squaring and averaging yields

$$I_2 = \tfrac{1}{4}(\varepsilon_0 c)[\langle {E_{0x}}^2\rangle + \langle {E_{0y}}^2\rangle + \langle 2E_{0x}E_{0y}\cos\delta] \tag{34}$$

where $\delta = \delta_y - \delta_x$, it follows, from the fact that $S_2 = 2I_2 - 2I_0$, then

$$S_2 = \tfrac{1}{2}(\varepsilon_0 c)\langle 2E_{0x}E_{0y}\cos\delta] \tag{35}$$

Only one more parameter S_3 remains, it requires the evaluation of I_3, the irradiance emerging from a right circular polarizer. Suppose that we construct such a device using the $+45^0$ linear polarizer considered above, followed by a quarter-wave plate. Position the wave plate so that its fast axis is along the y direction. The y component of the field will then lead the x component by $\frac{i}{2\pi}$, and the resulting beam will be right handed. The filter under consideration is supposed to be opaque to left circular states, which is tantamount to saying

that the beam must impinge on the retarder or output side of the circular polarizer. After traversing only the retarder portion, E_y would lead E_x by 90°. Because the phase was written using wt, a phase advance of 90^0 in one component corresponds to the addition of $-\frac{1}{2}\pi$ in the phase of that component. After passing through the linear polarizer, the electric field is again given by Eq. (34), this time including the $-\frac{1}{2}\pi$ phase shift. Thus, δ in Eq. (34) becomes $\delta - \frac{1}{2}\pi$ and

$$I_3 = \tfrac{1}{4}(\varepsilon_0 c)[\langle {E_{0x}}^2\rangle + \langle {E_{0y}}^2\rangle + \langle 2E_{0x}E_{0y}\sin\delta\rangle] \tag{36}$$

Since $S_3 = 2I_3 - 2I_0$

$$S_3 = \tfrac{1}{2}(\varepsilon_0 c)\langle 2E_{0x}E_{0y}\sin\delta\rangle \tag{37}$$

It has become common practice to drop the constant $\frac{\varepsilon_0 c}{2}$ appearing in Eqs. (32), (35), and (37) and write the Stokes parameters as

$$\begin{aligned} S_0 &= \langle {E_{0x}}^2 + {E_{0y}}^2\rangle \\ S_1 &= \langle {E_{0x}}^2 - {E_{0y}}^2\rangle \\ S_2 &= \langle 2E_{0x}E_{0y}\cos\delta\rangle \\ S_3 &= \langle 2E_{0x}E_{0y}\sin\delta\rangle \end{aligned} \tag{38}$$

Or given in the vector form by: $S = \begin{bmatrix} S_0 \\ S_1 \\ S_2 \\ S_3 \end{bmatrix} = \begin{bmatrix} \langle E_{0x}^2\rangle + \langle E_{0y}^2\rangle \\ \langle E_{0x}^2\rangle - \langle E_{0y}^2\rangle \\ 2\langle E_{0x}E_{0y}\cos\delta\rangle \\ 2\langle E_{0x}E_{0y}\sin\delta\rangle \end{bmatrix}$ (39)

The different polarization states can also be described in term of phase and amplitudes (see below table)

Polarization state[symbol]	Phase	Amplitude	Equation
Horizontal[H]	$\delta = \pm n\pi$ $n = 0,1,...$	$E_{0y} = 0$ $E_0 = E_{0x}$	$E = E_x + E_y = E_x$ $E_x(z,t) = iE_0\cos(kz - wt)$
Vertical[V]	$\delta = \pm n\pi$ $n = 0,1,...$	$E_{0x} = 0$ $E_0 = E_{0y}$	$E = E_x + E_y = E_y$ $E_y(z,t) = jE_0\cos(kz - wt)$
$+45^0$[P]	$\delta = \pm n\pi$ $n = 0,1,...$	$E_{0y} = E_{0X}$ $= E_0$	$E = E_x + E_y = E_y$ $E(z,t) = (i + j)E_0\cos(kz - wt)$
-45^0[M]	$\delta = \pm n\pi$ $n = 0,1,...$	$E_{0y} = E_{0X}$ $= E_0$	$E = E_x + E_y$ $E(z,t) = (i - j)E_0\cos(kz - wt)$
Right circular[R]	$\delta = \pm n\pi/2$ $n = 1,2,...$	$E_{0y} = E_{0X}$	$E = E_0[i + E_0\cos(kz - wt) + jE_0\sin(kz - wt)]$
Left circular[L]	$\delta = \pm n\pi/2$ $n = 1,2,...$	$E_{0y} = E_{0X}$	$E = E_0[i + E_0\cos(kz - wt) - jE_0\sin(kz - wt)]$

Table 2.1 The polarization states and their representing equations

2.2 Jones calculus and polarization of light

The electric field of any polarized beam propagating along the z-axis may be written as [45],

$$E = E_x i + E_y j \tag{40}$$

where $E_x = A_x\exp(kz\text{-}wt+\varphi_x)$, $E_y = A_y\exp(kz\text{-}wt+\varphi_y)$.

We can write the components as a column vector, which is called a Jones vector.

$$E = \begin{bmatrix} E_x \\ E_y \end{bmatrix} = \begin{bmatrix} A_x e^{j(kz-wt+\phi_x)} \\ A_y e^{j(kz-wt+\phi_y)} \end{bmatrix} \tag{41}$$

We may factor out and the dependence on z and t and just write

$$E = \begin{bmatrix} E_x \\ E_y \end{bmatrix} = \begin{bmatrix} A_x e^{i\phi_x} \\ A_y e^{i\phi_y} \end{bmatrix} \tag{42}$$

The intensity of the beam is proportional to $A_x^2 + A_y^2$. The most general Jones vector of a polarized beam propagating along the z-axis is given by the above equation.

The Jones vector for horizontally polarized light is given by

$$E = \begin{bmatrix} A_x e^{i\phi_x} \\ 0 \end{bmatrix} = A_x e^{i\phi_x} \begin{bmatrix} 1 \\ 0 \end{bmatrix} \tag{43}$$

Similarly, the Jones vector for vertically polarized light is given by

$$E = \begin{bmatrix} 0 \\ A_y e^{i\phi_y} \end{bmatrix} = A_y e^{i\phi_y} \begin{bmatrix} 0 \\ 1 \end{bmatrix} \tag{44}$$

The normalized Jones vector for light polarized at 45° is given by

$$E = \begin{bmatrix} Ae^{i\phi} \\ Ae^{i\phi} \end{bmatrix} = Ae^{i\phi} \begin{bmatrix} 1 \\ 1 \end{bmatrix} \tag{45}$$

where $A_x = A_y = A$ and $\varphi_x = \varphi_y = \varphi$. Now if $A = 1/\sqrt{2}$ and $\varphi = 0$, then

$$E = \frac{1}{\sqrt{2}} \begin{bmatrix} 1 \\ 1 \end{bmatrix} \tag{46}$$

The normalized Jones vector for right-hand circularly polarized light, $A_x = A_y = 1/\sqrt{2}$ and $\varphi_x = \varphi_y = 0$ is given by

$$E = \begin{bmatrix} Ae^{i\phi} \\ Ae^{i(\phi - \pi/2)} \end{bmatrix} = \frac{1}{\sqrt{2}} \begin{bmatrix} 1 \\ -i \end{bmatrix} \tag{47}$$

For the normalized vectors we have,

$$\frac{1}{\sqrt{2}}\begin{bmatrix}1\\-i\end{bmatrix}=\frac{i}{\sqrt{2}}\begin{bmatrix}i\\1\end{bmatrix} \tag{48}$$

If a polarized beam with field vector E is incident on a polarization-changing medium such as a polarizer or a wave plate, and the result is a beam in another polarization state given as:

$$\begin{bmatrix}E_x'\\E_y'\end{bmatrix}=\begin{bmatrix}m_{11} & m_{12}\\m_{21} & m_{22}\end{bmatrix}\begin{bmatrix}E_x\\E_y\end{bmatrix} \tag{49}$$

Here the 2 x 2 transformation matrix is called the Jones matrix. Table 2.2 lists the Jones matrices for common optical elements. If we require the Jones matrix for an optical element which has been rotated through an angle θ with respect to the direction given in the table above, we must multiply the above matrix by the usual matrices for rotation.

$$M(\theta) = R(\theta)\, M\, R(-\theta) \tag{50}$$

where $R(\theta)=\begin{bmatrix}\cos\theta & -\sin\theta\\ \sin\theta & \cos\theta\end{bmatrix}$

To find the Jones matrix for a sequence of polarization transformations, for example a linear polarizer followed by a quarter wave plate, we simply multiply the individual Jones matrices together in the correct order. If an incident beam of light with field vector E passes through a sequence of four polarizing elements, M_1 followed by M_2, M_3 and M_4, then the resultant field vector E' is given by $E' = M_4 M_3 M_2 M_1 E$, So Jones calculus deals with polarized beam of light passing through optical devices.

Optical Element	**Jones matrix**
Horizontal linear polarizer	$\begin{bmatrix} 1 & 0 \\ 0 & 0 \end{bmatrix}$
Vertical linear polarizer	$\begin{bmatrix} 0 & 0 \\ 0 & 1 \end{bmatrix}$
Linear polarizer at 45^0	$\begin{bmatrix} \cos^2\theta & \cos\theta\sin\theta \\ \cos\theta\sin\theta & \sin^2\theta \end{bmatrix}$
Quarter wave plate (fast axis vertical)	$e^{i\pi/4}\begin{bmatrix} 1 & 0 \\ 0 & -i \end{bmatrix}$
Quarter wave plate (fast axis horizontal)	$e^{i\pi/4}\begin{bmatrix} 1 & 0 \\ 0 & i \end{bmatrix}$

Table 2.2 Jones matrices for some optical elements.

2.3 Mueller matrix

In 1943, Hans Mueller developed a matrix that relates the Stokes vector of the light impinging on a sample to the Stokes vector leaving the sample [43]. Using the method with the input and output polarization states (Stokes vectors) known, the 4x4 Mueller matrix can be used to describe the polarization properties of a sample. The Mueller matrix is defined as a matrix which transforms incident Stokes vectors into exiting Stokes vectors with each element seen as a coupling between corresponding Stokes vector elements [45]. Despite this simple and elegant definition, the polarization properties associated with the Mueller matrix the diattenuation, retardance, and depolarization are not readily apparent from the matrix for two reasons. First, the Stokes vector has an unusual coordinate system in which the different elements do not represent orthogonal polarization components. Instead, positive and negative values on each component separately represent orthogonal polarization components. Second, the phenomenon of depolarization greatly complicates the matrix properties.

The package describing the light beam is simply the four-parameter Stokes vector, described as before. The wave length range (bandwidth) of the light is assumed to be broad enough that the light may, for example, be un-polarized, and narrow enough that the optical devices in question may be regarded as achromatic within this range. The package describing the polarizer, retarder, scatterer, or other optical device is called a Muller matrix. This has the general form [43]:

$$[M]=\begin{bmatrix} m_{11} & m_{12} & m_{13} & m_{14} \\ m_{21} & m_{22} & m_{23} & m_{24} \\ m_{31} & m_{32} & m_{33} & m_{34} \\ m_{41} & m_{42} & m_{43} & m_{44} \end{bmatrix} \tag{51}$$

It is a 4 x 4 matrix, and thus contains 16 elements. The individual matrix is indicative not only of the composition of the device but also of its orientation; thus the matrix of a linear polarizer whose transmission axis is horizontal is different from the matrix of a similar polarizer that has been turned so that its axis is at, say, 37°. The main rules used in performing the multiplications are the standard rules of matrix algebra. One must also observe the following convention, the vector representing the incident beam must be written at the right, and the successive matrices representing the successively encountered devices must be arranged in order, the matrix of the last-to-be-encountered device being written at the left [45].

The Mueller matrix can be calculated using 16, 36, or 49 polarization images, with 36 and 49 images corresponding to an over determined system. Sometimes it is necessary to use more than 16 images to reduce the error due to noise associated with the Mueller matrix calculation [70].

M_{11}=HH+HV+VH+VV	M_{12}=HH+HV−VH−VV	M_{13} = 2PH+2PV−M_{11}	M_{14} = 2RH+2RV−M_{11}
M_{21}=HH−HV+VH−VV	M_{22}=HH−HV−VH+VV	M_{23} = 2PH−2PV−M_{21}	M_{24} = 2RH−2RV−M_{21}
M_{31} = 2HP+2VP−M_{11}	M_{32} = 2HP−2VP−M_{12}	M_{33}=4PP−2PH−2PV−M_{31}	M_{34}=4RP−2RH−2RV−M_{31}
M_{41} = 2HR+2VR−M_{11}	M_{42} = 2HR−2VR−M_{12}	M_{43}=4PR−2PH−2PV−M_{41}	M_{44}=4RR−2RH−2RV−M_{41}

(a)

M_{11} = HH+HV+VH+VV	M_{12} = HH+HV−VH−VV	M_{13} = PH+PV−MH−MV	M_{14} = RH+RV−LH−LV
M_{21} = HH−HV+VH−VV	M_{22} = HH−HV−VH+VV	M_{23} = PH−PV−MH+MV	M_{24} = RH−RV−LH+LV
M_{31} = HP−HM+VP−VM	M_{32} = HP−HM−VP+VM	M_{33} = PP−PM−MP+MM	M_{34} = RP−RM−LP+LM
M_{41} = HR−HL+VR−VL	M_{42} = HR−HL−VR+VL	M_{43} = PR−PL−MR+ML	M_{44} = RR−RL−LR+LL

(b)

M_{11} = OO	M_{12} = HO−VO	M_{13} = PO−MO	M_{14} = RO−LO
M_{21} = OH−OV	M_{22} = HH−HV−VH+VV	M_{23} = PH−PV−MH+MV	M_{24} = RH−RV−LH+LV
M_{31} = OP−OM	M_{32} = HP−HM−VP+VM	M_{33} = PP−PM−MP+MM	M_{34} = RP−RM−LP+LM
M_{41} = OR−OL	M_{42} = HR−HL−VR+VL	M_{43} = PR−PL−MR+ML	M_{44} = RR−RL−LR+LL

(C)

Table 2.3 Mueller matrix equations for acquisition of (a) 16, (b) 36, and (c) 49 polarization images

The Mueller matrices are shown in Table 2.3, where the first term and second terms represent the input and output polarization states respectively. [70] The polarization states are defined as: H=Horizontal, V=Vertical, P=+45°, M=-45°, R=Right circular, L=Left circular and O=Open (i.e. no polarization).

For example, the Mueller matrix of material irradiated with Stokes vectors is given as:

$$S_{out} = MS_{in}$$

$$S_{out} = \begin{bmatrix} m_{11} & m_{12} & m_{13} & m_{14} \\ m_{21} & m_{22} & m_{23} & m_{24} \\ m_{31} & m_{32} & m_{33} & m_{34} \\ m_{41} & m_{42} & m_{43} & m_{44} \end{bmatrix} \begin{bmatrix} S_0 \\ S_1 \\ S_2 \\ S_3 \end{bmatrix} \tag{52}$$

and according to the usual rules of the matrix multiplication, the product has the form,

$$S_{out} = \begin{bmatrix} m_{11}S_0 + m_{12}S_1 + m_{13}S_2 + m_{14}S_3 \\ m_{21}S_0 + m_{22}S_1 + m_{23}S_2 + m_{24}S_3 \\ m_{31}S_0 + m_{32}S_1 + m_{33}S_2 + m_{34}S_3 \\ m_{41}S_0 + m_{42}S_1 + m_{43}S_2 + m_{44}S_3 \end{bmatrix} \tag{53}$$

It is to note that each row of the product contains terms that are connected by plus signs. Accordingly each row consists, essentially, of a single element. Thus the expression is a column vector, not a 4 x 4 matrix. When, say, four optical devices are inserted in the beam, four matrices must be used and four multiplications are called for. If the four matrices are called $[M_1]$, $[M_2]$, $[M_3]$, $[M_4]$, and if $[V_i]$ represents the Stokes vector of the incident beam, the procedure for finding the specification $[V_o]$ of the emerging beam is indicated schematically thus

$$[M_4][M_3][M_2][M_1][V_i] = [V_o] \tag{54}$$

2.4 Mueller matrix of a train

It is often advantageous to combine a given series of matrices (representing a given train of optical devices) into one single matrix, called the matrix of train. One advantage is that the combined matrix gives direct insight into the essential function of the train. A more important advantage is that, once the matrix of train has been computed, the outcome for any given incident beam can be found merely by one multiplication. For example if the Mueller matrices for a train of optical devices are $[M_1]$, $[M_2]$, $[M_3]$, $[M_4]$, then the matrix of train, $[M_t]$ is computed as follows

$$[M_t] = [M_4][M_3][M_2][M_1] \quad (55)$$

Now outcome can be computed by only one multiplication, i.e.,

$$[M_t][V_i] = [V_o] \quad (56)$$

Compressing the information into one matrix is, of course, an important simplification in problems that involve a large number of devices and many different choices of incident beam.

2.5 Derivation of Mueller matrix for polarizer

The matrices of the Mueller Calculus are not derived from the electromagnetic theory of light or any other theory. Rather, they rest on a phenomenological foundation. They were initially discovered by experimentation, or by reliance on previous experimentation. One makes a guess as to what the elements of 4 x 4 matrixes must be, then tries out the matrix to see whether it performs satisfactorily. To be deemed fully satisfactory, it must lead to results that are known to be correct for four independent types of incident beam, for example, (1) unpolarized light, (2) light that is horizontally polarized, (3) light that is linearly polarized at 45°, and (4) light that is right-circularly polarized.

The task of finding the matrix $[P_\theta]$ of a polarizer at some general azimuth 0 is easy, once one knows the matrix $[P_0]$ of the polarizer in its principal orientation, that is, with its transmission axis horizontal. Using a convention procedure of matrix algebra, one computes the product, which is standard and given in [70] is:

$$[P_\theta] = [T(-2\theta)][P_0][T(2\theta)] \quad (57)$$

where $[T(2\theta)]$ is the well-known standard rotator matrix [45],

$$\begin{bmatrix} 1 & 0 & 0 & 0 \\ 0 & C_2 & S_2 & 0 \\ 0 & -S_2 & C_2 & 0 \\ 0 & 0 & 0 & 1 \end{bmatrix} \quad (58)$$

where C_2 and S_2 are abbreviations for cos (2θ) and sin(2θ), and [T(-2θ)] is the counter-rotator matrix, the same as [T(2θ)] except that the signs of the sine elements, S_2, are changed.

As standard Mueller matrix for polarizer [P_0] is given by,

$$\begin{bmatrix} 1/2 & 1/2 & 0 & 0 \\ 1/2 & 1/2 & 0 & 0 \\ 0 & 0 & 0 & 0 \\ 0 & 0 & 0 & 0 \end{bmatrix} \tag{59}$$

So performing the indicated multiplication one finds, for the matrix [P_0] of an ideal homogeneous linear polarizer with transmission axis at angle θ

$$[P_\theta] = \begin{bmatrix} 1 & 0 & 0 & 0 \\ 0 & C_2 & -S_2 & 0 \\ 0 & S_2 & C_2 & 0 \\ 0 & 0 & 0 & 1 \end{bmatrix} \begin{bmatrix} 1/2 & 1/2 & 0 & 0 \\ 1/2 & 1/2 & 0 & 0 \\ 0 & 0 & 0 & 0 \\ 0 & 0 & 0 & 0 \end{bmatrix} \begin{bmatrix} 1 & 0 & 0 & 0 \\ 0 & C_2 & S_2 & 0 \\ 0 & -S_2 & C_2 & 0 \\ 0 & 0 & 0 & 1 \end{bmatrix} \tag{60}$$

$$[P_\theta] = \frac{1}{2} \begin{bmatrix} 1 & C_2 & S_2 & 0 \\ C_2 & C_2^2 & C_2 S_2 & 0 \\ S_2 & C_2 S_2 & S_2^2 & 0 \\ 0 & 0 & 0 & 0 \end{bmatrix} \tag{61}$$

The same procedure applies to a retarder: the matrix of a device at a non-principal azimuth is computed from that of the device at the principal azimuth with the aid of the rotator matrix and counter-rotator matrix.

2.6 General Mueller matrix for retarder

If ρ is the angle of axis (fast axis) of retarder with respect to the X-axis, then $a_x = \cos\rho$ & $a_y = \sin\rho$ as shown in Figure 2.2. The standard Mueller matrix for the retarder at fast axis is given by [45],

$$[M_R]=\begin{bmatrix} 1 & 0 & 0 & 0 \\ 0 & D^2-E^2+G^2 & 2DE & -2EG \\ 0 & 2DE & -D^2+E^2+G^2 & 2DG \\ 0 & 2EG & -2DG & 2G^2-1 \end{bmatrix} \quad (62)$$

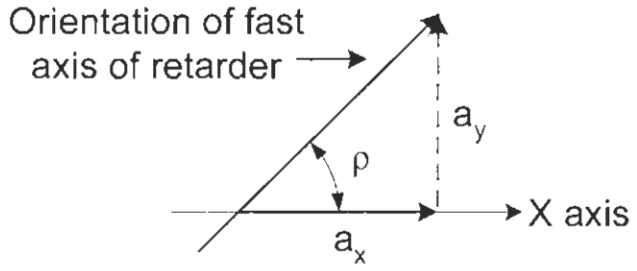

Figure 2.2 The orthogonal components due to orientation of retarder.

Here $D = S_1 \sin\frac{\delta}{2}$, $E = S_2 \sin\frac{\delta}{2}$, $F = S_3 \sin\frac{\delta}{2}$ & $G = \cos\frac{\delta}{2}$ and δ is the phase difference (required to produce for rotation of polarization of light for two components of light beam passing through the retarder and S_1, S_2 & S_3 are the 2nd, 3rd & 4th components of the Stokes vector respectively. That is $S_1 = a_x^2 - a_y^2$, $S_2 = 2a_x a_y \cos\delta$, $S_3 = 2a_x a_y \sin\delta$

2.7 Degree of polarization

The degree of polarization (DOP) can be calculated through output intensities and the values of measured intensities lie between -1 and 1, and they represent the tendency of the measured light to be polarized linearly, $\pm 45^{o}$, and right or left- handedness. Using the values of the Stokes vector the degree of polarization (DOP) can be computed [45],

$$DOP = \frac{\sqrt{S_1^{\,2} + S_2^{\,2} + S_3^{\,2}}}{S_0} \tag{63}$$

The DOP is 1 for completely polarized light, zero for totally depolarized light, and assumes a fractional value for any case in between. From the Stokes vector, the degree of polarization (DOP), the degree of linear polarization (DOLP), and the degree of circular polarization (DOCP) are derived as:

$$DOLP = \frac{\sqrt{S_1^{\,2} + S_2^{\,2}}}{S_0}$$

$$DOCP = \frac{S_3}{S_0} \tag{64}$$

DOP is a measure of the polarization purity of light. DOP = 1 means the light is completely polarized; DOP = 0 means the light is completely depolarized; DOP <1 means the light is partially polarized. When DOP = 1, we have

$$\begin{aligned} S_0 &= E^2{}_{0H} + E^2{}_{0V} \\ S_1 &= E^2{}_{0H} - E^2{}_{0V} \\ S_2 &= 2E_{0H}E_{0V}\cos\delta \\ S_3 &= 2E_{0H}E_{0V}\sin\delta \end{aligned} \tag{65}$$

where E_{0H} and E_{0V} are the amplitudes of the horizontal and vertical components of the electric vector of the light, respectively, δ is the phase difference between the vertical and horizontal components of the electric vector.

Chapter 3

MATERIALS AND METHODS

This chapter presents a detailed description of the Mueller matrix imaging system (Polarimeter) implemented in this research, an overview of the system setup, calibration procedure, optics defects and detailed description of the system and sample preparation.

3.1 Mueller matrix polarimeter

To measure the Mueller matrix elements for sample characterization we developed a Mueller matrix polarimetric system. This dual rotating retarder Mueller matrix polarimeter is one of the most common Mueller polarimeter. Figure 3.1 shows the configuration : light from the source passes first through a fixed linear polarizer , then through a rotating linear retarder and focusing lens, the sample , a rotating linear retarder , and finally through a fixed linear polarizer and detector. In the most common configuration the polarizer are parallel, and the retarder are rotated in angular increments of five-to-one. This five-to-one ratio encodes all 16 Mueller matrix elements onto the amplitudes and phases of 12 frequencies in the detected signal [71]. The detected signal is Fourier analyzed, and the Mueller matrix elements are calculated from the Fourier coefficients. This polarimeter design has an important advantage that the polarizers do not move. The polarizer in the generator accepts only one polarization state from the source optics, making the measurement immune to instrumental polarization from the source optics. If the polarizer did rotate, and if the beam incident on it were elliptically polarized, a systematic modulation of intensity would be introduced which would require compensation. Similarly, the analyzer does not rotate only one polarization state is transmitted through the analyzing optics and onto the detector.

Any diattenuation in the analyzing optics and any polarization sensitivity in the detector will not affect the measurements. Henceforth , the polarization analyzer is considered as the polarization elements used for analyzing the polarization state together with any and all optical elements (lenses , mirrors , etc .) , and the detector contained in the polarimeter . The polarization effects from all elements are included in the measurement and data reduction procedures for the polarimeter. A polarization analyzer is characterized by an analyzer v vector containing four elements and is defined in a manner analogous to a Stokes vector. Let P_H (polarizer at horizontal direction) be flux measurement taken by the detector (the current or voltage generated) when one unit of horizontally polarized light is incident. Similarly $P_V, P_{+45}, P_{-45}, P_R, P_L$ are the detector's flux measurements for the corresponding incident polarized beams with unit flux.

The polarization characteristics of a sample are characterized by its Mueller matrix. Since the Mueller matrix is a function of wavelength, angle of incidence, and location on the sample, these are assumed to be fixed.

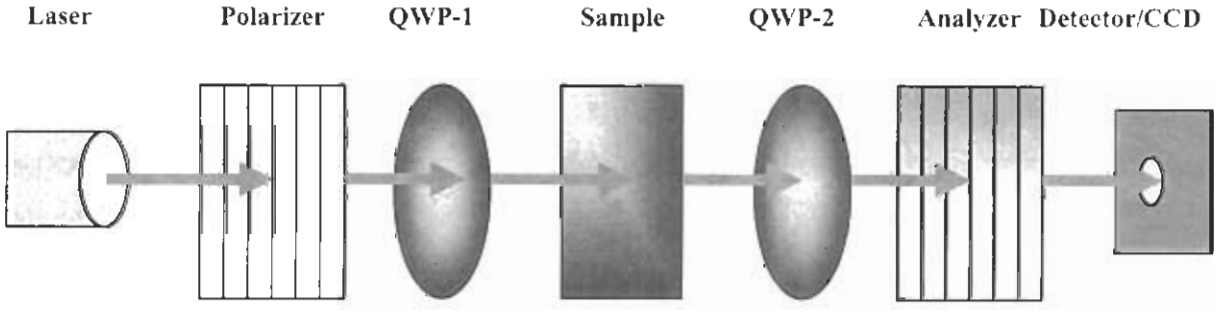

Figure 3.1 The dual rotating retarder polarimeter consists of a source , a fixed linear polarizer , a retarder which rotates in steps , the sample , a second retarder which rotates in steps , a fixed linear polarizer , and the detector .

3.2 Experimental setup for Mueller matrix imaging system

3.2.1 Optical components

The Mueller Matrix Polarization Imaging System consists of two branches: an input and an output. A laser (He-Ne 632.8 nm) wavelength is used because the amount of scatter and absorption in a turbid medium, such as skin, falls off with increasing wavelength in the visible to near-infrared region. The beam is sent through the input branch that consists of a linear polarizer set at $+45^{o}$ (to the horizontal) and a variable retarder. The rotator, which rotates the polarization vector of the initially polarized beam, produces all the necessary states of linearly polarized light (horizontal, vertical, and $\pm 45^{o}$), and the retarder, which changes the relative phase between the two components of the electric field vector, produces left and right circular polarization states. After passing through the input optics, the polarized light hits the sample and the transmitted light passes through the output optical branch, which consists of the same components as the input branch except in the reverse order with the polarizer set at -45^{o}. The charge coupled device (CCD) camera is placed at the end of the output branch and is used to capture the resulting images. Automation of the system is accomplished via a Lab View program.

This polarimeter measures the full Mueller matrix. It accepts only one polarization state from the source, and transmits only one polarization state to the detector. Several data reduction methods have been published to account for additional imperfections in the polarization elements, leading to considerably more elaborate expressions than those presented here developed an algorithm to compensate for the linear diattenuation and linear retardance of the retarder [72].

3.2.2 Polarimetric optical arrangements

The experimental setup for studying the transmitted polarized light is illustrated in Fig 3.2. The linear polarizer was placed in front of the laser when the laser was arranged to produce light polarized in the plane parallel to the table. This direction was labeled the horizontal axis for future consistency. A photo detector attached to a voltmeter placed after the polarizer could indicate the orientation of the polarizer which admitted the least amount of light.

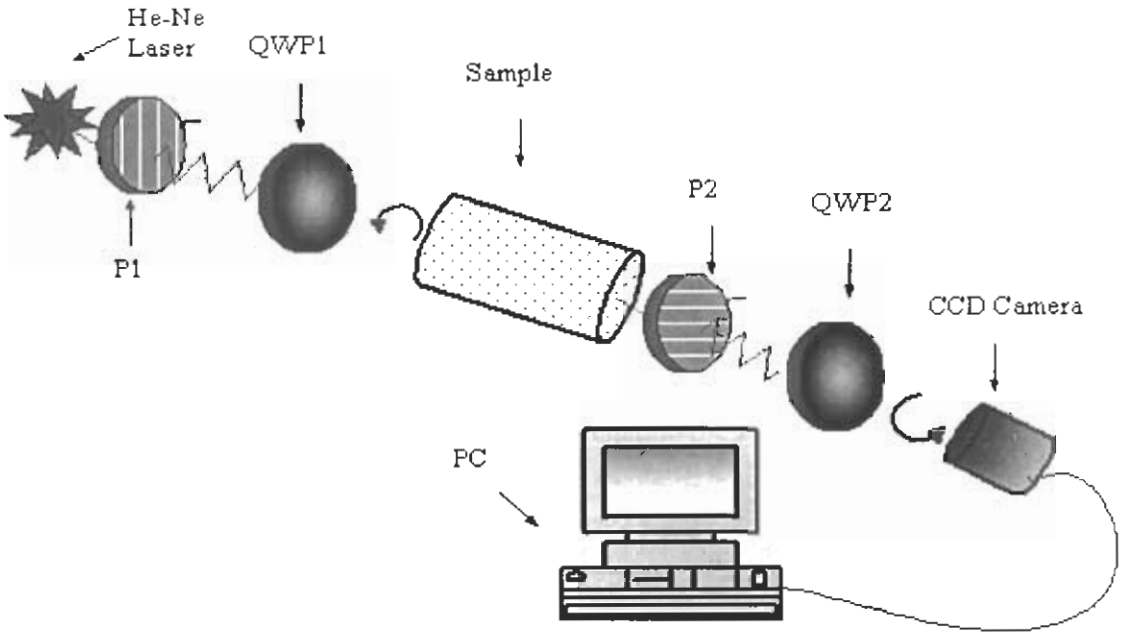

Figure 3.2 The experimental setup for the measurements of transmitted Mueller matrix elements of the medium. A He-Ne laser beam with an output power of 10 mW at a wavelength of 632.8 nm is used as the light source. The laser light is focused on sample. The circularly polarized light is generated, by inserting a quarter mica retardation plates behind the linear polarizer. The out put polarized light is focus to turbid medium or tissue sample, and again pass through quarter wave plate, linear polarizer, and recorded on photodiode detector or CCD camera, which is controlled and operated with Lab software.

At this orientation, the polarizer was labeled to be oriented to admit only electric fields parallel to y-axis or vertical axis. The quarter wave plates were more difficult to characterize. One at a time, they were placed directly in front of the laser, which was turned to produce vertically polarized light. After the wave plate was a linear polarized already tested, turned to allow only horizontally polarized light. At the point where a photo detector indicated the least amount of laser light passed through both elements, the quarter-wave

plate did not have any effect on the polarization of the light. Therefore it was oriented so that electric field was parallel to either the fast or slow axis of the plate. While knowing which axis was truly parallel to the vertical electric field of the polarized laser light would allow the handedness to be known of the circularly polarized admitted light, it is not essential to find this out. Our definition of any axis or direction is completely arbitrary; there is no standard for naming directions of polarization. Some standards were adopted in order to have a consistent procedure for the experimentation. The polarizer and quarter wave plates would also be uniformly arranged so the 360 degree rotation stage would face away from the laser. When an optical beam interacts with matter, such as an optical polarizing element, its polarization state is almost always changed. The polarization state can be changed in three ways and is governed by the fundamental amplitude and phase nature of field equations. The polarization state of an optical field can be changed by 1) changing the orthogonal amplitude, 2) changing the phase, or 3) changing the direction (orientation) of the components. A polarizing element that changes the orthogonal amplitudes unequally is called a polarizer and is an anisotropic attenuator. The detail description of different optics used is given as:

Polarizer

The Polarizer may be linear, circular, or elliptical, depending , linear polarizers that transmit a linear state are the most common and are often simply called polarizer. The transmission axis of a linear polarizer corresponds to the direction of the output light's electric field oscillation. When linearly polarized light is incident on a linear polarizer, the transmittance T from the polarizer follows Malus's law,

$$T = \cos^2\theta \tag{66}$$

where θ is the angle between the input polarization's azimuth and the polarizer's transmission axis.

For an imperfect polarizer Malus's law becomes,

$$T = (T_{max} - T_{min})\cos^2\theta + T_{min}, \tag{67}$$

where T_{max} and T_{min} are called the principal transmittances, and transmittance T varies between these values. The extinction ratio T_{min} / T_{max} provides a useful measure of polarizer performance.

Retarder

Retarders are devices that induce a phase difference, or retardation, between orthogonally polarized components of a light wave. Linear retarders are the most common and produce a retardance $\Delta\varphi = \varphi_y - \varphi_x$ between orthogonal linear polarizations. Circular retarders cause a phase shift between right and left-circular polarizations and are often called rotators because circular retardance changes the azimuthal angle of linearly polarized light. The polarization state of light is determined by the relative amplitudes and phase shifts between orthogonal components, retarders are useful for altering and controlling a wave's polarization. In fact, an arbitrary polarization state can be converted to any other state using an appropriate retarder.

Wave plates are linear retarders made birefringent medium of length L yields [73],

$$E(z = L, t) = \mathrm{Re}\{E_x \exp[i(wt - k_0 n_x L)] + E_y \exp[i(wt - k_0 n_y L)]\} \quad (68)$$

where the x and y directions coincide with eigen polarizations and the absolute phases are initially equal (at $z = 0$, $\varphi_x = \varphi_y = 0$). The retardance $\Delta\varphi = k_o (n_x - n_y) L$ is the relative phase shift between eigen polarizations and depends on the wavelength, the propagation distance, and the difference between the refractive indices of the eigen polarizations. If the z axis is an optic axis, then $n_x = n_y = n_o$, and there is no retardance, if is perpendicular to an optic axis, the retardance is $\Delta\varphi = \pm kz\hat{}(n_o - n_e)L$. In general, the retardance over a path of length L in a material with birefringence Δn is given by,

$$\Delta\varphi = 2\pi\Delta nL / \lambda \quad (69)$$

Retardance may be specified in radians, degrees. A wave plate that introduces a π-radian or 180° phase shift between the eigen polarizations is called a half-wave plate. Quarter-wave plates are another common component and provide phase shifts of 90° or $\pi / 2$.

Detectors

The type of optical detector and the method of detector conditioning used offer a wide scope of both possibilities and sensitivities. The light that emerges after traveling through many centimeters of highly scattering tissue is no longer coherent to any degree. Therefore any detection method which relies on the coherent properties at optical frequencies cannot be used. The maximum size of a detector which can be considered for direct attachment to a sample is 1 cm^2. The photo detector used in this experiment is constructed locally and details are given as. Circuit diagram of the photo-detector circuit is shown in Fig. 3.3

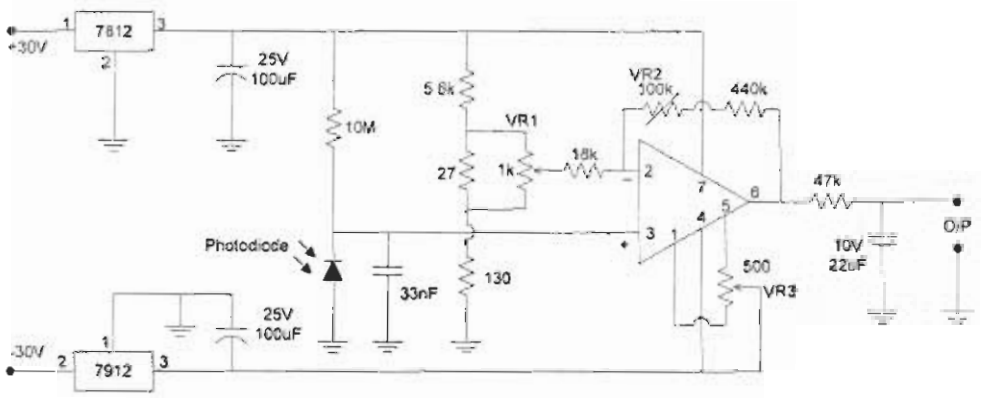

Fig. 3.3 Diagram of photo detector circuit.

Here the operational amplifier used was uA741 which has ±18V as limitation for its supply. As we used the same power supply for all the circuits with ±30V so if we want to operate uA741 at ±12V then we have to use the regulators 7812 & 7912 for both +12V and –12V voltages. Theses regulators not only attenuate but also filter out any variations in the supply. The photodiode used is compatible to a fiber cable coupling for wave length of light, λ = 632.8 nm. The photodiode is connected in reverse biased configuration while the operational amplifier is connected in non-inverting configuration such that output of the amplifier is directly proportional to the light input to the photodiode. The variable resistance of 100 kΩ is used to adjust the gain of the amplifier, variable resistance of 1 kΩ is primarily used to

adjust the output offset voltage when there is no input light to the photodiode. Then the variable resistance of 500 Ω is used for the fine adjustment of output offset voltage. To remove the effect of these high frequency components we connect an integrator at the output of uA741. The time constant of this integrator is 1.03 seconds and the low-pass frequency range is 0 Hz to 0.17 Hz that is this integrator is a perfect filter for filtering all the variations due to scattering event of 1 Hz. But at the same time there is draw back of using this integrator that we have to wait for nearly 3 seconds to get the stabilized value of the output from this circuit.

The ultimate noise determining factor is that of light itself, i.e. photon noise. Under circumstances of the random arrival of photons at the detector, the probability that n photons will arrive in the measurement interval τ is given by the Poisson distribution

$$P(n,r) = \frac{(nN_p r)^n}{n} e^{-nN_p r} \tag{70}$$

where Np is the average photon arrival rate and the variances are then

$$\mu_P = nN_p r \,,\ \sigma^2{}_p = \mu_p \tag{71}$$

Hence the signal to noise ratio (SNR) is given by

$$S_r = \sqrt{nN_p r} \tag{72}$$

There is an additional noise contribution from detected dark emission in the measurement interval, arising either from unwanted background light sources or thermal emission from the detector. Hence the overall signal to noise ratio S_r including the effect of shot noise. To obtain a high SNR in a fixed detection interval, the dark emission should be much less than the optical signal, the quantum efficiency near unity and the photon arrival rate high. Note that in situations where the dark emission noise term is negligible in comparison with the photon noise term, the detector is then operating photon noise limited i.e. its SNR is only dependent upon the intensity of the light striking it. An improved signal to noise ratio is always available at the expense of increasing the measurement interval.

$$S_r = \frac{nN_P r}{\sqrt{nN_P r + N_P r}} \tag{73}$$

If I the diode current and I_0 is the reverse bias saturation current, then I and I_0 are related by the standard diode equation as:

$$I = I_0[e^{\frac{eV}{eT}} - 1] \tag{74}$$

Here V is the diode bias voltage, k Boltzman's constant and T is the absolute temperature. A photodiode is typically used in one of two modes of operation. Firstly consider the diode with a zero bias voltage applied across it. As the photodiode is unbiased, it behaves like a Johnson noise source with a shunt resistance R_{sh} calculated from the gradient (dV/dI) at zero voltage.

The zero bias noise current is then

$$R_u = \sqrt{\frac{KT}{qI_0}} \tag{75}$$

$$I_0 = \sqrt{\frac{4KTB}{R_u}} \tag{76}$$

However, in most situations, the photodiode is used reverse biased to obtain a lower shunt capacitance and hence greater speed, then $I = -I_0$ and the shot noise current is given by

$$I_0 = \sqrt{2QI_0 B} \tag{77}$$

When the diode is illuminated, the current resulting from incident photons is i_p, related to the photon arrival rate. The overall signal to noise should be minimum.

$$S_r = \frac{i_p}{\sqrt{2qI_P B + 2qI_0 B}} \tag{78}$$

The CCD Camera

The camera and software used to acquire the images of scattered light is a critical element of the whole apparatus [121]. In the present experiments, individual photons scatter off small particles repeatedly until they finally leave the scattering substance and are focused towards

the CCD camera which analyzes them. Because the incident light in polarized, the intensity of the outgoing light will not be uniformly distributed in all areas of the sample. A dipole pattern is expected to be captured by the camera when linearly polarized light is directed onto a uniform substance. The presence of an axis perpendicular to two symmetrical areas of high intensity near the center of the image is caused by the inability of particles in the scattering medium to re-radiate light along that one plane. However, this occurs near the center of the image, as areas further away represent photons that have been scattered so many times that their polarization is lost, or decided by chance.

Image processing software

Mat lab Imaging software allows files to be imported and manipulated in all the ways necessary in this experiment. The intensity values of individual pixels can be determined, and an adjustable scale of false-coloring can group pixels of the same intensity value by color. A histogram can be created for the image in its entirety, graphing the amount of pixels of each value present in the file. A profile can also be made of a single straight line of pixels, showing their relative values in a graph. In short, the software is capable of every function required for the creation of a full 4x4 Mueller matrix. The Mat lab software was installed and run in the same P-II computer used to operate the camera.

3.2.3 Optical properties of phantom and bio-tissues

We use two types of samples for our experiment, turbid medium and for bio-materials in vitro (chicken skin tissue).The sample used in the experiment as a turbid phantom to characterize the tissue like materials was Intralipid 10% (soybean oil + distilled water) and polystyrene sphere of different suspension. The constituents of phantom are i.e. in a 500 mL bottle according to the manufacturer are soybean oil 10% and water 90%. There is sufficient bottle-to-bottle variation in the optical properties of commercially available Intralipid, or other brand name products, those optical properties should be verified experimentally for each bottle at the time of use. Therefore, the properties reported here are simply approximate.

3.2.4 Mueller matrix polarimetric system calibration

Main calibration

The Mueller matrix imaging system must be precisely calibrated so that errors are not induced in the measured Mueller matrices [70]. This process is carried out in several steps so that each optic is calibrated separately. For calibration, the system is setup in transmission mode, and the polarizer and analyzer are placed in the input and output arms respectively and the desired angles ($+45^{o}$ for polarizer, -45^{o} for analyzer) are determined. This is accomplished by first setting the polarizer to horizontal and analyzer to vertical so that minimum intensity is found, then the horizontal position for the analyzer is found by subtracting (or adding) 90^{o} to the vertical angle setting. The analyzer horizontal position is verified by detecting maximum intensity. The polarizer is then set to vertical by adding (or subtracting) 90^{o} to the angle setting for horizontal and with the analyzer set to horizontal, the minimum intensity is found. The polarizer and analyzer are also set to vertical and maximum intensity is verified.

Now that the horizontal and vertical angles for both the polarizer and analyzer have been determined, the desired angles ($+45^{o}$ for polarizer, -45^{o} for analyzer) can be found. The polarizer is then set to $+45^{o}$ with the analyzer at vertical and horizontal and the half intensity value is verified. The half intensity should be (max intensity + min intensity)/2. Next retarder (2) is placed in the output arm to verify polarizer and analyzer settings. If the polarizer and analyzer are set properly then the retarder should have no effect when the analyzer is set to vertical and horizontal and polarizer at 45^{o} (P_H=P_V).

Fine tune calibration

Once a rough calibration has been obtained, a fine tune calibration is needed. For this calibration, the intensity of each case is observed independently, and the angles to the polarizer and retarders are adjusted so that the appropriate intensity value is achieved. For the cases where input and output are the same polarization state, the intensity is maximum and when the input and output are 90 degrees out of phase the intensity is minimum. All the other cases the theoretical intensity is maximum plus minimum divided by 2 (half intensity).

For each case, there are four variables (voltages) that attribute to the intensity, and in order to determine the correct voltage to adjust, a system model that is a function of the four components is needed. The system is modeled using Mueller-Stokes calculus and is shown below

$$S_{out} = MS_{in} \tag{79}$$

$$M_{system} = M_{polarizer} * M_{retarder1} * M_{sample} * M_{retarder2} * M_{analyzer} \tag{80}$$

where S_{out} and S_{in} are the output and input Stokes vectors respectively and M' is the Mueller matrices of all the optical components in the system. For calibration, the system is setup in transmission mode with air as the sample and the initial polarization set to $+45^{o}$. The following shows the calculation of S_{out}, where θ_1 and θ_2 are the rotation of rotator 1 and 2 respectively, and δ_1 and δ_2 are the retardance of retarder1 and retarder 2 respectively. [45]

$$S_{out} = \begin{bmatrix} S_0 \\ S_1 \\ S_2 \\ S_3 \end{bmatrix} = \frac{1}{2}\begin{bmatrix} 1 & 0 & -1 & 0 \\ 0 & 0 & 0 & 0 \\ -1 & 0 & 1 & 0 \\ 0 & 0 & 0 & 0 \end{bmatrix}\begin{bmatrix} 1 & 0 & 0 & 0 \\ 0 & \cos 2\theta_1 & \sin 2\theta_2 & 0 \\ 0 & -\sin 2\theta_1 & \cos 2\theta_2 & 0 \\ 0 & 0 & 0 & 1 \end{bmatrix}\begin{bmatrix} 1 & 0 & 0 & 0 \\ 0 & 1 & 0 & 0 \\ 0 & 0 & \cos\delta_1 & \sin\delta_2 \\ 0 & 0 & -\sin\delta_1 & \cos\delta_2 \end{bmatrix}$$
$$\begin{bmatrix} 1 & 0 & 0 & 0 \\ 0 & 1 & 0 & 0 \\ 0 & 0 & 1 & 0 \\ 0 & 0 & 0 & 1 \end{bmatrix}\begin{bmatrix} 1 & 0 & 0 & 0 \\ 0 & 1 & 0 & 0 \\ 0 & 0 & \cos\delta_1 & \sin\delta_2 \\ 0 & 0 & -\sin\delta_1 & \cos\delta_2 \end{bmatrix}\begin{bmatrix} 1 & 0 & 0 & 0 \\ 0 & \cos 2\theta_1 & \sin 2\theta_2 & 0 \\ 0 & -\sin 2_1 & \cos 2\theta_2 & 0 \\ 0 & 0 & 0 & 1 \end{bmatrix}\begin{bmatrix} 1 \\ 0 \\ 1 \\ 0 \end{bmatrix} \tag{81}$$

$$S_{out} = \begin{bmatrix} S_0 \\ S_1 \\ S_2 \\ S_3 \end{bmatrix} = \frac{1}{2}\begin{bmatrix} 1+\sin 2\theta_2 \sin 2\theta_1 - \cos 2\theta_2 \cos 2\theta_1 (\cos\delta_2 \cos\delta_1 - \sin\delta_2 \sin\delta_1 \\ 0 \\ -1-\sin 2\theta_2 \sin 2\theta_1 + \cos 2\theta_2 \cos 2\theta_1 (\cos\delta_2 \cos\delta_1 - \sin\delta_2 \sin\delta_1 \\ 0 \end{bmatrix} \tag{82}$$

Since the quantity that the system measure is intensity, S_0 is the Stokes parameter of interest, and the output vector can be simplified as:

$$S_0 = \frac{1}{2}\left[1 + \sin 2\theta_2 \sin 2\theta_1 - \cos 2\theta_2 \cos 2\theta_1 (\cos\delta_2 \cos\delta_1 - \sin\delta_2 \sin\delta_1\right] \quad (83)$$

3.2.5 Effect of source parameters and polarization optics

The important variables that need to be considered for polarimetric results are the wavelength of the source, its polarization state and spectral width. When, we are considering the effect of polarization state of light on the imaging performance. The key points have been listed below:

1. Depolarization of scattered light depends on the initial polarization of the photons.
2. Few scattering events are needed to randomize circular polarization in Rayleigh regime and linear polarization in Mie regime. Many scattering events are required to randomize circular polarization in Mie regime.
3. In dilute suspensions of micro spheres, where independent scattering can be assumed, the DOP decreases as the scatterer concentration increases. However, for dense suspensions, the DOP increases with the scatterer concentration, and further, preferential propagation of linear over circularly polarized light is observed.
4. For biological tissues, the widths of the point-spread functions do not depend on whether the incident light is linearly or circularly polarized.
5. Polarization discrimination of ballistic and snake photons based on circularly polarized light gives rise to a wider point-spread function than the one based on linearly polarized light.
6. Circularly polarized light cannot be used to discriminate between weakly and strongly scattered photons for media containing spheres of large diameter. The converse is true in media containing small spheres.
7. The DOP decays at the same rate for both incident linear and circular polarization states for small detector apertures and it is independent of the anisotropy parameter.

8. In Rayleigh regime, the depolarization rates for both the incident linear and circular polarization states are nearly the same.
9. Circular depolarization length strongly depends on material concentration and systematically decreases after each scattering event, whereas, linear depolarization length decreases with the randomization of directions. This is true, independent of the size parameter and the refractive indices of the scatterers and the size of the receiver's field of view.
10. The criterion to choose the initial polarization state of the probe beam, when the optical properties of the scattering medium are known, is addressed in. For Rayleigh scatterers, linear polarization has been recommended, and for Mie scatterers, circular polarization has been suggested. There are a ways in which the polarization state of the input light affects imaging performance. It should however be remembered that only in active imaging schemes, we can choose the polarization state. Many applications use passive imaging schemes, in which case, the above review will not be able to help predict the imaging performance [74].

3.3 Common defects of the polarization element.

Here we list some common defects found in real polarization elements:

1. The absorption of polarizer and wave plates can be slightly different by coated values.
2. Retarders have the incorrect retardance. Thus, there will be some deviation from a quarter-wave or a half-wave of retardance, for example, because of fabrication errors or a change in wavelength.
3. Retarders usually have some diattenuation because of differences in absorption coefficients (dichroism) and due to different transmission and reflection coefficients at the interfaces. For example, birefringent retarders have diattenuation due to the difference of the Fresnel coefficients at normal incidence for the two eigen polarizations since $n_1 \neq n_2$. This can be reduced by antireflection coatings.
4. Polarizer usually has some retardance, there is a difference in optical path length between the transmitted (principal) eigen polarization and the small amount of the extinguished (secondary) eigen polarization. For example, sheet polarizer and wire-

grid polarizer show substantial retardance when the secondary state is not completely extinguished.

5. The polarization properties vary with angle of incidence, for example, Glan-Thompson polarizer polarizes over only a 4^0 field of view. Birefringent retarders commonly show a quadratic variation of retardance with angle of incidence which increases along one axis and decreases along the orthogonal axis [75]. For polarizing beam-splitter cubes , the axis of linear polarization rotates for incident light out of its normal plane (the plane defined by the face normal and the beam-splitting interface normal) .
6. The polarization properties vary with wavelength, for example, for simple retarders made from a single birefringent plate, the retardance varies approximately linearly with wavelength.
7. For polarizer, the accepted state and the transmitted state can be different. Consider a polarizing device formed from a linear polarizer oriented at 0^0 followed by a linear polarizer oriented at 0^0. Incident light linearly polarized at 0^0 has the highest transmittance for all possible polarization states and is the accepted state. The corresponding exiting beam is linearly polarized at 0^0, which is the only state exiting the device. In this example, the transmitted state is also an eigen polarization. This rotation between the accepted and transmitted states of a polarizer frequently occurs, for example, when the crystal axes are misaligned in a birefringent polarizing prism assembly such as a Glan-Thompson polarizer.
8. A nominally linear element may be slightly elliptical (have elliptical eigen polarizations). For example, a quartz linear retarder with the crystal axis misaligned becomes an elliptical retarder. Similarly a circular element may be slightly elliptical. For example, an (inhomogeneous) circular polarizer formed from a linear polarizer followed by a quarter-wave linear retarder at 45^0 becomes an elliptical polarizer as the retarder's fast axis is rotated.
9. The eigen polarizations of the polarization element may not be orthogonal, a polarizer may transmit linearly polarized light at 0^0 without change of polarization while extinguishing linearly polarized light oriented at 45^0. Such a polarization element is referred to as inhomogeneous. Sequences of polarization elements, such

as optical isolator assemblies, often are inhomogeneous. A polarization element may depolarize, coupling polarized light into un-polarized light. A polarizer or retarder with a small amount of depolarization, when illuminated by a completely polarized beam, will have a small amount of un-polarized light in the transmitted beam. Such a transmitted beam can no longer be extinguished by an ideal polarizer. Depolarization results from fabrication errors such as surface roughness, bulk scattering, random strains and dislocations, and thin-film microstructure [76].

Chapter 4

STOKES VECTOR MODELING OF TURBID MEDIUM AND BIOLOGICAL TISSUES

4.1 Polarimetric system for spatially resolved Stokes vector imaging of biological turbid samples.

The biological tissues exhibit their distinct optical characteristics, and their point-to-point compositional variation could either be determined by the optical parameters or reconstruction of the transmitted images. The image of the turbid sample is reconstructed by polarimetric system and shows point-to-point variation for differentiation in the medium. A procedure for making spatially resolved, the Stokes vector images map of polarized light is described. The imaging system consists of a He-Ne laser, linear and circular polarizer and a charge coupled device (CCD) camera. A series of output Stokes images are captured and the polarization maps are computed and displayed. By these procedures the structural variation in healthy and diseased tissues through change in optical birefringence can be determined and their relevance to early detection of tumor.

In this section, we presented our detailed, quantitative investigation of Stokes vector images by means of polarized light and discussed the implications of our findings for clinical applications. The output optical images provide all the polarimetric properties of the sample i.e. diattenuation, dichroism, retardance, birefringence and depolarization capability simultaneously. These quantities could be of major importance for studying pathologies that involve a change of structure. Laser radiation possesses nearly single frequency, high degree

of temporal and spatial coherence, enormous intensity and highly plane polarized characteristics. Due to low absorption, the penetration of light within the 'therapeutic window' (600–1300 nm) is more, which also leads to high scattering from the surface after deep penetration [76]. The spatial distribution of the scattered and transmitted components related to medium birefrengent contains information on the metabolic, physiologic or possibly structural status of tissues [77-78]. Mc-Gary et al. show how to separate subsurface from surface scatter using crossed polarization images [79]. Demos and Alfano report an optical polarization technique utilizing temporally resolved, crossed polarization images in a biomedical imaging application [80].

We discussed the Stokes formalism in detail and extensively used these vectors for sample characterization using linear polarizer and a circular polarizer as a polarization generating optics for sample. The imaging capability of our instrument is demonstrated for all the Stokes polarization vectors. We measured the depolarization of the sample at different polarization states and computed its diattenuation, polarization, and retardance as a function of wavelength [81].

4.1.1 Experimental results

The measurement system can be tested by placing the linear polarizer and the quarter wave plates without sample. Rotating the analyzer from 0^0 to 360^0 verifies measurement techniques and computational algorithms. The value of S_0 is always 1 for the normalized Stokes vector and we have not considered it for imaging as it describes only the illuminating light properties. The resultant images of Fig.4.1 show the accuracy of the measurements to be within 0.1 of the actual values. Spatially resolved Stokes vector (S_1, S_2, S_3) measurements are shown by forming the image of the output surface of the sample at the CCD camera and can clearly seen the spatial distribution of the medium induced, crossed polarization. We have used two types of samples, first 50% diluted soybean oil representing normal tissues, and other is pure for malignant tissue representation. The calculated, spatially resolved Stokes vector images for the sample test pattern are shown in Figs.4.2 and 4.3. These images clearly show polarization variation and regions that have undergone a change of polarization for both the materials.

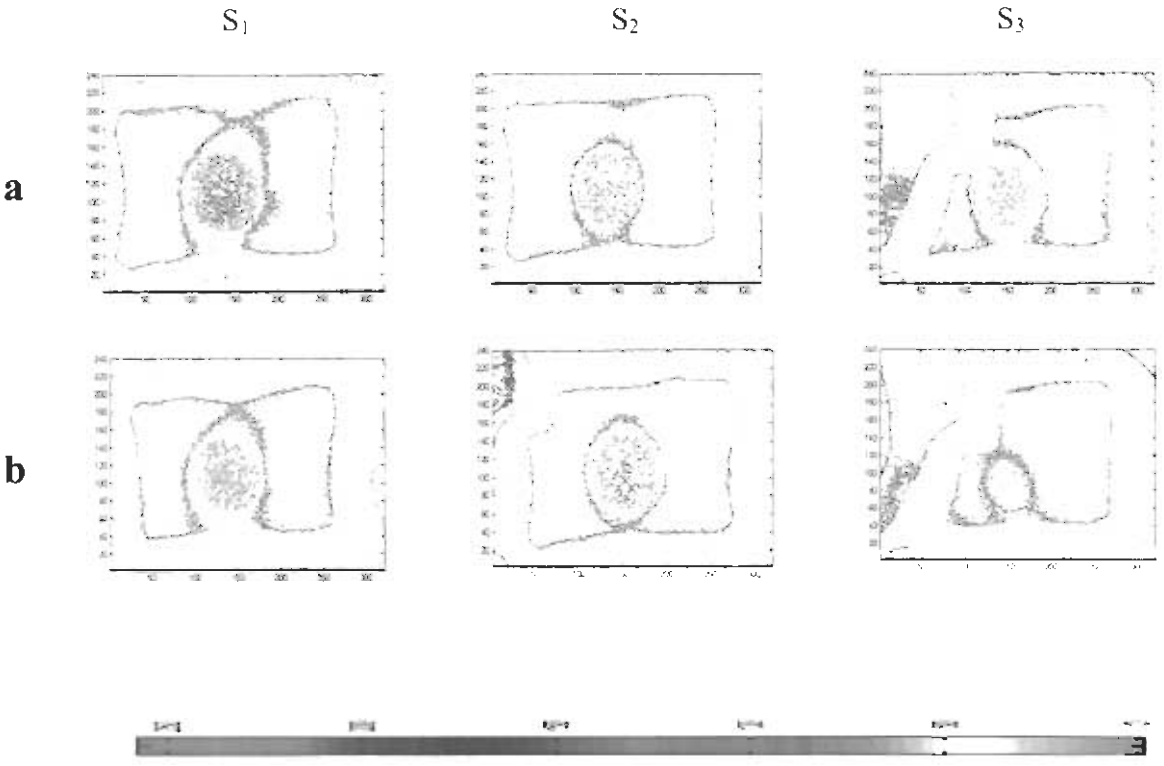

Figure 4.1 The direct transmitted intensity for all the Stokes vectors, where S_1, S_2, S_3 are shown, S_1 for horizontally polarized light, S_2 for $\pm 45^0$ polarized incident light and S_3 the right circular polarized light. (a) the 50% diluted solution (soybean oil) representing normal tissues. (b) the Stokes vector images of pure intralipid solution for malignant tissue representation.

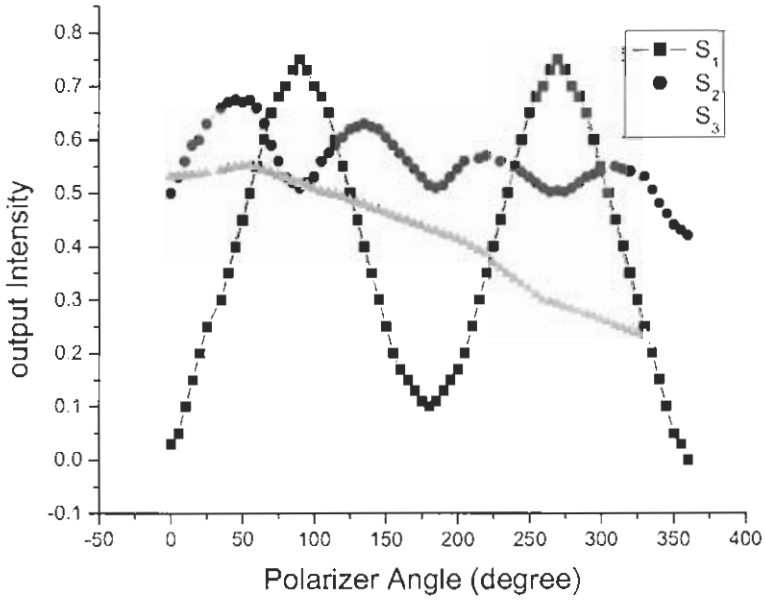

Figure 4.2 The Stokes polarization vector (S_1, S_2, S_3) for transluminated intensity across the normal tissue like turbid medium.

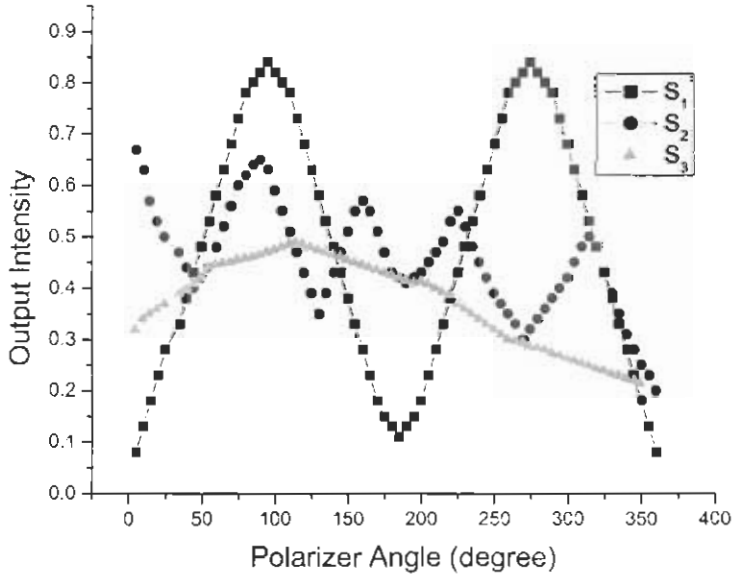

Figure 4.3 The Stokes polarization vector (S_1, S_2, S_3) for transluminated intensity across the malignant tissue like turbid medium.

In Fig.4.2 we have taken the Stokes vector S_1 having fixed polarizer at zero degree and rotating analyzer through 0^0 to 360^0 without quarter wave plates. For S_2 the polarizer is fixed at $\pm 45^0$ and analyzer is again rotated through 0^0 to 360^0 without quarter wave-plate. For the imaging S_3 the polarizer is fixed at $+ 45^0$, the quarter wave plate at its fast axis and analyzer is rotated through 0^0 to 360^0. The Stokes polarization vectors of Fig. 4.2 & 4.3 describe the different behavior for both types of samples. In Fig.4.2 S_1 goes from minimum to maximum intensity up to 90^0 change in polarization and repeat cycle for 0^0 to 360^0. The output intensity in Fig.4.3 for S_1 decreased up to 10% for malignant one, as to dominant scattering in dense medium. The Stokes vector $S_{2\ decreases}$ with variation in its polarization and present different behavior for both the mediums, S_3 is taken through circular birefringence and depolarizes rapidly for dense medium. So the linear polarization preservation is dominant compared to circular polarization. One can clearly differentiate the changing of birefringence for polarized input illumination for characterization of material under investigation.

The present Stokes vector polarimetric system consists of laser source and detection system separated by a fixed distance and the phantom is placed at the centre. This separation decreases with change in position of the scanning system as this is moved towards the sample. The incidence of light on the phantom is through the light source and the trans-illuminated component is received after a fixed separation. Due to this increase in source detector separation, the contribution due to scattering at the detector is decreased. The Stokes vector polarimetric system makes it possible not only to receive the straight propagating photons but also the less scattered. The transmitted data is collected for a small duration and finally these are averaged over 10 observations. This procedure further averages out any variation in the output signals of detector. The transillumination reconstruction procedure has greater detection efficiency compared to that of reflection one. Further processing of the Stokes vector polarimetric images can helps in viewing the various details within the sample under investigation. The steady-state, spatially resolved, diffuse transmitted profile is characteristic of a sample structure. By analyzing this profile, one can get the structural and functional details of the turbid medium across the penetration depth of the photons. The influence of any optical in-homogeneity (structural or rapid metabolic changes) in the sample could easily be detected by this technique.

Determination of the optical parameters is an integral part of tissue characterization. Optical parameters, which depend on the variation in a sample composition, are determined by the best-fit of experimental and theoretical curves. These parameters further depend on the measurement techniques and conditions, sample preparations and accuracy used during experimental procedures. The Stokes polarization vectors as measured by the present procedure are in agreement with literature [65]. Clinically, if the tumor is at a fairly advanced stage, the transmitted image reconstructed by this procedure can diagnose it. The resolution of the images obtained for a sample can further be improved by changing the scale, to provide details of pathological changes in the medium.

4.1.2 Conclusion

In conclusion, the principal motive behind the development of optical Stokes vector polarimetry, which is cost-effective compared to time-resolved and frequency-domain techniques, is to provide a safe and effective method of detecting and specifying diseases in the soft-tissue structures. The applications of Stokes vector polarimetric system to tissue-phantoms and biological tissues show that the present technique could be employed to detect structural changes. This technique is sensitive to detect changes in absorption coefficient and other properties of the particles of the medium. Due to its simplicity and versatility, this may prove to be an ideal system for structural analysis of turbid sample and soft tissues. Optical parameters quantify the medium and tissue changes, and imaging could further provide data on variability of tissue composition below the skin over an entire organ.

4.2 Stokes polarimetry for the characterization of bio-materials using liquid crystal variable retarders

We demonstrate significant differences in the propagation of polarized light through biological tissue phantom. The Stokes vectors along with degree of linearly and circularly polarized light were measured with stokes polarimetry techniques. The measurements were performed on dense and diluted tissue phantoms, consisted on soybean oil intralipid. Liquid crystal variable retarder (LCVR) Stokes polarimeter is used for either rotating the major axis of elliptically polarized light or for converting an input linearly polarized beam into an arbitrary elliptically polarized beam. This system makes possible a direct measurement of a component of the Stokes vector with phase change detection of polarization modulation for polarimetric measurements of turbid media in small interval of time i.e., less than 20 second. We also describe that polarized light is maintained differently in dense versus diluted sample. The results indicate that, for dense suspensions where independent scattering is assumed, the Stokes parameters and degrees of linear and circular polarization decrease, compared for dilute suspensions, where the degree of polarization begins to increase. The preferential propagation of linear over circular polarization states in diluted and dense suspensions is similar to results seen in biological tissue.

4.2.1 Stokes vectors formulism

The Stokes vector provides all the necessary information related to the polarization state of the light beam. Stokes polarimeter provide high sensitivity and speed for polarization modulation experiments involving Stokes polarimetry, magneto-optical Kerr effect, optical rotation, ellipsometry, linear dichroism, and circular dichroism. Polarization is the state or behavior of the transverse electric field of a light wave. Since the electric component of light is measurably affected by interaction of light with matter and energy, the polarization characteristics of light can provide diagnostic information for a broad range of biomedical and material characterization applications.

In many turbid media such as tissue, scattering structures have a large variance in size and are oriented in a complex and sometimes apparently random manner. Because each scattering event can modify the incident polarization state differently, the scrambling effect

of single scattering events accumulates, until finally the polarization state is completely random i.e., uncorrelated with the incident polarization state. A detailed description of the depolarization effect of polarized light in heterogeneous media discussed briefly in the hand book of optics by R. A. Chipman [86]. Materials interact with incident light by scattering or absorbing light energy. For some materials, when birefringence effects are present or when multiple scattering occurs, the polarization of the scattered light is altered and may be used to detect processes of interest. Demos and Alfano report an optical polarization technique utilizing temporally resolved, crossed polarization images in a biomedical imaging application.

The electric field of a plane wave can be described as the vector sum of two orthogonal components, typically horizontal and vertical components (E_x, E_y). The two components are characterized by their amplitudes and the relative phase between them. When viewed along its direction of propagation, the tip of the electric field vector of a fully polarized wave traces out a regular pattern. In its most general form, the pattern is an ellipse, as shown in Fig. 4.4.

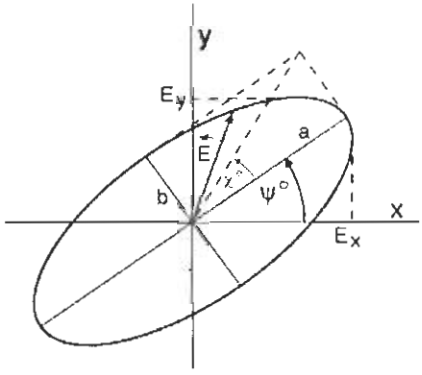

Figure 4.4 Polarization ellipse showing the orientation angle ψ and ellipticity χ, which are a function of the semi-major and semi-minor axes, a and b [86].

For a fully polarized wave, the ellipticity χ is defined as the arc tangent of the ratio of the polarization ellipse's minor and major axes (b and a in Fig. 4.4). If the ellipticity is zero, the

wave is linearly polarized. If the ellipticity is $\pm 45^0$ to the wave-plate, the wave is circularly polarized. For ellipticities between zero and 45 degrees, the wave is elliptically polarized. Fig.4.5 gives Stokes vector representation in term of Poincare sphere. The x-axis poles are the linear polarization states of 0 and 90^0. The y-axis poles are the linear polarization states of 45^0 and -45^0. The z-axis poles are the polarization states of left circular and right circular.

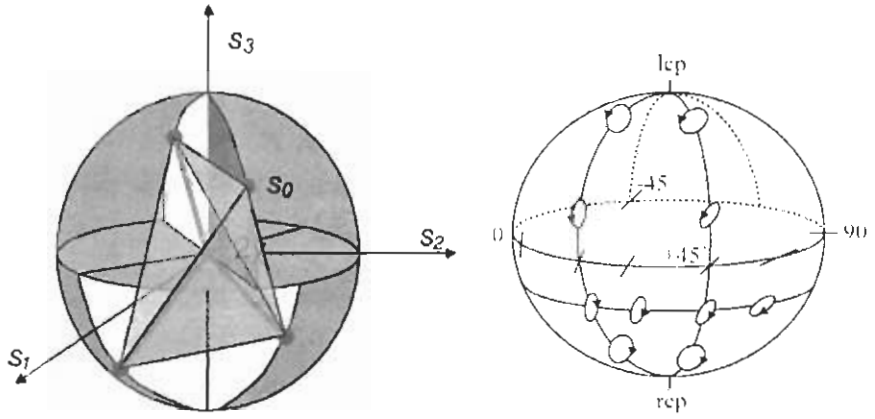

Figure 4.5 Stokes vectors representation of polarized light on Poincare sphere, (a) Optimal locations for measuring the polarization states are when the diattenuation vectors inscribe a regular tetrahedron inside the Poincare sphere. (b) Representation of linear (0^0, 90^0, $\pm 45^0$) along equatorial plane, circular (right and left) on poles and elliptical polarized around the sphere [83].

There are several parameters that frequently occur as alternatives to describing the state of polarization (SOP) of a light wave by a Stokes vector. These include the degree of polarization (DOP), degree of linear polarization (DOLP), and degree of circular polarization (DOCP). They relate to the Stokes vector as

$$DOP = \frac{\sqrt{S_1^{\,2} + S_2^{\,2} + S_3^{\,2}}}{S_0},\ DOLP = \frac{\sqrt{S_1^{\,2} + S_2^{\,2}}}{S_0},\ DOCP = \frac{S_3}{S_0} \qquad (113)$$

Polarization is often rendered as an ellipse, indicative of the precession of the electric field in a plane as a light wave passes normally through the plane. The ellipticity ε is a measure of the linearity or circularity, an ellipticity of zero indicates linearly polarized light and an ellipticity of 1 indicates circularly polarized light. The ellipticity of a polarization ellipse relates to the Stokes components as:

$$\varepsilon = \frac{S_3}{1+\sqrt{S_1^{\,2}+S_2^{\,2}}} \tag{114}$$

If the ellipticity is negative, the rotation of the tip of the electric vector around the ellipse is clockwise, looking in the direction of propagation (referred to as right-handed following the right hand rule). If the ellipticity is positive, the rotation of the electric vector is counter-clockwise, or left-handed.

The location on the poincare sphere (Fig.4.5) can be determined by the wave's ellipticity χ and orientation ψ. The radius of the sphere is the power S_0 of the wave, the latitude is 2χ and the longitude is 2ψ. Linear polarizations are found at the equator, with horizontal and vertical polarizations opposite each other. Left-hand circular ($\chi > 0$) and right-hand circular ($\chi < 0$) lie on the north and south poles respectively. All other points on the sphere represent elliptical polarizations of various ellipticities and orientations. Points on the sphere that are directly opposite one another represent polarizations those are orthogonal, and are referred to as cross polarizations. Depolarization is the reduction of the degree of polarization of light. In the optical calculus depolarization can be pictured as a coupling of polarized into un-polarized light, where polarized light is incident and the exiting Stokes vector can be mathematically separated into a fully polarized and an un-polarized Stokes vector. Practically, degree of polarization is a measure of the randomness of polarization in a light beam, a property characterized by how much of this beam may be blocked by a medium.

The liquid crystal veriable retarders (LCVR's) consist of a material that changes birefringence in the presence of an electric field. Kerr cells, Pockels cells, and liquid crystal cells are all examples of variable retarders. Kerr cells generally use any of several specific organic compounds that change birefringence when a high voltage (~1 kV) is applied across

the material [84]. Pockels cell consist of a solid crystal material that undergoes a change in birefringence upon application of high voltage (~1 kV). LCVR's are commonly used in low-voltage (~10V) applications. A liquid crystal cell with no voltage applied acts as a retarder, with a retardance proportional to the liquid crystal thickness and LC material birefringence. Application of a voltage causes the liquid crystal molecules to align to the electric field (parallel to the direction of light propagation), thereby reducing (or nearly nullifying with sufficient voltage) the birefringence of the cell. Layer in which the molecules are aligned parallel to each other. The extraordinary index of refraction decreases as voltage is applied to the pixel while the ordinary index of refraction remains constant. Therefore the device acts as an electrically controllable wave plate with a voltage-dependent phase.

This paper investigates the way that a general depolarizing Stokes polarimeter affects degree of polarization DOP data, thus providing new methods for classifying Stokes polarimeter and their behaviors. The DOP of medium are explored by examining separately the changes imparted to the output by the diattenuation, retardance, polarizance, and depolarization properties encoded in a Stokes polarimeter.

4.2.2 Measuring the Stokes vectors

The S_1-component of the Stokes vector can be measured with a single LCVR. This component is defined as the intensity difference between the horizontal and vertical linearly-polarized components of the input beam. An LCVR is placed with its optic axis at 45° to a beam splitting polarizer as shown in Fig.4.6. The LCVR is switched between 0 and half wave. In the zero-wave state the polarization state of the input beam is unchanged. In the half-wave state the LCVR rotates the vertical component into the horizontal direction and vice versa. The S_1-component has been normalized to the total intensity. With this normalization the I-component is always equal to unity. The first term is the S_1-parameter measured using the detector in the transmitted arm (I_T) of the polarizer and the second term results from the detector in the reflected arm (I_R). The accuracy can be improved by adding a clean-up polarizer in the reflected arm.

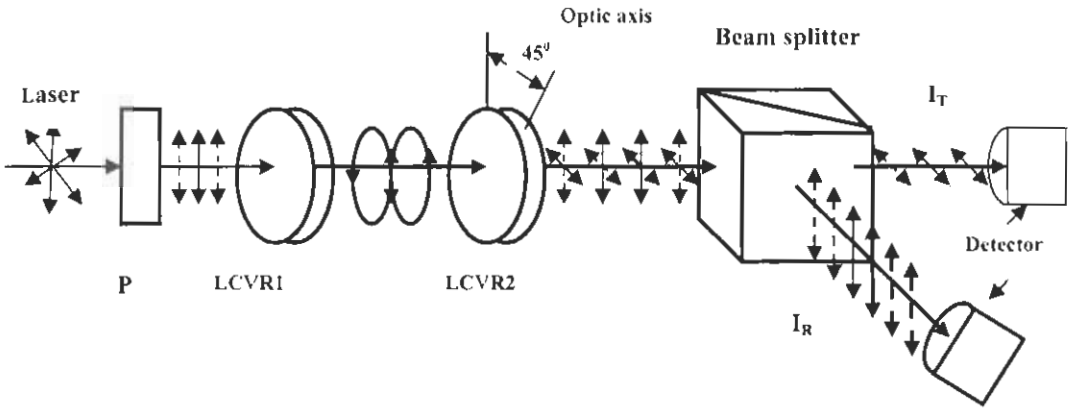

Figure 4.6 the experimental setup for Stokes liquid crystal variable retarder(LCVR) polarimeter. Where P is polarizer, I_T and I_R are the transmitted and reflected polarization field vectors through polarizing beam splitter.

The S_3-component describes the circular polarization of the incoming light beam. In Fig. 4.6, we resolved the input beam into two orthogonal linear polarization components in the horizontal and vertical directions. The S_2-component of the Stokes vector requires two LCVRs for its measurement. We imagine the input light to be decomposed into orthogonal linear polarizations oriented along directions ±45° to the vertical. This transforms the input linear components into right- and left-hand circular polarized components.

A complete Stokes polarimeter requires two LCVR. During the measurement of the S_1 and S_3 components the first LCVR is held to zero retardance. It is then tuned to a quarter wave of retardance for the measurement of the S_2 component. It should be noted that, while the Stokes vector is valid for laser light, the wavelength sensitivity of the LCVR limits the bandwidth of light that can accurately be tested.

4.2.3 Material and methods

The experiment proceeded as follows: polarized, monochromatic (633 nm) light was directed through a sample to a liquid crystal polarimeter (LCPM-3000 by Meadowlark Optics, Inc.) to measure the Stokes vectors and SOP of the polarized beam as shown in Fig. 4.6. In this way, the vertical, horizontal, and combined intensity components of the SOP

were measured with the photo-detector. The liquid crystal polarimeter was calibrated and a background reading was taken according to the manufacturer's instructions. A background measurement was acquired with the photo-detector and subtracted from each reading.

The linear SOP was measured as Stokes components with the polarimeter, and the vertical and horizontal, and combined intensity components of the linear SOP were measured with the photo-detector. The scattering medium (soybean oil) is placed in a cylindrical thin-walled quartz cell (3x2 cm) with flat parallel walls [85]. The Stokes vectors and degree of polarization for each sample was measured as a function of scatterer concentration. Each point is an average of ten measurements. Soybean oil is an inexpensive, non-toxic liquid with dielectric properties similar to very low-water-content fatty tissue. For this reason, it is used as the tissue phantom.

4.2.4 Experimental results

A He-Ne laser light was used to determine the Stokes parameters of light transmitted from a sample. In the present analysis, we demonstrate that coherent detection of the laser images in two orthogonal polarization states allows determination of all four Stokes parameters simultaneously. In this study we recovered the information of turbid sample by selectively detecting a transmitted component of the scattered photon flux that has its initial polarization state preserved. These photons transmitted through or re-emitted from a multiple scattering medium by using relatively inexpensive Stokes vectors polarimeter provides the basis for several potential applications. Consider polarized light source incident on a birefrengent sample, the polarization state of transmitted light from sample undergone a phase retardation and is orthogonal to the incident polarization state.

The degree of polarization measured in each sample is shown in Fig.4.7. For dilute concentrations, the degrees of both linear and circular polarization decrease. Linearly polarized light is depolarized more quickly than circularly polarized light, as reported earlier [86]. Above a critical concentration of scatterers, however, the degrees of linear and circular polarization begin to increase with increasing scatterer concentration [87]. However, a collection of densely packed, dependently scattering medium attenuates less light than is predicted by results for dilute solutions. Thus, as shown in Table 4.1, the Stokes vectors in dense solutions are less than that in dilute solutions.

For diluted medium, circularly polarized light is depolarized more quickly than linearly polarized light. As the concentration increases (i.e., Mie scattering), linearly polarized light is depolarized more quickly than circularly polarized light. In the transition region between Rayleigh and Mie scattering, both polarization states are depolarized similarly. For dense sample, we see that, similarly to the intensity attenuation results shown in Table 4.1, polarized light propagation through a dense medium of (Mie) scatterer is similar to polarized light propagation through a diluted medium of smaller (Rayleigh) scatterer.

Material	S_0	S_1	S_2	S_3	DOP	DOLP	DOCP	Ellipti city	Axis of ellipse
Air	1.061	-0.92	-0.03	0.001	0.926	0.926	0.001	0.001	85.20
Diluted	1.235	-0.89	-0.01	0.024	0.89	0.89	0.024	0.012	85.29
Dense	1.137	-0.87	-0.01	0.012	0.874	0.874	0.012	0.006	87.65

Table 4.1 Results of Stokes LCVR polarimeter data showing Stokes vectors and degree of polarization for air and both diluted and dense tissue phantom.

Circularly polarized light, either present as right or left circular, is characterized by $\lambda/4$ phase difference between the equal-intensity orthogonal E-field components. The interaction of circularly polarized light with tissue causes phase differences to be altered, thus, the ellipticity of the propagating and re-emitted light is changed according to the polarization-sensitive optical properties of the sample. The DOLP (Fig. 4.7) indicate regions of the sample that have converted the incident linear polarization (LCP) state to a more linear form. The DOCP data indicate regions of the sample that re-emit light retaining a fraction of the linear polarized state. One should note that degree of total polarization

would indicate regions of the sample that re-emit any type of polarized light (both linear and circular).

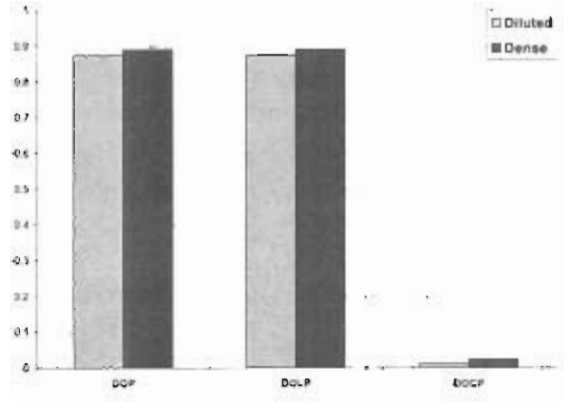

Figure 4.7 The difference in the degree of polarization by Stokes output polarimetric data for both dense and diluted sample. Linearly polarized light have higher value compared to circular.

The DOLP data (Fig. 4.7) indicate that the birefringence and multiple-scattering events within the turbid medium changes incident circularly polarized light to be converted to elliptically polarized light, i.e., where the polarization state contained more linear components. Linear birefringence was a major contributing source to these phase changes because of the natural difference in refractive indices along the orthogonal axes of the samples. The data for degree of polarization is consistent with time in both the medium Fig 4.8(a) and 4.8(b)

In short, the conversion of one pure state of polarization, either linear or circular, into elliptically polarized light (i.e., towards a more circular form or towards a more linear form, respectively), is analogous to optical effects created by classical optical components. For example, a polarizer-retarder or polarimeter can be used to transform linearly polarized light to circularly polarized light or circularly polarized light to linearly polarized light by allowing the light to pass through the optics. In our studies, we have observed similar

effects, though not with the exact phase-shifts caused by an engineered polarimetric system. Further, the experiments are performed in transmission mode rather than in reflection mode.

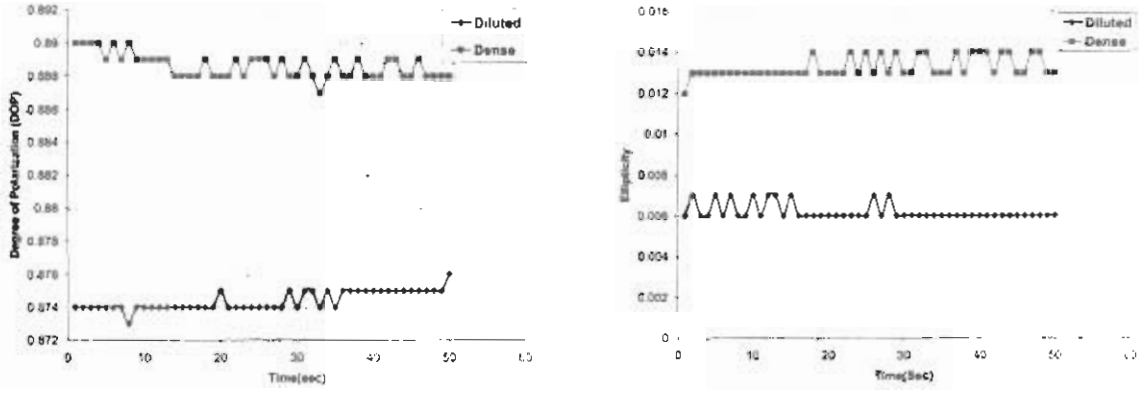

Figure 4.8 The error analysis for the output Stokes polarimetric measured data. (a) The consistency in degree of polarization. (b) The ellipticity measurement of turbid medium.

An interesting relation was found between the maximal and minimal polarization states with respect to that of the incoming wave, i.e., these points constitute a points on the Poincare sphere and that they form a Stokes vector signature on the circle. Therefore, in Fig.4.9, if the polarization of the incoming wave is given, these maximal and minimal polarization points can be determined graphically on the Poincare sphere instantaneously. Right and left circular polarization are represented on opposite ends of the sphere [88], As right or left circularly polarized light undergoes scattering events, its representation on the sphere moves away from the right and left ends of the sphere, respectively, and goes towards the middle of the sphere. Navigating away from either one of these extreme points on the Poincare′ sphere (Fig. 4.9) indicates polarization states that are elliptical and have the same respective handedness, but may have different ellipticities and azimuths. Because the tissue was birefrengent, the azimuth parameter had a greater influence than ellipticity on the polarization state of the re-emitted light. Depending on whether phase was added or subtracted into the left- or right-handed propagating beam, the azimuth of the ellipticity was different. In summary, the DOLP data in Fig 4.7, showed that the conversion of incident

circularly polarized light into a more linear form appears to show great sensitivity to a number of material and optical geometrical factors of the phantom, the handedness of elliptically polarized light, the azimuth of elliptically polarized light with respect to the sample orientation angle.

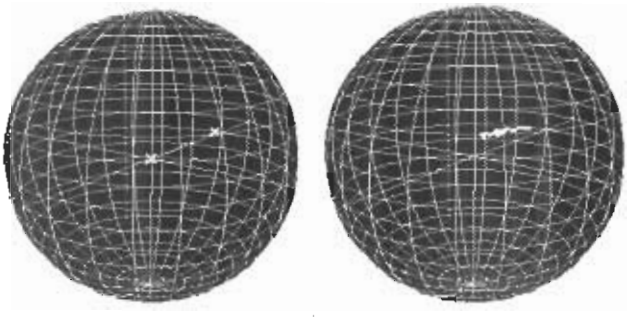

Figure 4.9 The pincare sphare for linear and circular polarization representation of diluted and dense tissue phantom. The output linear polarized light is marked as points for small interval of time (20 sec).

The Stokes additively property is that, the detected Stokes parameters are a sum of beams coming from the medium (Fig 4.10). Mathematically, un-polarized light has no influence on the detected Stokes parameters as the Stokes representation is $[S_0, S_1, S_2, S_3]$.

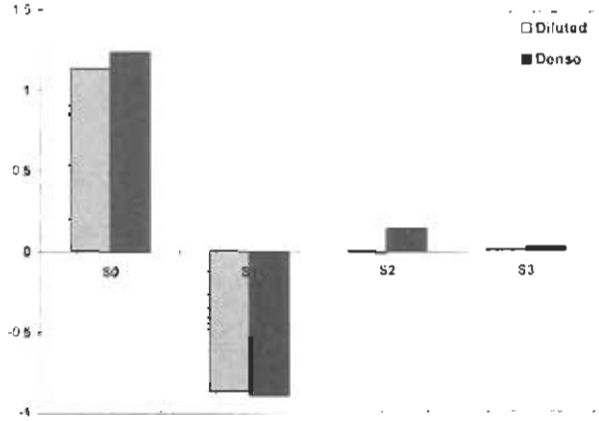

Figure 4.10 The four Stokes vectors measured by polarimeter for diluted and dense Intralipid sample, where S_0 and S_1 have major portion of incoming light compared to S_2 and S_3.

The Stokes image the S_0 shows total intensity of the illuminating beam and provides less information compared to others. The image S_1 and S_2 describe linear polarization and play significant role for material characterization being preserved for longer distance in dense medium. The transmitted intensity maintains the original polarization states at different points in the total intensity pattern and statistically different from each other because the phase between the orthogonal intensity patterns vary from point to point. The Stokes vector for an area including more than one such point is then determined by summing the Stokes vectors of all of the points in the area. The Stokes vectors for diluted phantom are less then the dense one. The S_1-component is –ve in both the cases, which means the output is vertically polarized. Therefore, the Stokes parameters of the mostly un-polarized light from the sample added to the somewhat polarized light from the turbid medium resulted in a detected signal that was elliptical with moderate DOCP. For Fig 4.7, the presence of degree of linear polarization means that parameter S_1 is nonzero. Of course, to obtain a more complete understanding of the impact of the increasing thickness of the turbid medium on the DOCP and DOLP data, one would need a measurement of the polarization properties of light incident on the sample, an understanding of the effect on light of various ellipticities, and a measurement of the polarization properties of the light re-emitted from a free medium

as a function of the thickness of the turbid medium. Finally, in dense medium the scattering effects of the turbid medium became dominant.

In summary, the experimental data show that degree of polarization measurements are sensitive to changes due to tissue morphology, geometry, and orientation and thus can provide difference between both the samples. Although the application of this technique so far has been limited to investigating ex-vivo tissue and phantoms in a bench top setting, we believe that the underlying imaging technique shows great promise for medical imaging in the clinic. Pathological or even cancerous tissues (dense) are known to have changes within the tissue matrix causing those regions to differ in cellular makeup from normal tissue (diluted). One advantage to using this Stokes polarimetry imaging technique is that it provides the ability to scan large regions of tissue efficiently (i.e., during a surgical procedure) while providing important tissue structural information not seen with conventional (un-polarized) optical imaging techniques. The suitability of creating DOLP and DOCP data should be disease/tissue specific, and can be parameterized as further research is performed. Another distinguishing feature of this imaging technique is that the discrimination of tissue structures is provided by the polarization properties of re-emitted light rather than by the color appearance or texture of the tissue, this provides an added dimension to viewing differences. In comparison to other imaging techniques, Stokes polarimetry imaging is unique. Optical coherence tomography (OCT) provides excellent microscopic level detail, however scanning large areas (i.e., greater than 10 cm^2) is rather inefficient. Furthermore, while both MRI and CT provide excellent anatomical information, they are inadequate in detecting differences within tissue matrix (especially for small lesions) and difficult to adapt to immediate identification and excision procedures.

4.2.5 Conclusions

We have demonstrated high-precision, low-noise polarimetric measurements in turbid media using LCVR Stokes polarimetric detection. The technique allows the polarized intensity measurements necessary to determine Stokes parameters in small interval of time. The surviving polarization fractions in turbid suspensions have been measured in the forward direction and are in reasonable agreement with literature. The measurements of optical rotation in turbid suspensions demonstrate the possibility of determining polarization change

in a highly scattering and depolarizing medium made of Intralipid. Measurements of optical rotation that is due to turbid scattering phantom solutions, is significant in dense and slightly smaller values in clear solutions [89].

In this research we used a phase-only LCVR Stokes polarimeter to demonstrate the difference between normal and malignant samples with polarization encoding of an incident beam. In our technique, each pixel of the LCVR can act as a wave plate having a different retardation. The LCVR Stokes polarimeter provides sufficient information for characterization of biomaterials in term of polarized Stokes vectors and degree of polarization changes in turbid medium.

Chapter 5

MUELLER MATRIX POLARIMETRY FOR OPTICAL MATERIALS CHARACTRIZATION

5.1 Optical imaging of turbid medium through scattering of polarized light for diagnostic and treatment of malignant diseases

The optical material can be characterized through their polarimetric properties. It is demonstrated that the degree of polarization of the scattered light is sensitive to the optical properties of turbid medium. Furthermore, it is shown that the polarization memory of polarized light enables scattering medium to be probed whereas linearly polarized light is more sensitive to surface of the medium. The imaging resolution in turbid medium is severely degraded by polarized light scattering. In this work the polystyrene micro sphere sample of 1.5μm diameter and semi-skimmed milk is analyzed through 632.8 nm linear polarized incident light for Ralyeigh and Mie type scattering. Through this study it will be possible to design quick and non destructive method for the identification of certain small object in turbid medium.

5.1.1 Experimental results

The polystyrene microsphere sample is illuminated through 632.8 nm linear polarized light in horizontal and vertical direction respectively. Fig. 5.1 shows scattering (S) and degree of polarization (D) for the polystyrene microsphere solutions. The experimental

observations are: At low scatterer concentrations output intensity is high as a significant amount of unscattered light is detected. Also less scattered light maintains its original polarization state. As the scatterer concentration increases, S increases and D decrease monotonically.

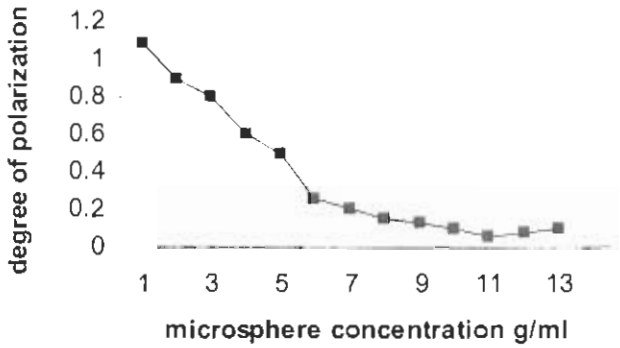

Figure 5.1 Parameters for microsphere solution. The degree of polarization, vs scattering concentration.

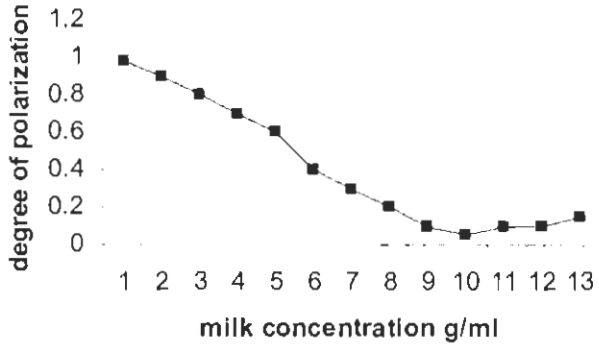

Figure 5.2 Parameters for semi -skimed milk solution. Degree of polarization and scattering concentration.

Fig. 5.1 and 5.2 shows degree of polarization for micro sphere and milk solutions. The trends are similar to those of the polystyrene micro sphere solutions except that the scattered light is completely depolarized for the range of scatterer concentration 7-9 ml, even when there is unscattered light detectable. Consider for example, typical detection system comprising a 1 mW input beam, a detector with a minimum detectable power of $1x10^{-10}$ W, and a 10-mm-thick container that contains a scattering solution. If one assume that un-scattered light can be separated from the scattering background, by using either a small aperture and pinhole or an electronic extraction method then Beer's law can be applied with $I_0 = 10^{-3}$ W. it yields a value of scattering coefficient $u_s = 1.6$ mm^{-1} at the limit of scattered light detection, which is independent of particle size. This means that the rate of depolarization of scattered light is dependent on the size of the particle. Fig.5.3 shows the scattering concentration for the micro sphere as scatterer concentrations increase for a solution of small particles. The solutions containing large particles maintain some degree of polarization even when there is no scattered light detectable, whereas the opposite is true for the solutions containing smaller particles.

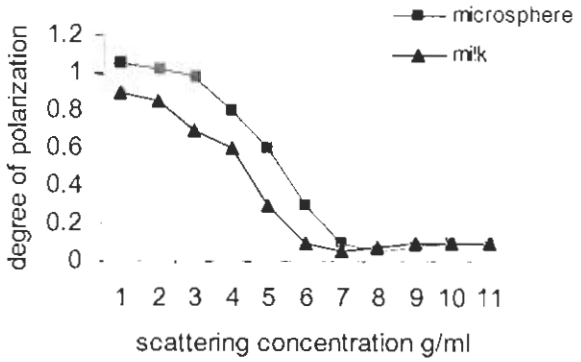

Figure 5.3 Compression of micro sphere and milk particles under linear polarized light illumination.

The value of the degree of polarization in Fig.5.3 is accurate approximation of the milk particles because the exact size or dielectric constant of the milk can not be determined. However, there is only a variation in the rate of depolarization for small quantity. Fig. 5.4

shows the degree of polarization of the detected light for different scatterer length. It can be seen that at low scatterer concentration linearly polarized light has a degree of polarization close to unity, which then decreases as the scatterer length increases.

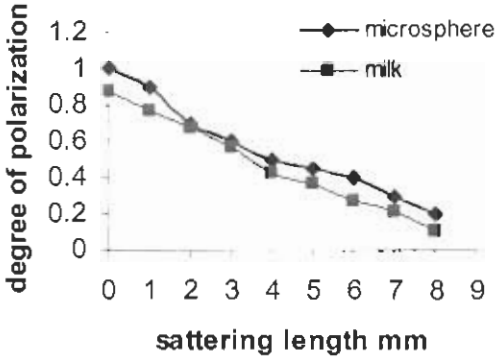

Figure 5.4 Degree of polarization with changing scattering length (mm).

At a high scatterer concentration there are a high proportion of photons that have been multiply scattered and return to the detector. These are generally depolarized and contribute equally to each polarization state, which results in a relatively low degree of polarization. As the concentration becomes weaker more depolarized light is transmitted by the sample and does not contribute to the detected signal. This causes an increase in the degree of polarization until the reflected light dominates and the degree of polarization is close to unity. At high scatterer concentrations the amount of polarization maintaining photons, dominate those detected on side, so the degree of polarization is positive. As there are more polarization maintaining photons than in linear the degree of polarization is higher. As the scatterer concentration decreases the amount of depolarized light transmitted through the sample increases and the degree of polarization initially increases. Decreasing the scatterer

concentration further demonstrates that polarization maintaining photons begin to be transmitted through the sample. The degree of polarization decreases when the sample side photons dominate. It is interesting to note that the light scattered is completely depolarized at a higher sample concentration, when the scattered and polarization maintaining photons cancel each other out. For linearly polarized light at high scatterer concentrations there is a small fraction of light detected that maintains its original polarization state. The degree of polarization is reduced as the amount of depolarized light increased.

5.1.2. Discussions

We have shown how polarization state can be used to discriminate the degree of scattering suffered by the light that emerges from a scattering medium. This may therefore be used to improve the imaging resolution. It is clear that when the medium has density of particles, all the detected light is both scattered and depolarized. At the other extreme there is a considerable amount of un-scattered light. The interesting region occurs for intermediate scattering concentrations in which different behavior was observed, depending on the particle size. For small particle sizes the scattered light is depolarized even when there is a small amount of unscattered light detectable. In this situation the light that emerges parallel to the incident polarization state will contain a mixture of scattered and unscattered light, where the light with polarization orthogonal to this direction will contain scattered light only. In this case the properties of the scattered light are similar regardless of polarization state so that subtraction of the two orthogonal components leaves the effect of the unscattered light only, which therefore dramatically improves the imaging resolution.

The successful operation of this technique requires some discussion. The fact that the imaging information carried by the scattered light at the two orthogonal polarizations is similar implies that on average the scattered light has suffered a large number of similar scattering events. On the other hand, for the technique to operate there must clearly be a measurable amount of un-scattered light detectable. Success, however hinges on the fact that the light is detected at the central pixels where a considerable degree of spatial filtering takes place. All the unscattered light is focused upon the central portion of the detector, whereas the scattered light is more or less uniformly distributed over the whole array. The proportion of unscattered light upon the detector is therefore considerably greater (by many order of

magnitude) for overall proportion that emerges from the medium. This very significant enhancement means that unscattered light may still be erected even though the average number of scattering events is large. The range over which this subtraction technique works is therefore dependent on two principal factors first the efficiency of the spatial filtering and second the particle size-the smaller the particle size the fewer scattering events are required to depolarize the emerging light and, therefore the technique will operate at lower scattering eoncentrations.

For larger particle sizes, such as those obtained with the micro sphere solution, a different situation prevails. Even when there is no measurable un-scattered light, the two orthogonal polarizations suffer different degrees of scattering. Therefore improved resolution may be obtained by extracting the light, it retains its original polarization state. We have examined the two effects of depolarization, un-scattered light attenuation and the possibility inproving the imaging resolution using these characteristics. The applicability of polarization to improve the imaging resolution has been discussed and emphasis has been placed on the most appropriate teehnique to be used with various particle sizes.

The results demonstrate that polarized light scattered from a scattering medium is sensitive to the state of input polarization and the optical properties and thickness of the medium, which indicate that as the number of scattering events decreases, simulating depth of decreasing thickness, the degree of polarization of the emerging light changes significantly. The Fig. 5.1 and 5.3 indicates that the polarization properties of the emerging light are also sensitive to the properties of the underlying medium. Larger differences are observed at low concentration as there is a higher probability of light being scattered from the second medium back to the detector. It is interesting to note that for smaller particles size the linear polarization is maintained for more scattering events. The linear polarization can be used to probe deeper in medium.

We are assisted in this problem by the fact that different polarization states maintain their polarization over different numbers of scattering events. Therefore a range of depths are probed by different polarization states, with linear probing nearer the surface and deepest. These photons are weighted in different ways by the distance they have propagated in either medium e.g. if the underlying layer has greater absorption than the upper layer then polarized light will be more heavily attenuated by this region. Plotting the degree of

polarization against polarization state will result in a curve that is weighted by different amounts depending on the thickness and optical properties of the medium. We are currently investigating whether the inversion is well conditioned by modeling the forward problem and obtaining a database of such curves and fitting to these to perform the inversion. Additional parameters can also be incorporated to improve performance such as the spatial distribution and additional wavelengths.

5.1.3 Conclusion

In conclusion, the polarization properties of light scattered from a scattering medium have been investigated. It has been shown that the degree of polarization is sensitive to the optical properties of the turbid medium and this offers a potential tool for characterizing the medium. The results demonstrate that polarized light scattered from a scattering medium is sensitive to the state of input polarization and the optical properties and thickness of the medium

5.2 Theoretical results for Mueller matrix polarimetry.

The measurements of the scattered polarized beam of laser radiation from turbid medium have been characterized through optics calculus. Stokes and Mueller parameters of polarized light are represented as a column matrices and optical turbid medium as 4x4 matrices. The tissue like turbid phantom system is considered homogeneous and scattering medium contains one kind of randomly distributed asymmetric particles. We used polarized light from He-Ne laser (λ=632.8 nm) focused on scattering medium. Different polarization components of backscattered light are obtained by varying the polarization state of incident laser light and the analyzer configuration. The calculation of the 16 element of the output Mueller matrix shows that theoretically only seven elements of backscattered light are independent and remaining nine can be calculated through symmetry relation. It also conformed through experiments. Matrix calculus concept for diffusely backscattered light fully characterized the turbid medium. The experimental and theoretical results are in good agreement

Results and discussion

5.2.1 Theoretical calculation of scattered Mueller matrices

For the theoretical calculation of scattered polarized light, all 16 element of effective scattered Mueller matrix calculation shows that only seven elements are independent. The remaining nine can be calculated through simple rotation or equality, due to axial symmetry of the system. The turbid medium illuminated with polarized laser light for the measurement of 16 Mueller matrix and state of polarization is used to make a linear transformation for measurement of the scatterer intensity. The arbitrary particles in turbid medium define the transformation applied to the amplitude of the incident wave and giving the amplitude of the backscattered wave. We assume homogeneous medium consist on cylindrical shaped particles turbid medium for our experiment.

Consider the general case in which the scattering medium contain one kind of randomly distributed asymmetric particles having scattering angle 'θ' and phase difference 'φ' in turbid medium, then the single scattering matrix is given as [90].

$$S = \begin{bmatrix} S_{11} & S_{12} & S_{13} & S_{14} \\ S_{21} & S_{22} & S_{23} & S_{24} \\ S_{31} & S_{32} & S_{33} & S_{34} \\ S_{41} & S_{24} & S_{34} & S_{44} \end{bmatrix} \tag{84}$$

The above single scattering matrix is effective backscattering Mueller matrix. This matrix is obtained by solving a radiative transfer equation with appropriate boundary conditions [91]. The Stokes vectors are calculated in detail in ref. [45], and concluded as:

$$S_{11}(\theta,\varphi) = S_{11}(\theta) \tag{85}$$

$$S_{12}(\theta,\varphi) = S_{12}(\theta)\cos 2\varphi + S_{13}(\theta)\sin 2\varphi \tag{87}$$

$$S_{13}(\theta,\varphi) = -S_{12}(\theta)\sin 2\varphi + S_{13}(\theta)\cos 2\varphi \tag{88}$$

$$S_{14}(\theta,\varphi) = S_{14}(\theta), S_{21}(\theta,\varphi) = S_{12}(\theta,\varphi) \tag{89}$$

$$S_{22}(\theta,\varphi) = \frac{S_{22}(\theta) - S_{33}(\theta)}{2} + \frac{S_{22}(\theta) + S_{33}(\theta)}{2}\cos 4\varphi + S_{23}(\theta)\sin 4\varphi \tag{90}$$

$$S_{23}(\theta,\varphi) = S_{23}(\theta)\cos 4\varphi - \frac{S_{22}(\theta) + S_{33}(\theta)}{2}\sin 4\varphi \tag{91}$$

$$S_{24}(\theta,\varphi) = S_{24}(\theta)\cos 2\varphi - S_{13}(\theta)\sin 2\varphi \tag{92}$$

$$S_{31}(\theta,\varphi) = -S_{13}(\theta), S_{32}(\theta,\varphi) = -S_{23}(\theta,\varphi) \tag{93}$$

$$S_{33}(\theta,\varphi) = -\frac{S_{22}(\theta) - S_{33}(\theta)}{2} + \frac{S_{22}(\theta) + S_{33}(\theta)}{2}\cos 4\varphi + S_{23}(\theta)\sin 4\varphi \tag{94}$$

$$S_{34}(\theta,\varphi) = S_{24}(\theta)\sin 2\varphi + S_{34}(\theta)\cos 2\varphi \tag{95}$$

$$S_{41}(\theta,\varphi) = S_{14}(\theta,\varphi) = S_{14}(\theta) \tag{96}$$

$$S_{42}(\theta,\varphi) = S_{24}(\theta,\varphi), S_{43}(\theta,\varphi) = -S_{34}(\theta,\varphi), S_{44}(\theta,\varphi) = S_{44}(\theta) \tag{97}$$

From this general form it follows that only seven independent elements are:

$S_{11}(\theta,\varphi), S_{12}(\theta,\varphi), S_{14}(\theta), S_{22}(\theta,\varphi), S_{23}(\theta,\varphi), S_{24}(\theta,\varphi), and S_{44}(\theta)$, and the other nine are:

$$S_{13}(\theta,\varphi) = S_{12}(\theta,\varphi + \tfrac{\pi}{4}), S_{21}(\theta,\varphi) = S_{12}(\theta,\varphi) \tag{98}$$

$$S_{31}(\theta,\varphi) = -S_{13}(\theta,\varphi) = S_{12}(\theta,\varphi - \tfrac{\pi}{4}) \tag{99}$$

$$S_{32}(\theta,\varphi) = -S_{23}(\theta,\varphi) = S_{23}(\theta,\varphi \pm \tfrac{\pi}{4}) \tag{100}$$

$$S_{33}(\theta,\varphi) = -S_{22}(\theta,\varphi - \tfrac{\pi}{4}) \tag{101}$$

$$S_{34}(\theta,\varphi) = S_{24}(\theta,\varphi - \tfrac{\pi}{4}) \tag{102}$$

$$S_{41}(\theta,\varphi) = S_{41}(\theta) = S_{14}(\theta), S_{42}(\theta,\varphi) = S_{24}(\theta,\varphi) \tag{103}$$

$$S_{43}(\theta,\varphi) = -S_{34}(\theta,\varphi) = S_{24}(\theta,\varphi + \tfrac{\pi}{4}) \tag{104}$$

The derived symmetry relations in Eq. 98 to104 and the general form of the reduced backscattering matrix of Eq. 85 hold, of course, if the assumptions made at the beginning of this section are satisfied, i.e., if the scattering medium contains one kind of randomly distributed asymmetrical particles, and homogeneous. It can be shown that Eq. 85 and 98 to 104 also hold when the medium that contains scattering particles is itself optically active because in that case, the effective scattering matrix S contains additional rotational matrices, which describe rotations that are due to optical activity. Finally, for the symmetry relation to hold, it is not necessary that the scattering medium fill the entire half-space; it is sufficient for it to have rotational symmetry around the initial laser beam, e.g., it can be a cylinder of finite size whose axis coincides with the direction of the initial laser beam.

The reduced backscattering matrix, Eq.85, can further simplify for the simplest, and important case of light scattering by homogeneous medium consist on spherical particles. In that case, the single-scattering Mueller matrix was calculated by solving Maxwell's equation with appropriate boundary conditions, Mie theory and it takes the relatively simple form [91].

$$\mathrm{S} = \begin{bmatrix} S_{11} & S_{12} & 0 & 0 \\ S_{21} & S_{22} & 0 & 0 \\ 0 & 0 & S_{33} & S_{34} \\ 0 & 0 & -S_{34} & S_{44} \end{bmatrix} \tag{105}$$

Substituting $S_{13}(\theta) = S_{14}(\theta), = S_{23}(\theta) = S_{24}(\theta) = S_{31}(\theta) = S_{34}(\theta) = S_{41}(\theta) = S_{42}(\theta) = 0$, in Eq. 85 to 97, the seven independent elements become:

$$S_{11}(\theta,\varphi) = S_{11}(\theta) \tag{106}$$

$$S_{12}(\theta,\varphi) = S_{12}(\theta)\cos 2\varphi \tag{107}$$

$$S_{14}(\theta,\varphi) = S_{14}(\theta) = 0 \tag{188}$$

$$S_{22}(\theta,\varphi)=\frac{S_{22}(\theta)-S_{33}(\theta)}{2}+\frac{S_{22}(\theta)+S_{33}(\theta)}{2}\cos 4\varphi \tag{109}$$

$$S_{23}(\theta,\varphi)=-\frac{S_{22}(\theta)+S_{33}(\theta)}{2}\sin 4\varphi \tag{110}$$

$$S_{24}(\theta,\varphi)=-S_{34}(\theta), S_{44}(\theta,\varphi)=S_{44}(\theta) \tag{111}$$

The other nine elements are obtained through symmetry relation Eqs. 98 to 104 or explicitly

$$S_{13}(\theta,\varphi)=S_{12}(\theta,\varphi+\tfrac{\pi}{4}), S_{21}(\theta,\varphi)=-S_{12}(\theta,\varphi)\sin 2\varphi \tag{112}$$

$$S_{21}(\theta,\varphi)=S_{12}(\theta,\varphi) \tag{113}$$

$$S_{31}(\theta,\varphi)=-S_{13}(\theta,\varphi), S_{32}(\theta,\varphi)=-S_{23}(\theta,\varphi) \tag{114}$$

$$S_{33}(\theta,\varphi)=-S_{22}(\theta,\varphi\pm\tfrac{\pi}{4})=-\frac{S_{22}(\theta)-S_{33}(\theta)}{2}+\frac{S_{22}(\theta)+S_{33}(\theta)}{2}\cos 4\varphi \tag{115}$$

$$S_{34}(\theta,\varphi)=S_{24}(\theta,\varphi-\tfrac{\pi}{4})=S_{34}(\theta)\cos 2\varphi \tag{116}$$

$$S_{34}(\theta,\varphi)=S_{24}(\theta)\sin 2\varphi+S_{34}(\theta)\cos 2\varphi \tag{117}$$

$$S_{41}(\theta,\varphi)=S_{14}(\theta,\varphi)=0 \tag{118}$$

$$S_{42}(\theta,\varphi)=S_{24}(\theta,\varphi), S_{43}(\theta,\varphi)=-S_{34}(\theta,\varphi) \tag{119}$$

From Eq. 106 to 119, we can see that, in the case of spherical scatterers, all matrix elements are defined by six functions, $S_{11}(\theta), S_{12}(\theta), S_{22}(\theta), S_{33}, S_{34}(\theta) and S_{44}(\theta)$ only.

5.2.2 Experimental Mueller matrix measurement

To determine each of the 16 experimental matrix elements, a total of 49 images are taken at various combinations of input and output analyzer polarization states [Table-5.1]. Adding or subtracting a series of images, calculates each of the 16 output Mueller matrix experimental elements. The individual images are represented by a two-letter combination that denotes the input polarization and output analyzer orientation. The turbid medium depolarize, mix polarization and changes the direction (θ,φ) of incident laser beam. The position of each matrix element S_{ij} depending on symmetry and certain optical properties can be described through Mueller calculus. The total transmitted intensity measurements together with 49 polarization combinations give total of 4x4=16 possible input-output Mueller matrix combinations to get the result for total information about the scatterer, and can be completely described by measuring its entire matrix element as a function of θ. We derived

theoretically that only seven element of turbid medium are needed to determine all the 16 output Mueller matrix elements, and measured experimentally, through the entire 49 polarization configuration.

The scatterer is usually an unknown. Therefore it is important to test the scattering instrument (optics, electronics, and mechanical stability), using perfect exactly known scattering sample such as small spheres turbid medium sample of known optical paramcters. This sample can be used to test theory and evaluate the entire scattering measurement because their interaction with the incident light can be predicted from fundamental electromagnetic theory. Unknown scatterers could consist of smoke, dust, bio-particles, or any other particulate suspended in air or in solution. Regardless of the nature of the scatterer, in most scattering experiments it is illuminated with a beam of light having wavelength, prepared into a particular incident Stokes vector while a particular scattered Stokes vector is measured as a function of θ. The scatterer *[S]* mixes the initially pure polarization state and produces a mixed final Stokes vector. The final Stokes vector will differ from the incident Stokes vector in intensity I, polarization, and direction θ. The main scattering problem is to define the scatterer in terms of its matrix elements via polarization measurements. We first illuminated the scatterer *[S]* with + 45° linear polarized light and analyze the scattered radiation with a horizontal polarizer.

We have $[S_{out}]=[V_+][S_{in}]=[V_s]$, where $[V_s]$ is the scattered Stokes vector. The resultant is,

$$S_{out}=\begin{bmatrix} S_{11} & S_{12} & S_{13} & S_{14} \\ S_{21} & S_{22} & S_{23} & S_{24} \\ S_{31} & S_{32} & S_{33} & S_{34} \\ S_{41} & S_{24} & S_{34} & S_{44} \end{bmatrix}\begin{bmatrix} 1 \\ 0 \\ 1 \\ 0 \end{bmatrix}=\begin{bmatrix} S_{11}+S_{13} \\ S_{21}+S_{23} \\ S_{31}+S_{33} \\ S_{41}+S_{43} \end{bmatrix}=\begin{bmatrix} I \\ Q \\ U \\ V \end{bmatrix}=[V_S] \qquad (120)$$

The scattered Stokes vector is a mixture of polarization states since its components *[I, Q, U, and V,]* created from the Stokes vector of initially + 45° polarized, are nonzero. It is also a mixture of certain matrix elements. Now analyze the scattered light with horizontal analyzer $[h]$ and measure the intensity I as a function of scattering angle θ, $[h][V_s]=[V_d]$

$$S_{out} = \begin{bmatrix} 1 & 1 & 0 & 0 \\ 1 & 1 & 0 & 0 \\ 0 & 0 & 0 & 0 \\ 0 & 0 & 0 & 0 \end{bmatrix} \begin{bmatrix} S_{11} + S_{13} \\ S_{21} + S_{23} \\ S_{31} + S_{33} \\ S_{41} + S_{43} \end{bmatrix} = \begin{bmatrix} (S_{11} + S_{13}) + (S_{21} + S_{23}) \\ (S_{11} + S_{13}) + (S_{21} + S_{23}) \\ 0 \\ 0 \end{bmatrix} = \begin{bmatrix} I \\ Q \\ U \\ V \end{bmatrix} = [V_d] \qquad (121)$$

In this case the Stokes vector $[V_d]$ entering the detector consists of only horizontally polarized light ($U=V=0$). But most important is that information about it contained in the matrix element combination $(S_{21} + S_{23})$ has been brought up into the first component by the horizontal analyzer. The total intensity seen by the detector is now $I = (S_{11} + S_{13}) + (S_{21} + S_{23})$ which can be observed or plotted as a function of scattering angle θ. We put the results of such calculations for all 16 Stokes vector combinations into a matrix array changing polarizer analyzer configuration to 49 combinations shown in table 5.1. Each matrix element label S_{ij} is in the uppermost left-hand corner of each matrix element block. The intensity states to the immediate right of S_{ij} represent the kind of light involved in the measurement. For example, in the above discussed matrix element position S_{23} are measured by illuminating the scatterer with 45°linear polarized light while analyzing the scattered light with a linear horizontal or vertical polarizer.

This is demonstrated by examining how each individual matrix element is measured. For example, a detector set up to measure the total intensity, scattered from a sample illuminated with horizontally linear polarized light measures the polarization intensity I_{h0} which connects the matrix elements S_{11} and S_{12} giving $I_{h0} = S_{11} + S_{12}$. Similarly when the input polarizer is rotated 90° to illuminate the scatterer with vertically linear polarized light the detector measures the polarization intensity I_{V0} which connects the same matrix elements $S_{21} + S_{23}$ but with $I_{0O} = S_{11} - S_{12}$. Subtracting these two signals gives $I_{h0} - I_{v0} = (S_{11} + S_{12}) - (S_{11} - S_{12}) = 2S_{12}$. This matrix element will be zero for scatterers that treat vertical and horizontal input polarization equally, that is, for scatterers equally efficient in completely depolarizing both vertical and horizontally polarized light. A scatterer can be completely described by measuring all of its matrix elements as a function of θ. This is often the goal of a scattering study. Only two measurements as shown above

are needed to determine the matrix elements of the first row S_{1j} and first column S_{i1}. S_{11} can be determined from a single measurement using un-polarized light for illumimition and measuring the total scattered intensity. Four measurements are needed to determine each of the other nine matrix elements S_{ij} (i and $j \neq 0$). For example, in order to compute the polarization measurements needed to determine S_{32} proceed as follows:

Measure $I_{h+} = S_{11} + S_{12} + S_{31} + S_{32}$ and $I_{h-} = S_{11} + S_{12} - S_{31} - S_{32}$

Subtract $I_{h+} - I_{h-} = 2(S_{31} + S_{32})$

Measure $I_{v+} = S_{11} - S_{12} + S_{31} - S_{32}$ and $I_{V-} = S_{11} - S_{12} - S_{31} + S_{32}$

Subtract $I_{v+} - I_{v-} = 2(S_{31} - S_{32})$

Compute $(I_{h+} - I_{h-}) - (I_{v+\_} - I_{v-}) = (I_{h+} + I_{v-}) - (I_{v+} + I_{h-}) = 4S_{32}$ (122)

Similar measurements and calculations will yield all 16-matrix elements of the scattering matrix [S]. The matrix showing the relationship between the S_{ij} and the polarization measurements is given in Table 5.1. Not all matrix elements are independent. Generally the matrix is diagonal with some $S_{ij} = \pm S_{ji}$ or zero. The degree of matrix symmetry and the number of nonzero elements depends on the degree of particle or symmetry of the scatterer. As mentioned above, a particle or particle distribution symmetry that treats various kinds of polarized light equally will have a zero for those matrix elements that are involved with that kind of polarized light, whether the polarized light is on the input or exit beam. This means that if $S_{ij} = 0$, then $S_{ji} = 0$. Making the above 16 measurements of polarized light from a scatterer will produce 16 matrix elements. Each one is a θ, dependent intensity measurement for a particular arrangement of input-output optics. These 16 elements contain all the information that can be learned from a scattering experiment. Choosing input-output optical combinations, different than the ones described above, will produce a set of elements drastically different in appearance but not fundamentally different in information content. They will simply be related by various coordinate transformations.

S_{11}(Parallel x Parallel)	S_{12} (horizontal x Parallel)	S_{13} (45^0x Parallel)	S_{14} (L.circulerx Parallel)
I_{00}	I_{h0}-I_{v0}	I_{+0}-I_{-0}	I_{L0}-I_{R0}
S_{21} (Parallel x horizontal)	S_{22} (horizontalx horizontal)	S_{23} (45^0x horizontal)	S_{24} (L.circularx horizontal)
I_{0h}-I_{0v}	(I_{hh}+I_{vv})-(I_{vh}+I_{hv})	(I_{+h}+I_{-v})-(I_{-h}+I_{-v})	(I_{Lh}+I_{Rv})-(I_{Rh}+I_{Lv})
S_{31} (Parallel x 45^0)	S_{32} (horizontal x45^0)	S_{33} (45^0x45^0)	S_{34} (L.circularx45^0)
(I_{0+}-I_{0-})	(I_{h+}+I_{v-})-(I_{v+}+I_{h-})	(I_{++}+I_{--})-(I_{-+}+I_{+-})	(I_{L+}+I_{R-})-(I_{R+}+I_{L-})
S_{41} (Parallel x L.circular)	S_{42}(horizontal x L.circular)	S_{43}(45^0xL.circular)	S_{44}(L.circularxR.circuler)
(I_{0L}-I_{0R})	(I_{hL}+I_{vR})-(I_{vL}+I_{hR})	(I_{+L}+I_{-R})-(I_{-L}+I_{+R})	(I_{LL}+I_{RR})-(I_{RL}+I_{LR})

Table.5.1 A matrix array showing the polarization measurements, necessary to measure each particular matrix element of the different configurations (polarizer and analyzer) setup.

For obtaining matrix signature of diffusely backscattered light from turbid medium the resultant equation is,

$$[S_{out}] = [M_{system}][S_{in}] \tag{123}$$

$$[M_{system}] = [P_\theta][M][m_1][m_2][A_\theta] \tag{124}$$

where $[P_\theta]$and $[A_\theta]$ are the ideal matrix for the polarizer and analyzer, m_1 and m_2 for mirrors and M for turbid medium. For finding ideal matrix $[P_\theta]$and $[A_\theta]$of a polarizer analyzer at some general azimuth $\theta$with its transition axis, we use conventional method of matrix algebra and compute the polarizer and analyzer for an ideal case:

$$[P_\theta] = [T(-2\theta)][P_0][T(2\theta)] \tag{125}$$

and for analyzer,

$$[A_\theta] = [T(-2\theta)][A_0][T(2\theta)] \tag{126}$$

Where $[T(-2\theta)]$ and $[T(2\theta)]$ are rotator and counter rotator matrix. The light passes through a cascade of optical components made up of a polarizer, and analyzer. The Mueller matrix for an ideal polarizer is given by [92].

$$[P_0] = \begin{bmatrix} 1 & C_2 & S_2 & 0 \\ C_2 & C_2^{\,2} & C_2 S_2 & 0 \\ S_2 & C_2 S_2 & S_2 & 0 \\ 0 & 0 & 0 & 0 \end{bmatrix} \tag{127}$$

Where $C_2 = \cos(2\theta)$, $S_2 = \sin(2\theta)$, $and C_2^{\,2} = \cos^2(2\theta)$ and 0 is the angle of polarizer Similarly, Mueller matrix for an ideal analyzer same to polarizer,

$$[A_\theta] = \begin{bmatrix} 1 & C_2 & S_2 & 0 \\ C_2 & C_2^{\,2} & C_2 S_2 & 0 \\ S_2 & C_2 S_2 & S_2 & 0 \\ 0 & 0 & 0 & 0 \end{bmatrix} \tag{128}$$

The Mueller matrix for an aluminum mirror used in our experiment is,

$$m_1 = \begin{bmatrix} S_{11} & S_{12} & 0 & 0 \\ S_{21} & S_{22} & 0 & 0 \\ 0 & 0 & S_{33} & S_{34} \\ 0 & 0 & S_{43} & S_{44} \end{bmatrix} \text{ and } m_2 = \begin{bmatrix} S_{11} & S_{12} & 0 & 0 \\ S_{21} & S_{22} & 0 & 0 \\ 0 & 0 & S_{33} & S_{34} \\ 0 & 0 & S_{43} & S_{44} \end{bmatrix} \tag{129}$$

the resultant Stokes vector for the system is,

$$[S_{out}] = [A_0][m_2][m_1][M][P_\theta][S_{in}]$$

$$[S_{out}] = \begin{bmatrix} (gd = he) + C_2(jd + ke) + S_2(mf) \\ C_2(gd = he) + C_2^{\,2}(jd + ke) + C_2S_2(mf) \\ S_2(gd = he) + C_2S_2(jd + ke) + S_2(mf) \\ 0 \end{bmatrix} \tag{130}$$

where d, e, f, g, h, j, k, and m are given as:

$$d = S_{11}a + S_{12}b + S_{13}c,$$
$$e = S_{21}a + S_{22}b + S_{23}c,$$
$$f = S_{31}a + S_{32}b + S_{33}c,$$
$$g = S_{11}^{\,2} + S_{12}S_{21},$$
$$h = S_{11}S_{12} + S_{12}S_{22},$$
$$j = S_{11}S_{21} + S_{22}S_{22},$$
$$k = S_{12}S_{22} + S_{22}^{\,2},$$
$$m = S_{33}^{\,2} - S_{32}S_{43}$$

as

$$a = I + C_2Q + S_2U,$$
$$b = C_2I + C_2^{\,2}Q + C_2S_2U,$$
$$c = S_2I + C_2S_2Q + S_2U$$

So the set of 16 measurements together with other optical components will stand as the signature or fingerprint of the diffusely back-scatterer as described by polarized scattered light. An important area of light back-scattering research is to characterize turbid systems by their matrix elements and to use the matrix element signals for changes in the system. This is a very powerful application of light scattering for biological and other complex system, even though the system is not amenable to theoretical treatment, because light scattering elements are often not unique and because certain large features of the scattering system could completely mask smaller features. An important current research area deals with establishing the information content of the various matrix element signals.

5.2.3 Conclusion

The introduction of the Mueller-matrix concept for the diffusely backscattered light provides detailed information about scattering media. Because the description of the optical characteristics with the Mueller matrix is complete, any information about particle size, refractive index, particle shape etc. has to be found in the Mueller matrix by careful analysis of the matrix elements and application of some mathematical calculations. However, further information may be gained, for example, by measuring the diffuse transmittance, the diffuse back reflectance at different incident and observation angles, or time-dependent polarization effects.

5.3 Mueller matrix polarimetry for characterization of optical materials.

The laser polarimeter has been constructed to measure the Mueller matrix of material samples in transmission. The instrument is ideally suited for calibrating visible polarization elements. It is also intended for studies of induced birefringence resulting from the application of electric field. Fundamental constants of materials, such as the linear or nonlinear electro-optic coefficients can then be obtained from measurements of the Mueller matrix as a function of applied field strength. With this polarimeter we can obtain a complete Mueller matrix, the full characterization of electro- optic materials that might be expected to produce scattering and depolarization, such as nitrobenzene or microcrystalline materials is also possible.

The emphasis of this investigation is the development and demonstration of an automated electro-optical imaging system for measuring the elements of the Mueller matrix calculus that overcomes most of the shortcomings of previously developed systems. Polarimetry is an experimental technique for measuring the polarization state of a light beam and for deducing the polarizing properties of materials in transmission. Polarimeters are commonly used to measure specific optical properties of media in diverse applications [93]. The most general information that can be obtained from a polarimeter is the Mueller matrix, a 4 x 4 real matrix that contains all information concerning the polarization properties of a medium. Optical polarization-imaging system has the potential to non-invasively detect cancerous lesions. The described system generates the full Mueller matrix image in seconds. The operation of the system was tested in transmission, using known samples, such as a nitrobenzene. The results of the known samples are in good agreement with their theoretical values [94].

We demonstrated an optical calculus method for the measurement of retardance with a polarimetric system for the measurement of turbid medium optical properties. The polarimeter used for this measurement was designed to give a high-precision, high-accuracy measurement of a polarizer and quarter-wave retarder at 632.8 nm He-Ne laser. The performance and precision is demonstrated by the variance of multiple polarization and retardance measurements on each optical component for characterization of sample through Mueller matrix algorithm. We have constructed a Mueller matrix polarimeter based on an

ellipsometric method proposed by Azzam [95]. My purpose in constructing and operating this instrument is to determine properties such as retardance, diattenuation, and depolarization of linear or nonlinear electro- -optic materials in the visible region of the spectrum using Mueller matrix calculus [96].

5.3.1 Mueller matrix rotating retarder polarimeter

The visible laser polarimeter described here is designed for operation with a He-Ne laser source in the 632.8 nm spectral regions. This spectral region is of great interest for the evaluation of materials used as elements of optical-processing systems, laser-modulation systems, or thermal-imaging systems. The polarimeter design is readily adapted for operation in other wavelength regions with different sources, detectors, and elements. This polarimeter configuration is based on designs described by Azzam and others [97, 98]. Mueller matrix elements, Jones matrix and Stokes vectors are used to represent the polarization elements and polarized light, respectively. The Mueller matrix formulation is used because it is preferable for experimental research where scattering and depolarization measurements are made routinely [99].

One of the great advantages of this configuration is that the polarization sensitivity of the detector is not important because the orientation of the final polarizer (analyzer) is fixed. The Mueller matrix of the sample is found through measurements of a series representing the modulation and the elements of the sample matrix.

The polarization elements are aligned relative to the laser beam. This dual-rotating retarder polarimeter technique requires a rotating linear retarder on both sides of the sample to modulate the various Mueller matrix elements onto intensity variations modulation frequencies. The retarders used with the He-Ne laser of zero-order wave plates, giving nominally a 90^0 phase shift between orthogonal polarization states at 632.8 nm. The final element in the sample measurement is a detector. Data are displayed on the computer screen or output to a printer and plotter. All the software necessary for calibration procedures, data acquisition, and preliminary processing is stored on the computer. The computer is programmed in Mat-lab for taking out put Mueller matrix images of sample material.

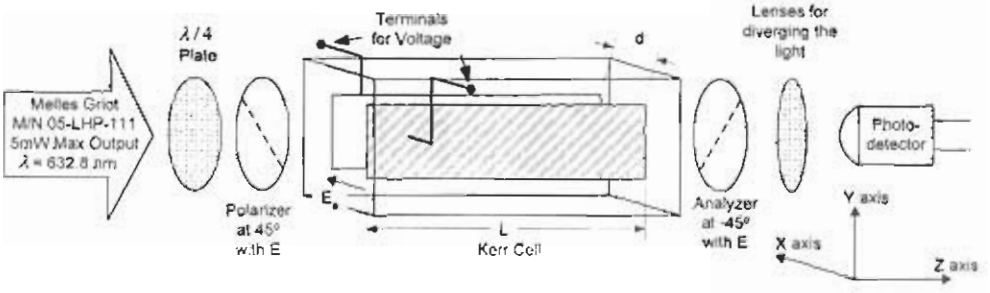

Figure.5.5 Experimental setup for the measurement of transmitted Mueller matrix elements electro-optical polarimeters. A He-Ne laser beam with an output power of 5 mW at a wavelength of 632.8 nm is used as the light source. The circularly polarized light is generated, by inserting a quarter mica retardation plate behind the linear polarizer. The out put polarized light is directed to sample (nitrobenzene) placed in a Kerr cell, and again pass through linear polarizer, quarter wave plate and recorded on photodiode detector, which is controlled and operated with lab view software.

The four polarizing elements in the polarimeter are required to be aligned with respect to the laser axis. The principal objective of the polarimeter calibration is to orient the linear polarizer so that its axis is parallel with the laser axis and then to orient the retarders so that their fast axes are parallel with the polarizer axis. This process is the subject of considerable effort, and the elimination of the remaining errors form a substantial part of this research.

The optical system of a polarized light obtained from the combination of a linearly polarized He-Ne laser and quarter wave plate for characterization of sample containing the optically active material nitrobenzene placed in a Kerr cell followed by a detector. The light source used is 5 mW He-Ne laser operating at a wavelength of 632.8nm. Length '*L*' and

separation'd' of the Kerr cell electrodes is 11.6 mm and 1.5 mm, respectively. The Kerr coefficient 'K' for nitrobenzene is 2.79 x 10^{-10} cm/volt^2. A high voltage power supply is used to generate voltage up to 6 kV. The laser system is fixed, so for controlling the electric field vector of the input light we used a quarter wave plates with a linear polarizer. The transmitted beam is measured with a photodiode detector behind the cell.

5.3.2. Optical properties from the Mueller matrix

The Mueller matrix can be thought of as the "optical fingerprint" of a sample. This matrix operates directly on an input or incident Stokes vector, a Stokes vector, a 4 x 1 vector, is a mathematical representation of the polarization state of light [100]. It can be represented as a set of six intensity measurements recorded through a set of various polarizing filters. The Stokes vector is composed of four elements, I, Q, U, and V and provides a complete description of the light polarization state. If the total irradiant intensity I_t incident on the sample and $I_{0^0}, I_{90^0}, I_{+45^0}, I_{-45^0}, I_{rc}$, and I_{lc} the irradiances transmitted by a polarizer-retarders and focused to the detector. Then, the Stokes parameters are defined by [101],

$$S = \begin{bmatrix} I \\ Q \\ U \\ V \end{bmatrix} = \begin{bmatrix} S_0 \\ S_1 \\ S_2 \\ S_3 \end{bmatrix} = \begin{bmatrix} I_t \\ I_{0^0} - I_{90^0} \\ I_{+45^0} - I_{-45^0} \\ I_{rc} - I_{lc} \end{bmatrix} = \begin{bmatrix} \langle E_{0x}^2 \rangle + \langle E_{0y}^2 \rangle \\ \langle E_{0x}^2 \rangle - \langle E_{0y}^2 \rangle \\ 2\langle E_{0x} E_{0y} \cos\delta \rangle \\ 2\langle E_{0x} E_{0y} \sin\delta \rangle \end{bmatrix} \tag{131}$$

After normalizing the Stokes parameters by the irradiance I, Q describes the amount of light polarized along the horizontal (Q= +1) or vertical (Q= -1) axes, U describes the amount of light polarized along the +45° (U= +1) or -45° (U= -1) directions, and V describes the amount of right (V= +1) or left (V= -1) circularly polarized light.

A Mueller matrix, a 4 x 4 matrix, is a mathematical description of how an optical sample interacts or transforms the polarization state of an incident light beam and given as [102].

$$[M] = \begin{bmatrix} m_{11} & m_{12} & m_{13} & m_{14} \\ m_{21} & m_{22} & m_{23} & m_{24} \\ m_{31} & m_{32} & m_{33} & m_{34} \\ m_{41} & m_{42} & m_{43} & m_{44} \end{bmatrix} \quad (132)$$

where, M is the 4 x 4 Mueller matrix of the media or sample and can be experimentally measured through the application of various incident polarization states and then by analyzing the state of polarization of the light leaving the sample. If the Mueller matrix is not known, all the elements can be determined experimentally. It can be shown that transmitted intensity measurements with various orientations of polarizers and analyzers are necessary to obtain the output elements of the Mueller matrix [103].

One objective of this study is to obtain electro- optic coefficients of material. The coefficients are derived from Mueller matrices measured as a function of applied field strength. The method by which this derivation is accomplished is described in Goldstein et al. [103], and is briefly summarized here. The application of an electric field across a nitrobenzene produces an index change. It is now clear that the electro-optic coefficient can be obtained from the measured Mueller matrix.

Note that for purposes of obtaining the electro-optic coefficient experimentally, the fast axis of an electro-optic material acting as an ideal retarder can be at any orientation. The (4, 4) matrix element of the matrix for a retarder with the fast axis at angle 0 is independent of fast-axis orientation, and the fast-axis orientation can be eliminated elsewhere by adding the matrix elements or squaring and adding elements in the row and column. Given a measured Mueller matrix of a material, a known applied voltage, and a known refractive index, one can easily obtain the electro-optic coefficient.

5.3.3 Error compensation

The true nature of the sample may be obscured by errors inherent in the polarimeter optical system. The Mueller matrix elements must be compensated for the known errors in retardance of the retarders and the errors caused by the inability to align the polarizing elements precisely. The fact that there are errors that cannot be eliminated through optical means led to an error analysis and a compensation procedure to be implemented during polarimeter data processing.

A summary of an error analysis of a dual-rotating retarder Mueller matrix polarimeter is presented in this section. The derivation of the compensated Mueller matrix elements using the small-angle approximation is documented in detail by Chipman and Shurcliff [70, 104]. Errors in orientation alignment are considered and the errors caused by non ideal retardation elements are also included in the analysis. A compensation for imperfect retardation elements is then made possible with the equations derived, and the equations permit a calibration of the polarimeter for the azimuthal alignment of the polarization elements.

The following calibration procedure is used. First, the polarimeter is operated with no sample and Fourier coefficients obtained from the measured modulated intensity. Second, using error- compensation equations with matrix elements of the identity matrix inserted for the Mueller matrix elements, we calculate the errors in the element orientations and retraces. Third, in the routine use of the polarimeter, the systematic errors in the Fourier coefficients arising from the imperfections are compensated for by using the error-compensated equations with experimentally determined error values to obtain the Mueller matrix elements as a function of measured Fourier coefficients. Thus, birefringence induced changes are relatively slow, and the Stokes parameters change according to the Mueller matrix of a linear retarder. However, an optic axis that varies with depth will give changes in the polarization state that will be difficult to distinguish from the random manner of multiple scattering. More research is necessary on this complex problem. We use coherent light source and standard optical filters to minimize these errors for our Mueller matrix polarimeter.

5.3.4 Mathematics for obtaining the Mueller matrix

This polarimeter measures a signal, which is modulated by rotating the polarizing optical elements. The elements of the Mueller matrix are encoded on the modulated signal. The output signal is then Fourier analyzed to determine the Mueller matrix elements. The implementation described here uses two aligned and fixed linear polarizers and two rotating quarter-wave retarders as shown in Fig. 5.5. This generates twelve harmonic frequencies in the Fourier spectrum of the modulated intensity. We used the Mueller matrix calculus for characterization of the optical material. The transformation of the Stokes vector for an optical system can be described as [104]:

$$[S_{out}] = [M_{system}][S_{in}], \tag{133}$$

where S_{out} is the output Stokes vector, M_{system} is the Mueller matrix for an optical system and S_{in} is the input Stokes vector. When light passes through the polarizer, Kerr cell, retarders and analyzer, then the corresponding Mueller matrix for the system is given by the following,

$$[M_{system}] = [A_M][M_{mi}][P_M], \tag{134}$$

where $[A_M]$ and $[P_M]$ are the Mueller matrices for the analyzer and polarizer respectively, and $[M_{mi}]$ for the electro-optic material sample , using the method as specified in [105, 106].

$$[M_{mi}] = \begin{bmatrix} \frac{1}{2}(A+B+U_1+U_2+U_3+U_4) & \frac{1}{2}(A-B+U_1-U_2-U_3+U_4) & 0 & 0 \\ \frac{1}{2}(A-B+U_1-U_2+U_3-U_4) & \frac{1}{2}(A+B+U_1+U_2-U_3-U_4) & 0 & 0 \\ 0 & 0 & \sqrt{AB}\cos(\Delta\phi) & \sqrt{AB}\sin(\Delta\phi) \\ 0 & 0 & -\sqrt{AB}\sin(\Delta\phi) & \sqrt{AB}\cos(\Delta\phi) \end{bmatrix}, \tag{135}$$

where A, B are the amplitude coefficients along x- and y-axis respectively, U_1, U_2, U_3, U_4 are the electric field dependent depolarization coefficients and $\Delta\varphi$ is the relative phase between the orthogonally polarized components. The input Stokes parameters for our system is given by,

$$[S_{in}] = \begin{bmatrix} 1 \\ 0 \\ 0 \\ 1 \end{bmatrix}. \tag{136}$$

For characterization of nitrobenzene sample as a function of applied voltages, we need an equation of measured intensity through which we can solve the seven unknowns A, B, U_1, U_2, U_3, U_4 and $\Delta\varphi$ in Eq. (135). Taking the first component of the output Stokes vector $S_{out} = I_{\theta_i,\theta_o}$ from Eq. (133) we have,

$$I_{\theta_i,\theta_o} = \frac{1}{8}\begin{bmatrix} (A+B+U_1+U_2+U_3+U_4)+(A-B+U_1-U_2-U_3+U_4)(C_{2i}) \\ +C_{2o}\{(A-B+U_1-U_2+U_3-U_4)+(A+B+U_1+U_2-U_3-U_4)(C_{2i})\} \\ +2\sqrt{AB}\,S_{2o}S_{2i}\cos(\Delta\phi) \end{bmatrix} \quad (137)$$

where $C_{2i} = \cos(2\theta_i)$, $S_{2i} = \sin(2\theta_i)$, $C_{2o} = \cos(2\theta_o)$, $S_{2o} = \sin(2\theta_o)$, and θ_i , θ_o are the input and output angle of the polarizers with respect to the electric field.

5.3.5 Measurements

The extensive measurements on commercial polarization elements and electro-optic nitrobenzene have been made with the polarimeter. Thus the experimental matrix results presented here show an example of a measured Mueller matrix without detailed analyses of the data. We have placed the nitrobenzene sample in parallel plate electrodes made of nickel plated copper. The transmitted optical intensity versus applied voltage is measured using polarizer-analyzer (extinction ratio of 10^{-3}) orientations with the He-Ne laser source. From the observation of the experimental data, we have

$$I_{0,0} \approx I_{90,90} = I_{\parallel} \text{ and } I_{0,90} \approx I_{90,0} = I_{\perp}. \quad (138)$$

It is clear from Eq. (138),

$$I_{\parallel} = \frac{1}{2}(A+U_1) = \frac{1}{2}(B+U_2), \quad (139)$$

$$I_{\perp} = \frac{1}{2}U_4 = \frac{1}{2}U_3, \tag{140}$$

For semi-isotropic scattering we assume that,

$$A = B, \quad U_1 = U_2 = U_{\parallel}, \quad \& \quad U_4 = U_3 = U_{\perp}. \tag{141}$$

Using assumptions from Eq. (141) in Eq. (138) we get,

$$MaxI_{45,45} = \frac{1}{4}\left[2A + U_{\parallel} + U_{\perp}\right], \tag{142}$$

$$MinI_{45,45} = \frac{1}{4}\left[U_{\parallel} + U_{\perp}\right]. \tag{143}$$

Moreover, absorption is found to be dependent on orientation of the polarizer (θ_i), i.e., the absorbance is given by $f(\theta_i)$. These In which, transmitted intensity is plotted against applied voltage, after removing polarizer retarder and analyzer from the setup shown in Fig.5.5. This intensity transmittance is normalized to 0.69, which is the convergence of intensity transmittance at $\theta_i = 45^{\circ}$, then we measured the intensity transmittance at every 5° of orientation of polarizer and normalized it to get transmittance ranging from 0 to 1. It is observed that the $sin^2(2\theta_i)$ function is in a good agreement with the experimentally observed normalized intensity, therefore we can assume that $f(\theta_i \propto sin^2(2\theta_i)$. the absorbed intensity factor, I_A is included in the intensity transmittance through Eqs. (142) & (143). Therefore we can write

$$MaxI_{45,45} + MinI_{45,45} = I_{\parallel} + I_{\perp} + I_A f(\theta_i). \tag{144}$$

By rearranging the above expression, we get

$$I_{\perp} - \left(MaxI_{45,45} - \frac{I_A f(\theta_i)}{2} \right) - \left(MinI_{45,45} - \frac{I_A f(\theta_i)}{2} \right) + I_{\perp} = 0 , \tag{145}$$

For any general orientation of θ_i intensity transmittance is as follows:

$$I_{\theta_i,\theta_o} = \frac{1}{4}\left[A + U_{\perp} + U_{\perp} + \left(A + U_{\parallel} - U_{\perp} \right) C_{2i} C_{2o} + A S_{2o} S_{2i} \cos(\Delta\phi) \right] + I_{kc} , \tag{146}$$

where I_{kc} incorporates the absorption factor of the two polarizers and retarder, which is 0.25 (nominal value given by manufacturer for 632.8 nm). In order to get a corrected simulations for the nitrobenzene device model, we eliminate the effect of the polarizer and retarder absorption from I_{kc} such that,

$$I_{kc} = 2 I_A f(\theta_i) . \tag{147}$$

We can also write an electric field dependent absorption Mueller matrix for the nitrobenzene device as [107]:

$$[M_A] = \begin{bmatrix} 2I_A f(\theta_i) & 0 & 0 & 0 \\ 0 & 2I_A f(\theta_i) & 0 & 0 \\ 0 & 0 & 2I_A f(\theta_i) & 0 \\ 0 & 0 & 0 & 2I_A f(\theta_i) \end{bmatrix} . \tag{148}$$

Combining Eq. (142) and Eq. (143) we have

$$[M_P] = \begin{bmatrix} A + U_{\parallel} + U_{\perp} + 2I_A f(\theta_i) & 0 & 0 & 0 \\ 0 & A + U_{\parallel} - U_{\perp} + 2I_A f(\theta_i) & 0 & 0 \\ 0 & 0 & A\cos(\Delta\phi) + 2I_A f(\theta_i) & A\sin(\Delta\phi) \\ 0 & 0 & -A\sin(\Delta\phi) & A\cos(\Delta\phi) + 2I_A f(\theta_i) \end{bmatrix} , \tag{149}$$

where *[M_P]* is the Mueller matrix responsible for the phase difference between orthogonal components of polarized light, scattering, and the absorption of light. Solving Eq. (149) for the present case, we get

$$I_{\theta_i,\theta_o} = 2I_A f(\theta_i) + \frac{1}{4}\left[A + U_{\parallel} + U_{\perp} + \left(A + U_{\parallel} - U_{\perp}\right)C_{2i}C_{2o} + A S_{2o}S_{2i}\cos(\Delta\phi)\right]. \qquad (150)$$

Now we are in a position to find the unknown coefficients required to simulate the intensity transmittance given by Eq. (180) at different orientations of θ_i and θ_o. For this purpose first we get curve fitted equations, up to 3rd degree of polynomial, from the graphical data.

To verify our model at the orientations of θ_i & θ_o other than defined above, we have simulated Eq. (150) and again found reasonable agreement between simulated and experimental transmittances. The model is checked for parallel polarizer and analyzer with θ_i ranging from 0 to $\pi/2$ with a step of 5 degrees for voltage corresponding to the phase change ofπ. Fig. 5.8 shows the simulation data [107].

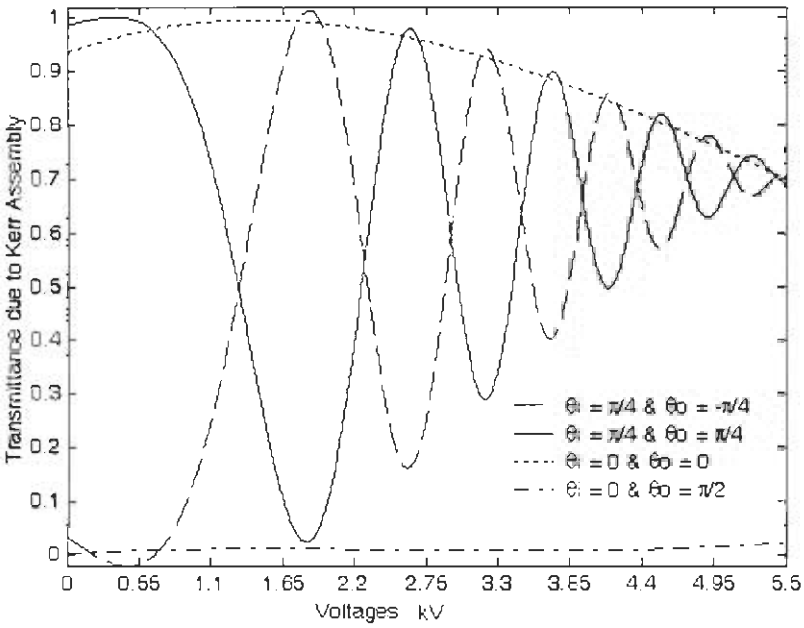

Fig. 5.6 Simulation of the transmittance for $\theta_i = \theta_o = \pi/4$, (solid curve), $\theta_i = \pi/4$ and $\theta_o = -\pi/4$ (dashed curve), $\theta_i = \theta_o = 0^\circ$, (dotted curve) and $\theta_i = 0^\circ$and $\theta_o = \pi/2$, (dash-dot curve).

5.3.6 Conclusions

This polarimeter has been designed to fulfill the specific need of an instrument that measures polarization and fundamental electro-optic properties of transmitted bulk materials in the visible. It has an advantage over other polarimeters and ellipsometers in that it measures the entire Mueller matrix, makes these measurements in the visible, and is designed to compensate, with novel hardware features and data-reduction techniques, for the major error sources (beam wander, non ideal retarders, and element-orientation misalignments). The polarimeter has been an effective tool in accurately characterizing polarization elements.

The Mueller matrix polarimeter having nitrobenzene device (having parallel-plate electrode geometry) between a pair of polarizers, we perform relatively simple experimental measurements to solve for the unknown coefficients. As we vary the electric potential across

the nitrobenzene device, we generate a dataset describing the coefficients of scattering, depolarization, absorption, and EO phase response as functions of the applied electric field. Our characterization shows distinctly different EO responses for weak, medium, and strong electric-field strengths. Therefore, for accurate simulation of changes in phase (or index of refraction) resulting from large electric field gradients, we used a higher order EO model. As nitrobenzene has anisotropic scattering, to reduce the number of unknowns in our Mueller matrix [Eq. (149)], we have made assumptions given in Eq. (150) to make the model simpler to solve. This can be justified on the basis of the similarity between the measured intensities for the various polarized, depolarized, and absorbed components. Now we have only five unknown coefficients (A, $U_{\parallel}$, $U_{\perp}$, I_A, and $\Delta\varphi$) to reduce the corresponding number of required experimental measurements. Finally, we applied our characterization study to computer aided device simulations and observed that the simulated graphs match the experimental graphs within an error range of 5% which could be further reduced by increasing the order of curve fitting.

Genius is one per cent inspiration, ninety-nine per cent perspiration (Thomas A Edison)

Chapter 6

MUELLER MATRIX POLARIZATION IMAGING

6.1 Mueller matrix polarimetry: characterization of turbid medium through polarization discrimination

The Mueller matrix polarization discrimination (MMPD) technique for two-dimensional imaging of a turbid medium with dual rotating polarizer and retarder setup is presented. We are interested to see the out put images of highly scattering media with low power polarized wave source. The error analysis and the axial symmetry of 16 Mueller matrix elements are consider in the experimental measurement procedures. The polarization and depolarization of scattered light in term of Mueller matrix images in transmission mode provides a fingerprint of the turbid medium under investigation. The Mueller matrix polarimetry does not decrease or increase the state and degree of polarization itself. The turbid medium is highly scattering and can be characterized by arbitrary and combined effect of birefringence, absorption and scattering properties. The results predict the presence of the significant surveying and preservation of polarization in optical scattering media up to certain distance. This technique has potential to investigate the turbid biological material for their optical properties (structure, size, shape and orientation of scatterer) through Mueller polarization matrix and for noninvasive diagnostic and treatment modalities of malignant tumors.

6.1.1 Optical properties of the scatterer that influence polarization

The scattering through turbid medium is the principle mechanism that modifies the initial polarization state of the incident light. The polarization state of light after a single scattering event depends on the direction of scatter and incident polarization state [108, 109]. In many

turbid media such as tissue, scattering structures have a large variance in size and are distributed or oriented in a complex and sometimes apparently random manner. Because each scattering event can modify the incident polarization state differently, until finally the polarization state is completely randomized. An important exception is when the media consists of organized linear structures, such as birefringent turbid medium, and then the phase retardation between orthogonal polarization components is proportional to the distance traveled through the birefringent medium. The phase retardation of the scattering medium is given as:

$$\delta = \frac{2\pi\Delta nx}{\lambda} \tag{151}$$

The phase retardation measurement through turbid media is aimed at retrieving useful information from such multiply scattered light. The behavior of light in random media is well-known from the extensive study of wave propagation. Light traveling in a random medium can be classified into three categories, the ballistic, the snake and the diffuse light [138, 139]. The ballistic light either remains un-scattered, or undergoes coherent forward scattering in the medium. This light travels undeviated and has the shortest path length in the medium. The snake light is that which undergoes near-forward scattering, and follows path that undulate about the ballistic path [105]. The diffuse photons, which largely exceed the other two categories in number, are those which undergo multiple scattering. We consider all three kinds of photons in our study.

A large number of different experiments are possible if one wants to study the polarization dependent scattering properties of turbid media. The probing light may be linearly polarized at various angles, right and left-hand circularly, or elliptically polarized. Light coming from the scattering medium can be analyzed in the same numerous ways. However, only a few measurements are needed to completely characterize the optical properties of any material. The necessary procedure is elegantly demonstrated by the Stokes-vector Mueller matrix approach to polarization and light scattering.

6.1.2 Determining the Mueller matrix

If the Mueller matrix is not known, all the elements can be determined experimentally. It can be shown that 49 intensity measurements with various orientations of polarizer and analyzers are necessary to obtain the 16 elements of the Mueller matrix [105].

$$
\begin{aligned}
m_{11} &= I_{00} \\
m_{12} &= I_{h0} - I_{v0} \\
m_{13} &= I_{+0} - I_{-0} \\
m_{14} &= I_{l0} - I_{r0} \\
m_{21} &= I_{0h} - I_{0v} \\
m_{22} &= (I_{hh} + I_{vv}) - (I_{vh} + I_{hv}) \\
m_{23} &= (I_{+h} + I_{-v}) - (I_{-h} + I_{+v}) \\
m_{24} &= (I_{lh} + I_{rv}) - (I_{rh} + I_{lv}) \\
m_{31} &= I_{0+} + I_{0-} \\
m_{32} &= (I_{h+} + I_{v-}) - (I_{v+} + I_{h-}) \\
m_{33} &= (I_{++} + I_{--}) - (I_{-+} + I_{+-}) \\
m_{34} &= (I_{l+} + I_{r-}) - (I_{r+} + I_{l-}) \\
m_{41} &= I_{0l} - I_{0r} \\
m_{42} &= (I_{hl} + I_{vr}) - (I_{vl} + I_{hr}) \\
m_{43} &= (I_{+l} + I_{-r}) - (I_{-l} + I_{+r}) \\
m_{44} &= (I_{ll} + I_{rr}) - (I_{rl} + I_{lr})
\end{aligned}
\qquad (152)
$$

where the first subscript term represents the input polarization state while the second subscript the output polarization state of light. The states are defined as: h = horizontal, v = vertical, + = +45°, - = -45°, r = right circular and l = left circular. Once all 16 elements of the matrix are obtained, the medium is completely described in terms of its optical properties.

6.1.3 Error analysis of Mueller matrix polarimeter

For the retardations close to 0^0 or 90^0 the background noise on the detectors introduces a significant and systematic error of 15^0 at a signal to noise ratio of 10 dB [110]. The coherent detection scheme which calculates the Stokes parameters has better immunity to the system. in the calculation of the Q parameter the spectral density in one polarization channel is subtracted from the spectral density in the orthogonal polarization channel, thus eliminating constant background noise terms, and the U and V parameters are calculated from the cross

correlation between the orthogonally polarized channels, eliminating autocorrelation noise. Noise will decrease the degree of polarization, since it will be present as autocorrelation noise in the Stokes parameter I. In the incoherent detection scheme only V is measured and the error in the phase retardation is introduced by the decrease of the amplitude of oscillations with increasing depth. In the coherent detection scheme, the Stokes parameters Q, U, and V can be renormalized on DOP, restoring the amplitude of the oscillations, and thus eliminating the systematic error.

We have analyzed system errors introduced by the extinction ratio of polarizing optics and chromatic dependence of wave retarders, and errors due to dichroism, i.e., the differences in the absorption and scattering coefficients for polarized light in turbid medium. System errors can be kept small by careful design of the system with achromatic elements, but can never be completely eliminated. Dichroism is a more serious problem when interpreting the results as solely due to birefringence. However, Mueller matrix polarimetry measurements have shown that the error due to dichroism is relatively small [111]. The variance in the computed Stokes vectors of transmitted light (excluding effect of birefringence) is due to multiple scattering, speckles, and shot noise (i.e., optimized system). At some depth, the detected signals are limited by shot noise. At shallower depths (i.e., before the shot noise limit) variance in the Stokes parameters is primarily due to the effects of multiple scattering and speckle. Multiple scattering scramble the polarization mainly in a random manner and this offers some means to distinguish it from birefringence. Thus, birefringence induced changes are relatively slow, and the Stokes parameters change according to the Mueller matrix of a linear retarder [112]. However, an optic axis that varies with depth will give changes in the polarization state that will be difficult to distinguish from the random manner of multiple scattering. More research is necessary on this complex problem. We use coherent light source and standard optical filters to minimize these errors for our Mueller matrix polarimeter.

The experimental setup for Mueller matrix polarimetry is shown schematically in Fig. 3.2. A He-Ne laser of wavelength 632.8 nm and the laser spot size is less than 2 mm passes through a plarizer (P1) and quarter wave-plate (QWP1) and impinges on the sample. The scattered light which emerges from the sample passes through an analyzer (P2) and quarter wave-plate (QWP2), and is then recorded by the detector connected to lock in amplifier or CCD

camera system. The CCD resolution is 12 bit and the lab view software is used for data analysis. The scattering medium (soybean oil) is placed in a cylindrical thin-walled quartz cell (3x1 cm). Soybean oil is an inexpensive, non-toxic liquid with dielectric properties similar to very low-water-content fatty tissue. For this reason, it is used as the tissue phantom [113].

6.1.4 Experimental results

In many medical applications, we need information about multiple scattering results. In this study we recovered that information by selectively detecting a transmitted component of the scattered photon flux that has its initial polarization state preserved. These photons transmitted through or re-emitted from a multiply scattering medium by using relatively inexpensive Mueller matrix polarimeter provides the basis for several potential applications. The measurement technique is based upon an operational principle, which involves the modulation of a polarization state. The resulting modulated light signal is collected by the detector or CCD camera and is analyzed pixel by pixel to calculate individual intensity patterns, which correspond respectively to the 16 components of the scattering Mueller matrix. In brief, the two polarizer and quarter-wave plates inserted in the probing and analyzing beam paths, are generate a periodic signal, which includes 12 harmonic terms and a dc term. This signal carries information about the properties of the medium which induces the transformation of the polarization state of the modulated probing light. The experimental procedure requires collecting of 16 intensity images at various orientations of the polarizing components. The described procedure provides the possibility to calculate the scattering Mueller matrix for a given sample.

The Stokes parameter I of the system in Fig. 6.1, 6.2 represents the magnitude of the intensity of the scattered light. Thus, any abrupt change in the detected signal indicates strong discontinuity in the refractive index of the specimen. Along with I, other Stokes parameters, Q, U and V can be used to detect structural changes that are not simply detected from I. Other Stokes parameter images of U and V show supplement information that there is no apparent level of stress inside the scatterer. Therefore, by analyzing the corresponding series of the polarization patterns one can trace scattering events of different order. Specifically, the data analysis of, Fig. 6.3, 6.4 suggests several interesting observations

regarding the general properties of the scattering Mueller matrix and Stokes matrix. First, the magnitude of the off-diagonal components of the scattering Mueller matrix is significantly smaller than the magnitude of the diagonal components.

In the present experiments, we are able to trace the polarization patterns and to verify that the existing magnitude distributions are preserved. The magnitude and the sign of most of the spatial extent of the matrix components for Fig.6.2, 6.3 closely resemble the form of the Mueller matrix for scattering medium. The next important observation is that the experimental results clearly display several symmetry properties of certain matrix components for homogeneous scattering medium. The seven out of sixteen are independent and other can be calculated through symmetry relation [114].

By comparing the images of Fig. 6.2, 6.3, and 6.5, one can identify the unique features of the Mueller matrix for scattering medium. The axial symmetry of the system provides relation between all the Mueller matrix components and reduces the number of measurements, which reduces the observation time. These symmetry relations describe that the seven independent elements are [115],

$$m_{11}(\theta,\varphi), m_{12}(\theta,\varphi), m_{14}(\theta), m_{22}(\theta,\varphi), m_{23}(\theta,\varphi), m_{24}(\theta,\varphi), m_{44}(\theta), \tag{153}$$

and the other nine

$$\begin{aligned}
&m_{13}(\theta,\varphi) = m_{12}(\theta,\varphi+\tfrac{\pi}{4}) \\
&m_{21}(\theta,\varphi) = m_{12}(\theta,\varphi)
\end{aligned},$$

$$m_{31}(\theta,\varphi) = -m_{13}(\theta,\varphi) = m_{12}(\theta,\varphi-\tfrac{\pi}{4}),$$

$$m_{32}(\theta,\varphi) = -m_{23}(\theta,\varphi) = m_{23}(\theta,\varphi\pm\tfrac{\pi}{4}),$$

$$m_{33}(\theta,\varphi) = -m_{22}(\theta,\varphi-\tfrac{\pi}{4}),$$

$$m_{34}(\theta,\varphi) = m_{24}(\theta,\varphi-\tfrac{\pi}{4}),$$

$$\begin{aligned}
&m_{41}(\theta,\varphi) = m_{41}(\theta) = m_{14}(\theta) \\
&m_{42}(\theta,\varphi) = m_{24}(\theta,\varphi)
\end{aligned},$$

$$m_{43}(\theta,\varphi) = -m_{34}(\theta,\varphi) = m_{24}(\theta,\varphi+\tfrac{\pi}{4}) \tag{154}$$

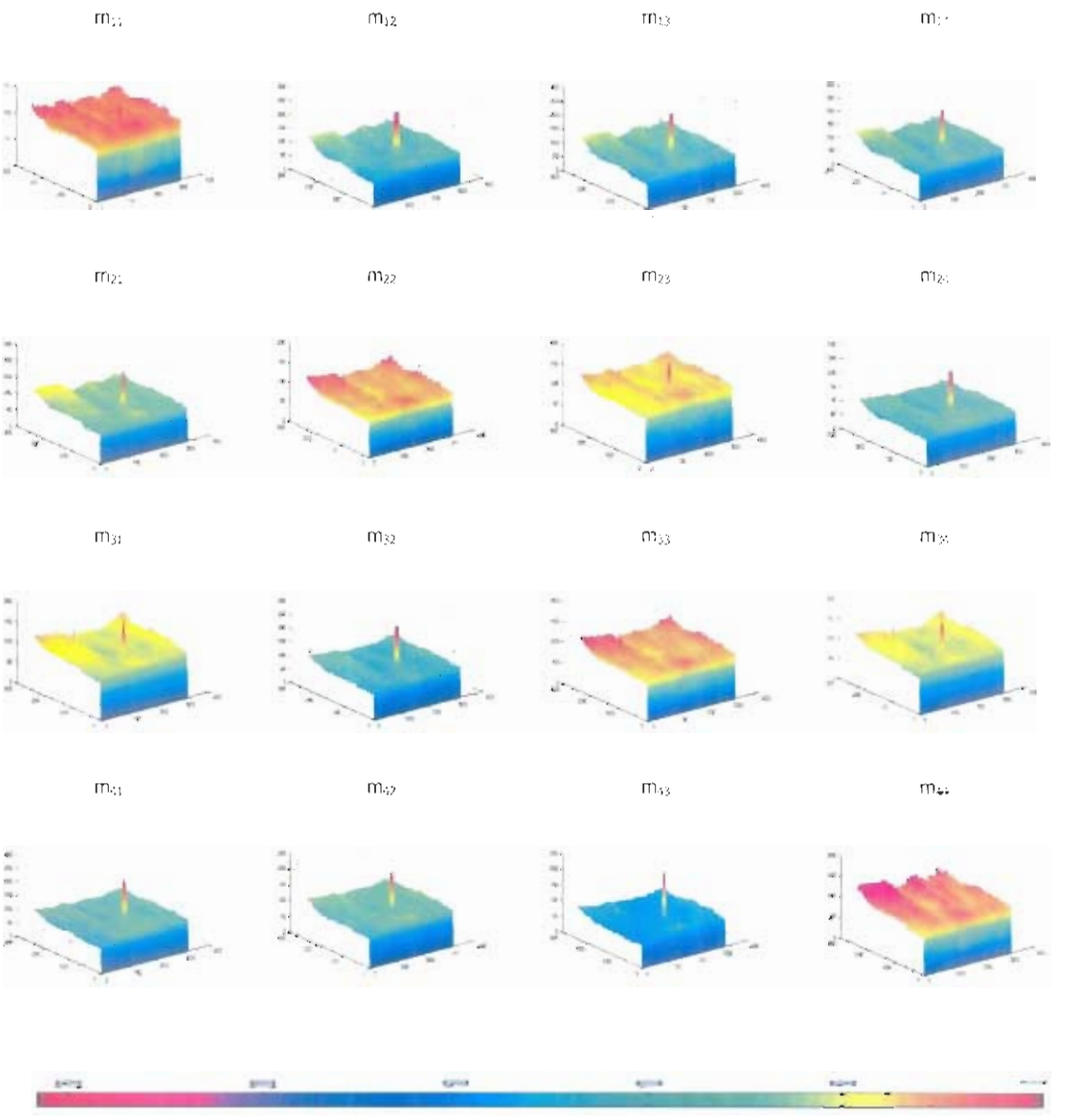

Figure 6.1 Transmitted Mueller matrix components (3D) corresponding to a 16 images of scattering medium. The images are taken with the experimental setup in Fig. 3.2. The scale bar is adjusted so that red represent the maximum irradiance, yellow to middle one, green for minimum irradiance and blue means "no light" or component change by an order of magnitude. All displayed images are 3x1 cm in phantom sample.

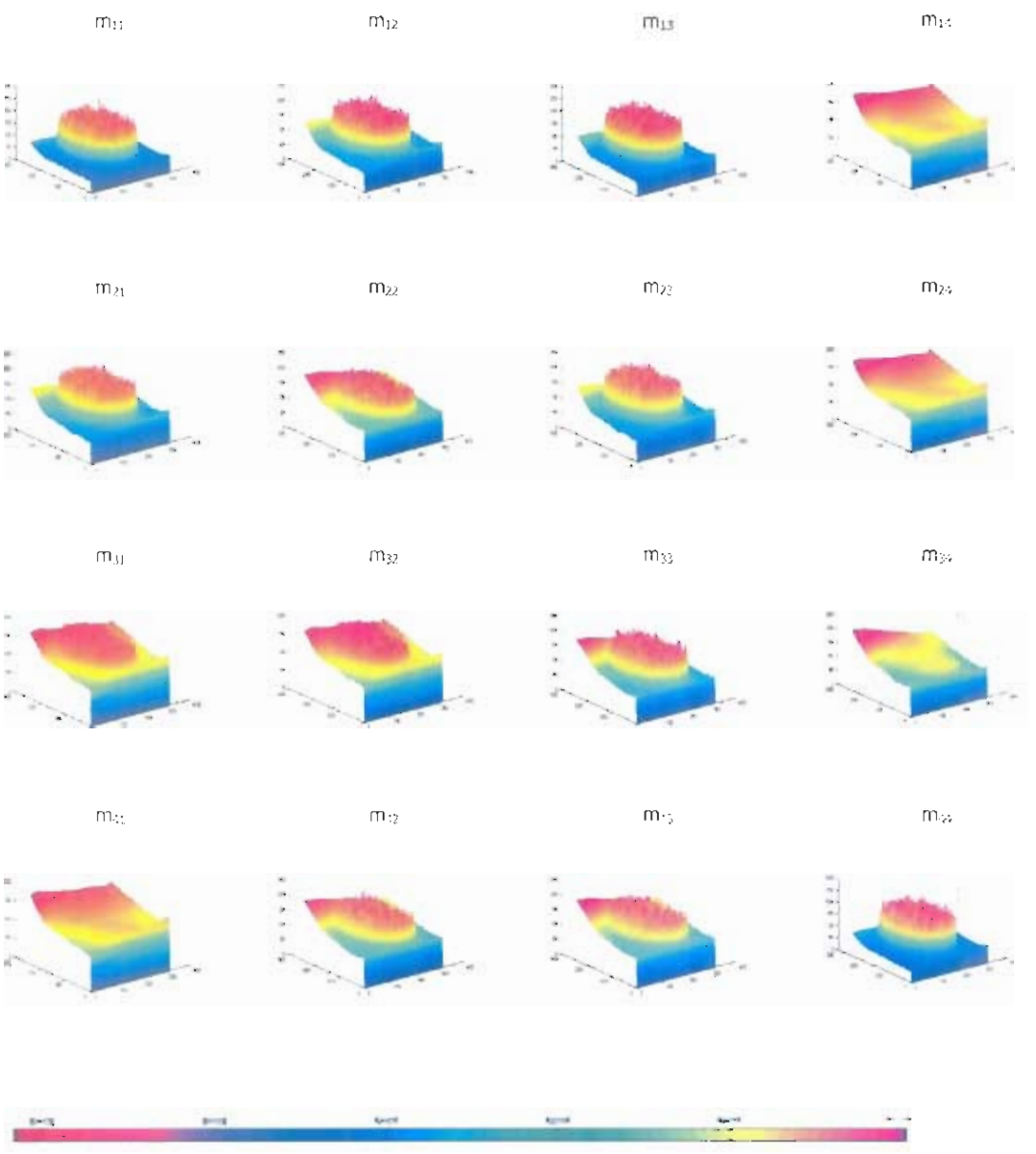

Figure 6.2 The three dimensional images of 16 Mueller matrix transmitted intensity elements for phantom.

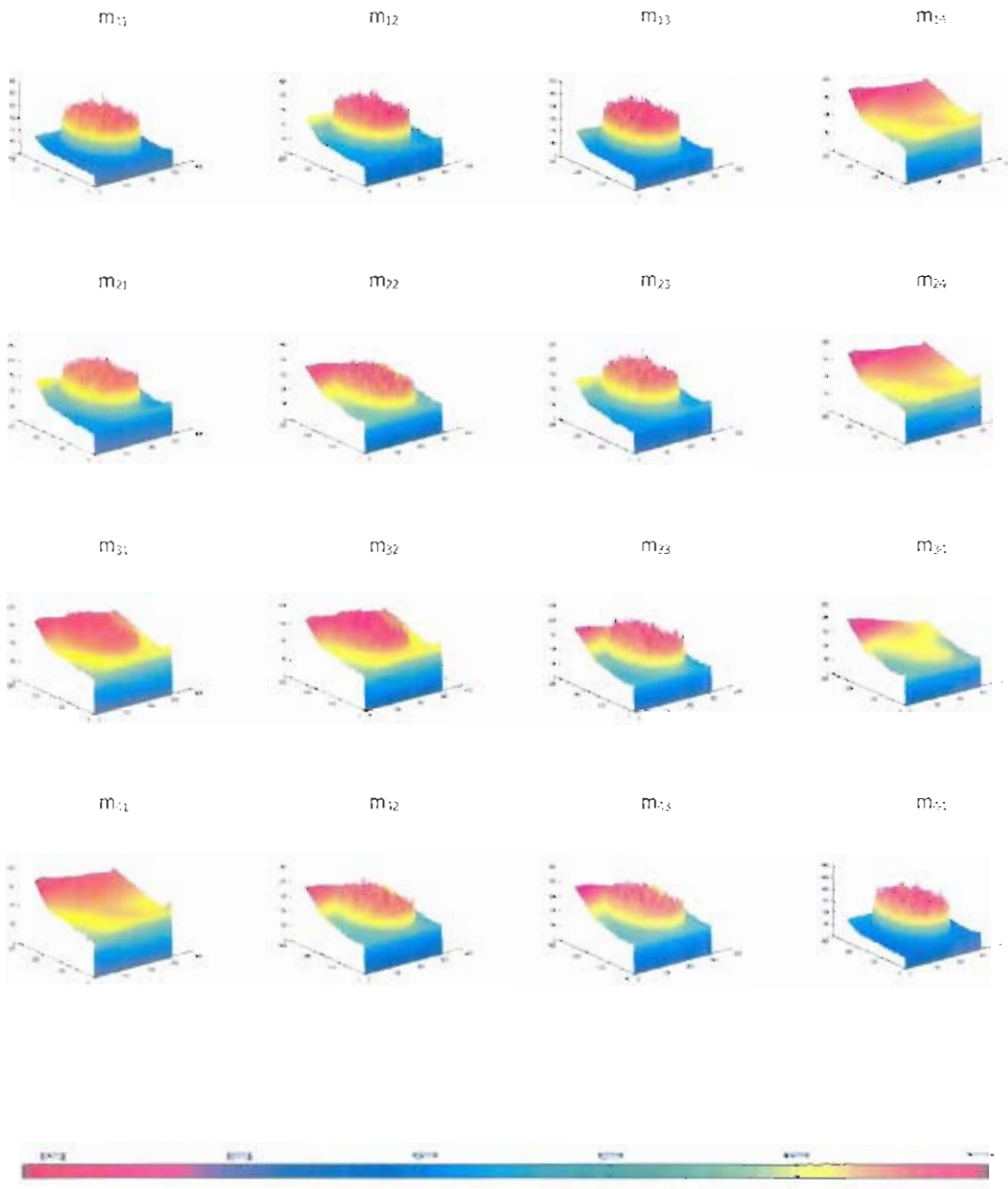

Figure 6.3 The three dimensional images of 16 Mueller matrix transmitted intensity elements for phantom.

Table 6.1, 6.2 displays the matrix array, which represents the detector reading specific to a linear polarizer lie in the first row, first column elements, those specific to a quarter wave plate lie in the fourth row, fourth column elements. Making the above 49 measurements of polarized light from a scatterer will produce 16 matrix element pattern. Each one is an polarization dependent intensity measurement for a particular arrangement of input-output optics. These 16 curves contain all the information that can be learned from a scattering experiment. Choosing input-output optical combinations, different than described above, will produce a set of patterns drastically different in appearance but not fundamentally different in information content. When the 16 matrix elements are measured the data is ready for analysis. For certain particles like spheres, fibers, and mixtures of particles, the matrix elements can be exactly predicted. So the set of 16 measurements will stand as the signature of the scatterer as described by polarized scattered light.

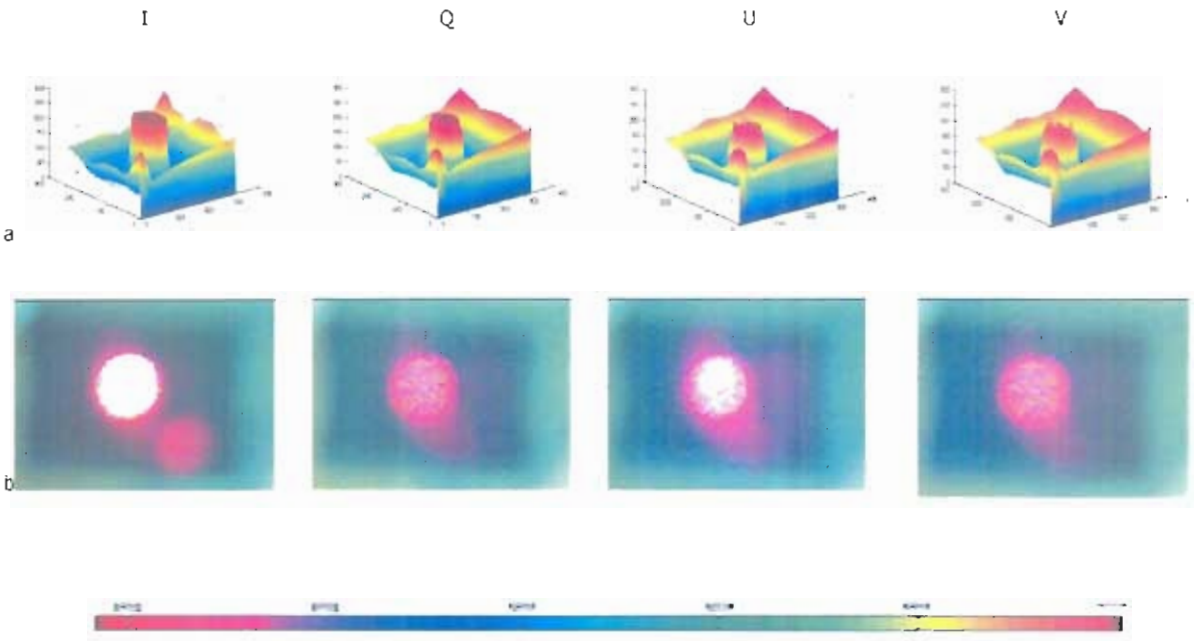

Figure 6.4. The Stokes vector I, Q, U, and V are shown, I present the total irradiant power profile, Q for horizontal polarized light, U for $+45^0$ polarized incidents light and V the right circular polarized light. (a) Represents the 3-D images and (b) represent the direct transmitted intensity for phantom.

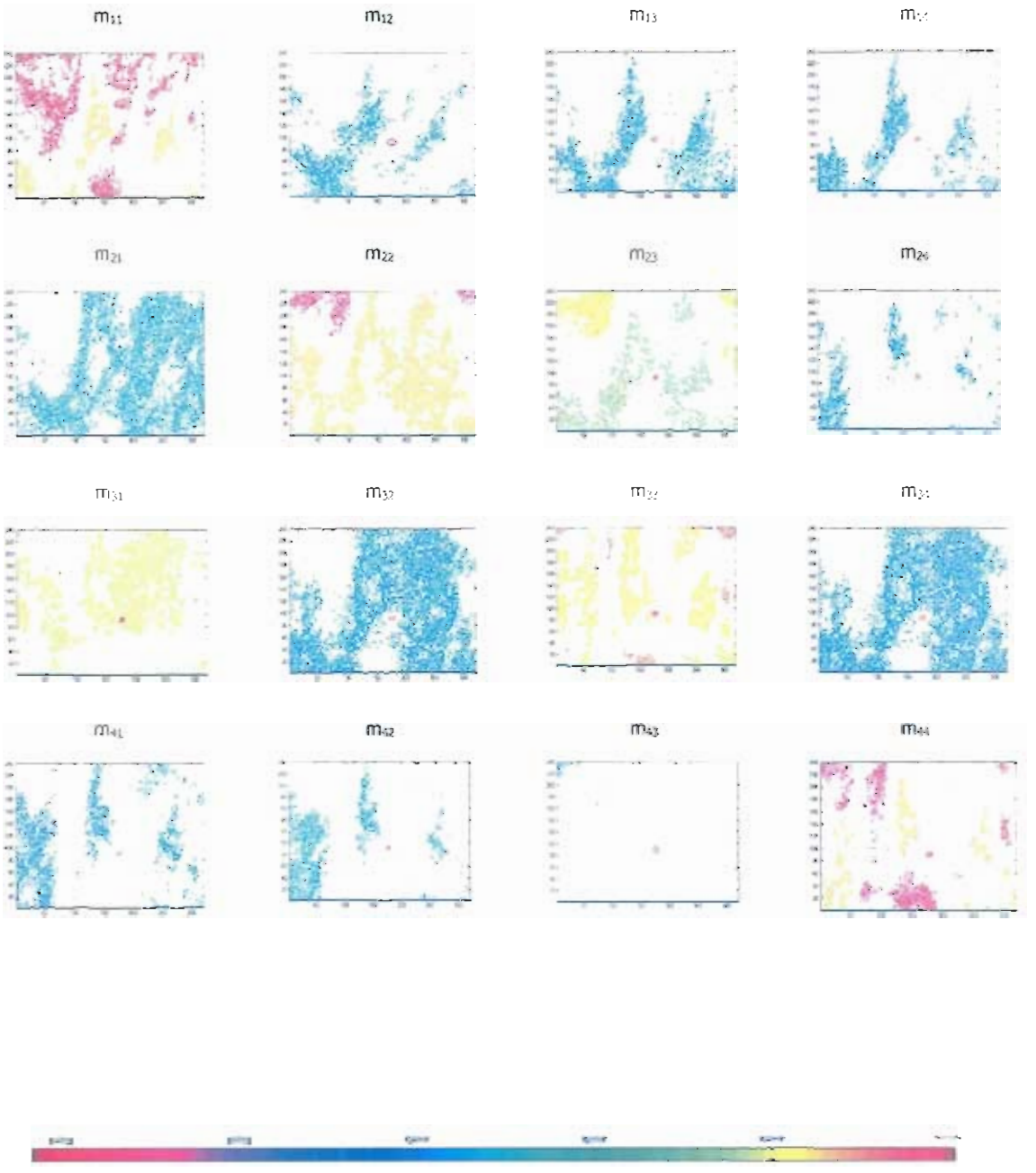

Figure 6.5. The sixteen Mueller matrix components (2D) corresponding to a phantom scattering and transmission.

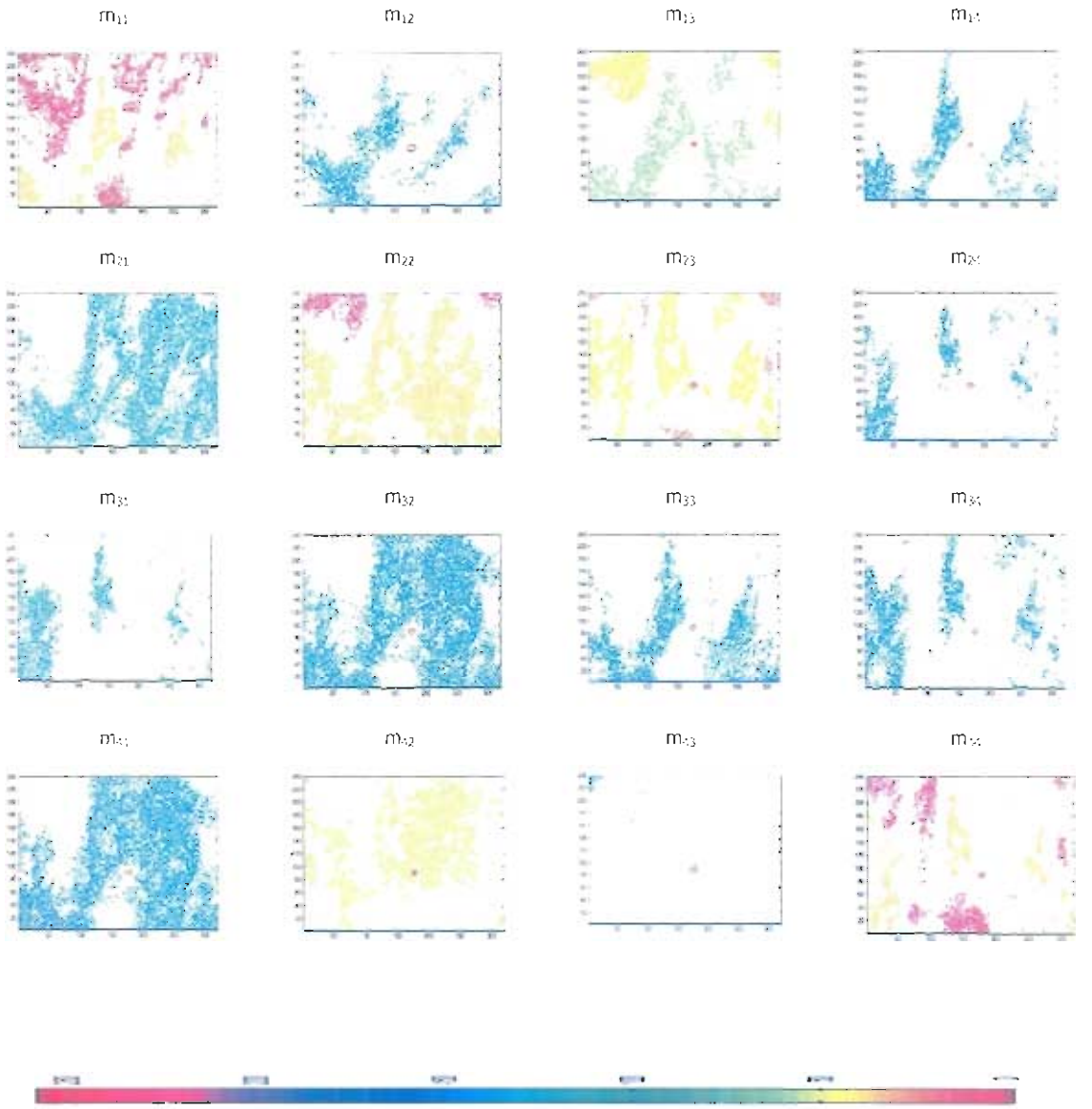

Figure 6.6. The transmitted Mueller matrix components (2D) corresponding to a turbid phantom scattering. These 2-D images are derived through 49 measurements of Mueller matrix polarimeter. The central spot presents the output transmitted irradiance by scatterer along with scattering pattern.

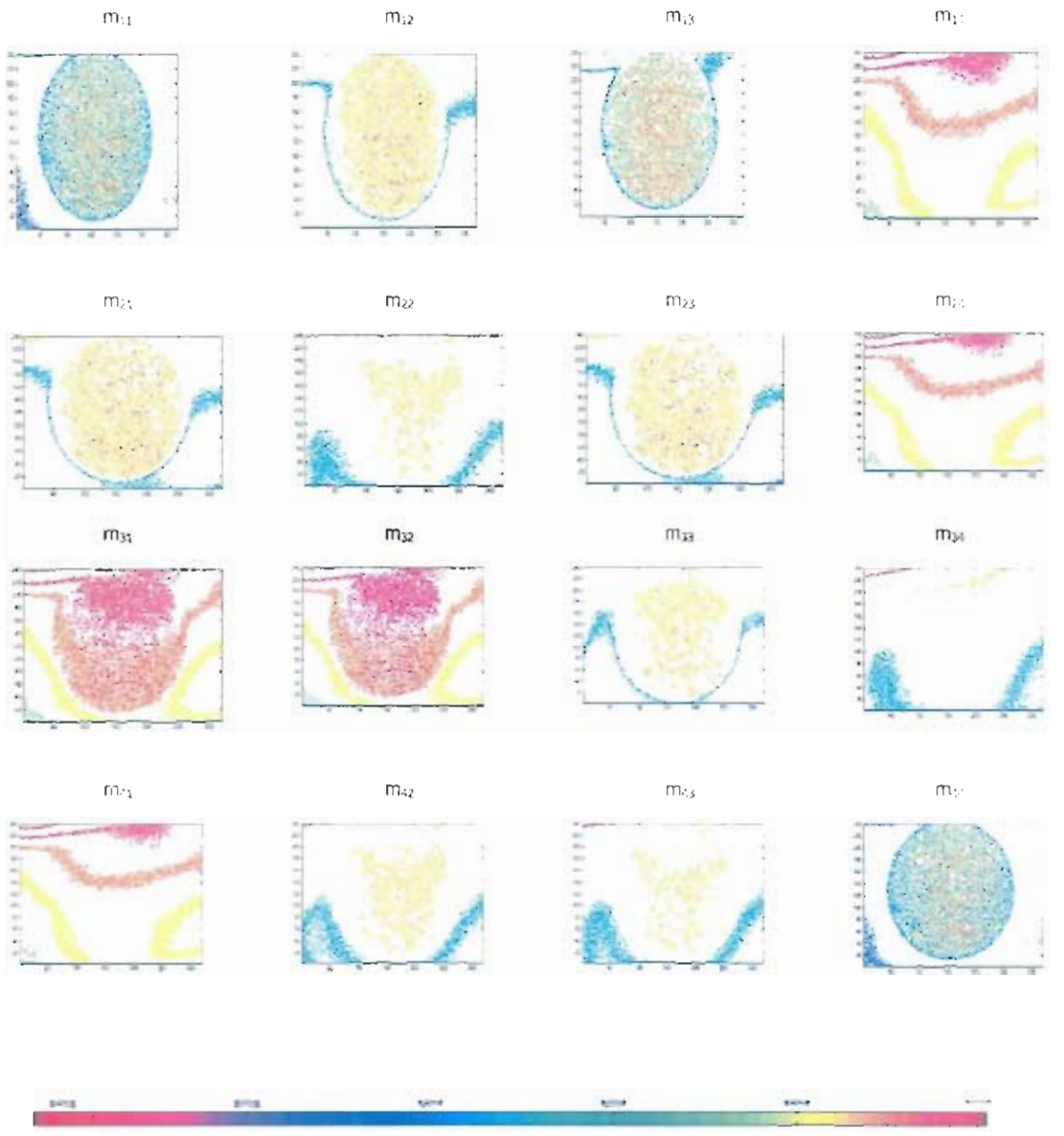

Figure 6.7 The two dimensional images of 16 Mueller matrix transmitted intensity elements for phantom.

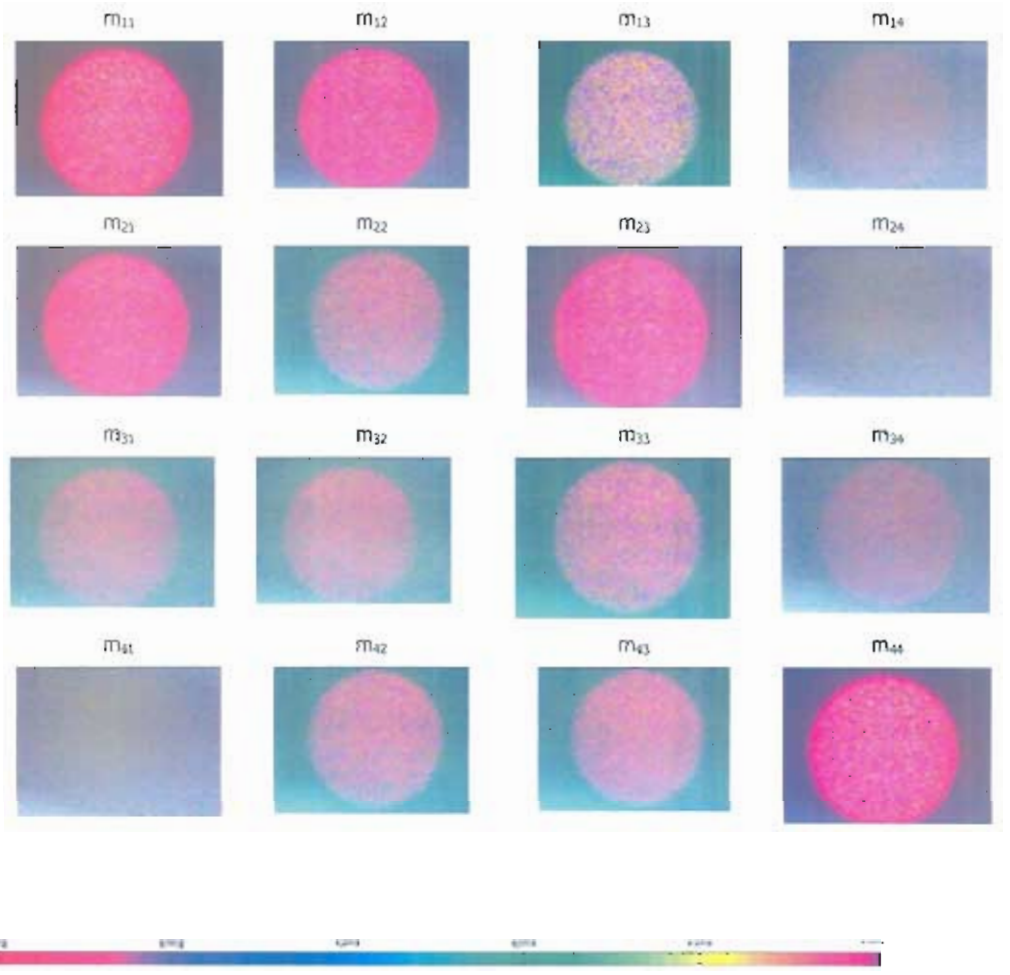

Figure 6.8 The shape of laser intensity profile by CCD camera for scattering phantom.

6.1.5 Discussions

Mueller matrix polarimetric pattern analysis predicts interesting information about the medium. The ballistic, snake and diffuse photons reaching the camera contributes to the formation of direct image. The diffuse photons have suffered multiple scattering before exiting the scattering medium. Ballistic photons completely preserve the polarization properties of the irradiant light after passing through scattering medium. The snake photons recorded by the detector are partially polarized but to the smaller degree then the ballistic photons, because snake photons partially preserve polarization. The diffuse photon

depolarized for thick sample. The collective image of these three photon provides useful information and characterizes the scattering medium.

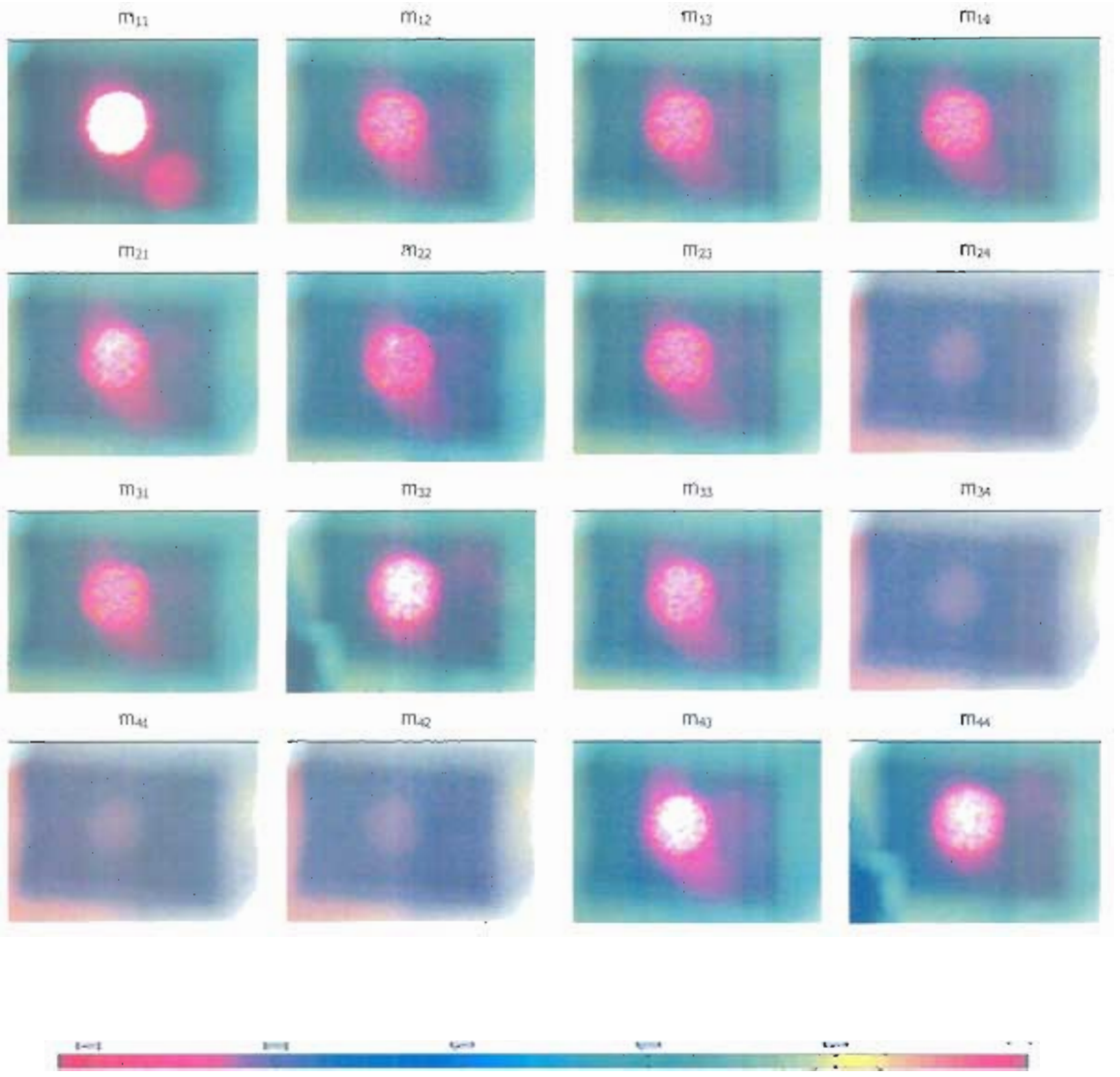

Figure 6.9 The experimental transmitted polarization images of Mueller matrix components corresponding to a scattering medium of randomly distributed particles of sample. The images corresponds the direct scatterer irradiance, measured through polarization discrimination technique.

The diagonal elements of Mueller matrix consist of linear and circular polarization pattern. The Mueller matrix m_{11} describe the properties of the total irradiance of light source and provides less information comparing to other elements of the matrix array, but all other elements are normalized through it. The m_{22} composed of linear horizontal and vertical polarization state. The liner polarization preserve through longer distance in the scatterer as compared to circular light. The concentration, size and shape of the particles in scattering medium can be predicted through careful analysis of this element along with other linear elements of the matrix. If the value of this element is zero or -ve, then the medium obey Raleigh theory and the size of the particle is small as compared to the irradiated wavelength. If its value is greater then zero than it can be explain through Mie theory and particles of the scattering medium are larger in size. m_{33} depend on $\pm 45^0$ linear polarization state and describes the properties almost close to m_{22} element. The last element m_{44} of the Mueller matrix compose on circular polarization. If the size of scatterer is larger, then the magnitude of this elements matrix will be in negative other wise greater then or equal to zero. The difference between normal and malignant biological tissues can be characterized through this element. But for larger scatterer concentration, it is less informative because the data is taken through diffuse photon and the preservation of circular polarization is not dominant in this medium. If this element is measured through the ballistic and snake photons contribution then it reviles a significant role in characterization of biological tissues. In our case the experimental data shows decline in the diagonal elements from top to bottom that conforms the preservation of linear polarization in diffuse medium for longer distance compared to circular one. As m_{44} is greater then zero, which predicts that the size of scatterer is larger then the irradiating wavelength. The size of the particle can be numerically calculated through Mie scattering theory [116].

First row and first column of the Mueller matrix except m_{14} and m_{41} describe the linear polarization pattern. Each and every element of this group is very informative, and describes the structure of the dense diffuse scatterer. From Fig. 6.1 to 6.9 we see that the intensity contrast reduces from left to right and top to bottom of the Mueller intensity matrices except m_{13}, which tells about the enriched optical activity and highly birefringence of the sample. The higher value of element m_{13} is due to randomization of the sample molecules, when the

incident light is of $\pm 45^0$ polarized. From analysis of the elements of this group the normality and abnormality of the medium can easily be defined.

The elements in the middle of this group m_{22}, m_{23}, m_{32}, and m_{33} can obtain through $\pm 45^0$ linear polarization. If some properties of the scatterer can not be obtain through the elements of other group they can be characterize through it. The elements m_{23} and m_{32} decline for dense scattering medium and the scattering angle for these elements is very small. The reduction of these elements directly related to the variation in structure of the scatterer. The last row and last column of this matrix set consist on circular polarization pattern. This group exhibits the depolarization properties of the medium. The depolarization is faster in dense as in case of circular one. The light is equally right and left-hand polarized and the effect is strongest in the center, near the laser entry point. Here the scattered light has undergone only a few scattering events and the polarization effects are strongest. With increasing distance from the point of light incident, the number of scattering events increases and eventually the polarization information is lost, the value of the m_{44} approaches zero. The majority of the elements of this group shows decline in the magnitude for dense medium and predict that the scattering cross-section of medium is small for this wavelength and the circular polarization preservation of light is weaker.

m_{11}	m_{12}	m_{13}	m_{14}	m_{11}	m_{12}	m_{13}	m_{14}
0.986	0.007	0.004	0.0003	0.910	0.657	-0.314	0.097
m_{21}	m_{22}	m_{23}	m_{24}	m_{21}	m_{22}	m_{23}	m_{24}
0.007	1.003	-0.007	0.009	0.739	0.732	0.793	0.083
m_{31}	m_{32}	m_{33}	m_{34}	m_{31}	m_{32}	m_{33}	m_{34}
0.008	-0.007	0.992	-0.003	0.435	0.243	0.620	-0.213
m_{41}	m_{42}	m_{43}	m_{44}	m_{41}	m_{42}	m_{43}	m_{44}
0.003	-0.006	-0.007	0.189	0.133	0.421	0.136	0.251

Table 6.1 Mueller matrix data for transmitted polarized laser beam (a) no sample (air) and (b) for scattering turbid sample.

m_{11}	m_{12}	m_{13}	m_{14}
1.021	0.567	-0.254	0.059
m_{21}	m_{22}	m_{23}	m_{24}
0.739	0.432	0.831	0.061
m_{31}	m_{32}	m_{33}	m_{34}
0.385	0.243	0.519	-0.213
m_{41}	m_{42}	m_{43}	m_{44}
0.0653	0.325	-0.136	0.183

Table 6.2 Mueller matrix data for transmitted polarized laser beam from phantom.

The next important observation is that the experimental results in Mueller matrix array display several symmetry properties and relations among them. This can be seen in Fig. 6.7, 6.8 and these derived symmetry relations hold, of course, if the scattering medium contains one kind of randomly distributed asymmetrical particles or optically active. Some elements of the matrix have same behavior and other one are of same shape but rotated through 90^0 as indicated in Eqs. 153, 154. All sixteen Mueller matrix components together provide a "finger print" of the scattering medium under investigation. As just shown, looking at the entire Mueller matrix often enables one to distinguish qualitatively between two media. Lot of information about particle size, refractive index, particle shape etc. has to be found in the Mueller matrix by careful analysis of the matrix elements. However, further information may be gained, for example, by measuring the diffuse backscattering and back-reflectance at different incident and observation angles, or time-dependent polarization effects.

In this study we presented a polarization discrimination scattering experiment and have taken care to establish unambiguously the coordinate systems involved, the redundancy of certain measurements and the importance of particular orientations of optical element combinations. We believe that these concepts are important for understanding and fully

appreciating optical polarization and that this approach is attractive because it discusses the inexpensive and non invasive procedures that are equally valid.

6.1.6 Conclusion

We describe the Mueller matrix polarization discrimination (MMPD) technique for characterization of highly scattering media through laser beam. From an experimental standpoint the scattering is most challenging and on the other hand, it is rich in information content because the low-order scattering events are responsible for non-trivial polarization features. Our results demonstrate that the Mueller matrix components satisfy symmetry relations. These measurements provide detailed information about the changes in the magnitude and sign of Mueller matrix components. This should offer more insight and could lead to novel procedures for characterizing scattering phenomena. We discuss the entire experimental measured Mueller polarized matrix in detail for extracting the information about the structure, size, and shape of the scattering particles. This has the potential of characterization of turbid sample for their optical properties through polarized laser radiations. The capability to measure polarization properties of multiple scattered light in vitro is exciting in that it yields several experimental observables which can be used to study and characterize turbid systems in vivo. Furthermore, the ability to acquire such measurements in a minimal time frame (approx 15 min) gives promise for the future application of such a system to differentiate between biological tissue in case of cancer and other malignant tissues.

6.2 Transmission and scattering matrix of polarization imaging for biological turbid medium

Laser transmission and scattering technique, including depolarization of wave applied to biological particles provide a simple way for diagnostic and treatment of skin lesion. Laser polarization imaging system is described for non invasive and non radioactive detection. The system described in this article generates 16 full out put Mueller matrix for characterization of turbid medium. In this work we describe the scattering and depolarization of electromagnetic radiation through biological turbid medium. This research work provides a base work for designing quick model of polarized laser tissues imaging.

6.2.1. Experimental results

Before collecting any sample data, the precision of the described system was tested after calibration. This was accomplished by determining the system variability between ten successive runs. Since the two post calibration precision results were similar, only the results obtained after calibrating the system for diffuse reflectance mode are presented. These results indicate accuracy within 97% and a standard deviation of 0.0084 using 16 polarization images and 99% accuracy with a standard deviation of 0.005 when 36 images were used to generate the Mueller matrix. In order to determine the average values for sample, the area used for the calculation was roughly 1 cm in diameter. The experimental calculations for the turbid medium with polarized laser beam are taken according to below mention order.

1. No sample (air).

As theoretically expected, the experimentally measured Mueller matrix for the case of no sample is in the form of the identity matrix for each reconstruction case, as depicted in below matrix. The maximum elemental error was 1.79% for the 36-image derived Mueller matrix, and 3.53% for the 16-image derived matrix.

$$[M]=\begin{bmatrix} 1 & 0.874 & 0.385 & -0.701 \\ 0.678 & 0.81 & 0.850 & -0.001 \\ 0.593 & 0.368 & 0.782 & -0.004 \\ 0.233 & 0.062 & 0.002 & 0.160 \end{bmatrix} \quad (155)$$

2. Sample reflection mode

To acquire specular reflection measurements, a mirror was installed between the realigned input and output branches such that the reflection from the mirror was directed through the detection optics branch. The system was then calibrated and tested for specular reflection mode.

$$[M]=\begin{bmatrix} 1 & 0.774 & 0.632 & -0.001 \\ 0.778 & 0.61 & 0.50 & -0.001 \\ 0.593 & 0.468 & 0.382 & -0.004 \\ 0.003 & 0.002 & 0.002 & 0.012 \end{bmatrix} \quad (156)$$

3. Mirror sample

The raw intensity values detected ranged from a 632.8 nm. As theoretically expected for the case of a mirror sample, the experimentally measured Mueller matrix for each reconstruction case is in the form of the reflection identity matrix, as depicted in section 2 and 3.The maximum elemental error was 1.48% for the 36-image derived Mueller matrix and 2.80% for the 16-image derived matrix.

$$[M]=\begin{bmatrix} 1 & 0.010 & -0.023 & -0.005 \\ 0.003 & -1.012 & 0.016 & 0.001 \\ -0.003 & -0.009 & 0.987 & -0.004 \\ -0.004 & -0.003 & -0.012 & -0.099 \end{bmatrix} \quad (157)$$

4. Glass transmitted mode

To test the system in transmittance mode, the angle of the system was adjusted to direct the sample to detection-optics branch. Measurements for the following cases were collected.

$$[M] = \begin{bmatrix} 1 & 0.774 & 0.632 & -0.001 \\ 0.778 & 0.421 & 0.50 & -0.001 \\ 0.593 & 0.468 & 0.510 & -0.004 \\ 0.003 & 0.002 & 0.002 & 0.094 \end{bmatrix} \quad (158)$$

5. Mirror sample

The raw intensity values detected ranged from a 632.8 nm. As expected from theory, the experimentally measured Mueller matrix for sample regardless of the reconstruction method. The maximum elemental error for the 36-image and 16-image derived Mueller matrix is 1.25% and 4.61%, respectively [45].

$$[M] = \begin{bmatrix} 1 & 0.774 & 0.732 & -0.001 \\ 0.778 & 0.70 & 0.50 & -0.001 \\ 0.693 & 0.468 & 0.832 & -0.104 \\ 0.033 & 0.002 & 0.102 & 0.250 \end{bmatrix} \quad (159)$$

The particles that shows up in the M_{21} element of above matrix disappears in the M_{12} and M_{21} cases, which are the crossed horizontal and vertical linear polarization cases. This subtraction of pigmentation from matrix elements, other than for elements M_{11} and M_{22}, which are the addition of the orthogonal horizontal and vertical linear polarization cases, confirms that polarization imaging can be used to eliminate pigmentation aliasing and allows the observation of the underlying tissue structure. In addition, the differences in the details of the underlying tissue structure between the elements other than M_{11} and M_{22}, which indicate that the retention of polarization information is also dependent on the system input and output polarization states. The specific experiments reported in this paper have concentrated on the measurement of the scattering in matrix of well defined spheres resembling the scattering matrix of biological particles. One of the major problems arising in this type of experiment is related to the extreme short sampling. In addition there is deficiency in our knowledge concerning which scattering matrix elements of biological particles are of fundamental interest.

Experiments in a turbid system are mainly concerned with finite particles. Therefore, characterization of complete population is of main interest. Fortunately, symmetry

conditions, especially valid for an ensemble of particles measured in a system reduce the number of independent matrix. Particles in a medium are randomly oriented on passing the laser beam. Therefore ensemble averaging can be applied. the characteristics, implicit in a experiment, contribute positively to the light scattering depolarization measurements of biological particles .On the other hand, however, the complete optical equipment demands some experimental and theoretical adaptations, the sharply focused laser beam constrains the theoretical description of the interaction of a particle with the laser beam.

To investigate the possibility of application of a system to measure the sixteen relevant scattering matrix elements of biological particles system with exactly known scattering characteristics must be studied. It is obvious that the measurement of spheres in the size regime of biological particles allows us to test the parameters of the adapted theory and the experimental setup. However, it is implicit in this test system of spheres that no major differentiation between M_{22} and M_{11} or M_{33} and M_{44} can be obtained. Therefore, the consistency of M_{22} and M_{11} was checked by additional measurement of the combinations. From these measurements M_{22} and M_{11} could be derived. No major differences in $M_{11}$and M_{22} were detected. Measurement of the M_{44} term was omitted since it requires a retarder analyzer. This would introduce inevitable complications especially for the measurement of the laser signal. The consistency of M_{33} =M_{44}in the directions of the beam was verified. To explore the extent to which the 16 scattering elements can be measured, a number of independent experiments were performed. We have demonstrated that quantitative measurement of the scattering matrix elements of biological particles. It has been shown that theoretical study of this type of experiment requires implementation of the beam shape into Mie scattering functions. In addition large cone integration must be applied to account for the relatively large detector surfaces. Furthermore a model is proposed to describe the scattering matrix of biological particles in the medium. It was illustrated that depolarization must occur in biological particles. In the near future we shall concentrate on the discrimination and subsequent separation of human tissues by means of depolarization information.

6.2.2 Conclusion

The presented results establish the ability of the described Mueller matrix imaging system to precisely mea- sure within a 97% accuracy the 16 elements of a sample in either transmission, specular reflection, or backscattering modes. In the current configuration, it is clear that using 16 polarization images in the Mueller matrix reconstruction process is a trade off between maximizing accuracy a benefit of using an over determined system and acquisition time. Thus depending on the reconstruction process, it takes approximately 70 or 150 s to reconstruct the 16-EMM using either the 16 polarization images, respectively, however, it should be noted that these times are not a direct reflection of the speed of either the electro-optic components or detector. The maximum sample calibration matrix element error of 6.00% and 3.74%, for 16 polarization images respectively, can be attributed, in part, to the laser beam in front of sample. This lack of spectral purity in the probing light beam has the effect of increasing the retardation errors, which are extremely wavelength dependent, therefore, resulting in noticeable errors in the circular polarization containing matrix elements. Going to an incoherent, coherence scrambled laser source, or using a narrower pass band filter could help compensate for this error.

Finally, the potential of the developed system for the detection of superficial cancerous lesions lies in its ability to remove pigmentation effects and to reject deeply backscattered light at different depths, based on the incident and backscattered polarizations within the tissue. These effects often mask the underlying superficial structures in laser tissue imaging. In addition, the ability to fully characterize the polarization properties of the sample under investigation can provide useful information in terms of the morphological structure differences present between normal and cancerous tissue. These changes can be used to help characterize and distinguish between tissue types. Furthermore, the ability to acquire such measurements in a minimal time frame gives promise for the future application of such a system to differentiate between normal, benign, and cancerous tissue. Future studies will be directed at exploring the angular dependence of such measurements and in the development of algorithms to aid in the characterization and differentiation process.

If you can imagine it, you can achieve it. If you can dream it, you can become it. (William Arthur Ward)

Chapter 7

MUELLER MATRIX POLARIMETRIC APPLICATIONS

7.1 Measurements of the optical properties of breast tissues in vitro using Mueller matrix Polarimetry

Laser transmission, absorption, and scattering technique for photon migration in tissues phantom with Mueller matrix polarimetry have been investigated in this study. Polarized laser transmittion, including depolarization of wave applied to biological tissues provide a comprehensive frame work and sample way for diagnostic and treatment of skin lesion. He-Ne Laser (λ=632.8 nm) imaging system is described for non invasive and non radioactive clinical procedure. The system generates 16 out put Mueller matrices for characterization of tissues. This matrix along with optical images can characterize the normal and malignant tissues for diagnostic as will as treatment procedures of breast cancer. Although the in vitro measurements are smaller then in vivo, but this research work provides a base for designing quick model of polarized laser tissues culturing and imaging. The optical polarimetric imaging system, shown in Fig.3.2, consists of two branches, which contain the optics necessary to create the input and output polarization states required for deriving the out put Mueller matrix of breast tissue like phantom. The sample is illuminated through He-Ne laser of output power 5 mW at a wavelength of 632.8 nm. Polarization optics is placed in front of the He-Ne laser, to generate linearly polarized light

Circularly polarized light is generated, by inserting a λ/4 mica retardation plate behind the linear polarizer, with the retarder principal plane at 45^0 with respect to the electrical field vector of the incident linearly polarized beam. The scattered light from the sample is focused to the analyzer and λ/4 plate for the desired variation of polarization of light. The out put light is then entered to the detector or CCD camera.

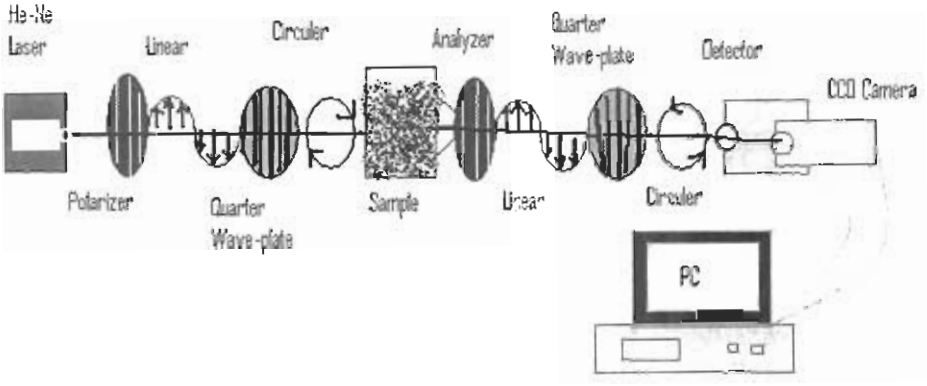

Figure 7.1 The experimental setup for measurements of transmitted Mueller matrix elements of breast phantom. A He-Ne laser beam with an output power of 5 mW at a wavelength of 632.8 nm is used as the light source. The laser light is directed on polarizer P1 for obtaining linearly polarized light. The circularly polarized light is generated, by inserting a quarter mica retardation plate behind the linear polarizer. The out put polarized light is directed to polystyrene sphere suspension turbid medium, and again pass through linear polarizer, quarter wave plate and recorded on photodiode detector and CCD camera, which is controlled and operated with Lab software.

7.1.1 Preparation of biological tissue sample

Freshly excised fat and liver tissues of goat were procured from a commercial butcher and cleaned thoroughly to remove dirt, if any. Thereafter, to remove traces of blood, these were soaked in physiological saline for 30 min. prior to measuring their reflectance, the saline and moisture from their surfaces were mopped with blotting paper. These tissues were used within 1 hour after collection.

7.1.2 Experimental results

The measurements of media with different absorption and scattering properties (water, vegetable oil, milk, Intralipid) and corresponding experimental phantom bodies (different absorbers such as balls, rods or tubes inside a highly scattering turbid medium) served as an approach to the subject [see Table.7.1]. Tissue-like media beside water and fat, the most important absorbers in all biological tissue are the blood pigments oxy- and deoxy hemoglobin (Hb and HbO). Thus all the other components play a secondary role. Fig 7.2 shows the transmission of these normal and malignant tissues pattern 632.8 nm.

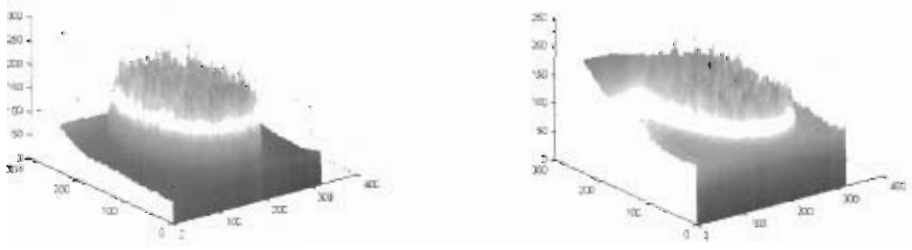

a b

Figure 7.2 The output transmitted intensity for (a) normal breast tissue and (b) malignant tissue.

The main absorption feature of phantom is melanin and the strength of the fat signal (or the oil shown here) will therefore be very variable, and differs from water. The local blood

content is especially important for transillumination of living tissues because total light absorption increases with the blood concentration. This can critically limit the transmittance of thick tissues, as the absorption coefficient of whole blood increases by several orders of magnitude below 600 nm. The absorption coefficients of the individual constituents oxy (HbO) and deoxyhemoglobin (Hb) have been taken from the literature and converted into transmission data to enable a comparison with the transmission characteristics of all the other contents. The mean adult hemoglobin concentration (HbO + Hb) is 2.3 mMol per litre blood with an HbO fraction of around 90 to 100% in arterial blood and from 20 to 70% in venous blood sample. Thus the prime absorbers blood and water form a diagnostic window for thick biological tissue, the limit for shorter wavelengths is approximately 550 nm [117]. Measurements of highly scattering media reflect reality more closely than the merely absorbing media, i.e. diluted milk and Intralipid. The results for the first medium (which consists entirely of fat) and the other two substances (which contain practically only water) clearly illustrate the spectral characteristics of these prime absorbers. In part, transmission spans three orders of magnitude (milk, Intralipid, at 10 mm thickness), the difference between water and fat characteristics between 600 and 850 nm remains small, even for highly scattering media with long path lengths [118].

The experimentally measured Mueller matrix from Fig. 7.1 in the case of no sample is in the form of the identity matrix for each reconstruction case, as described in below matrix.

$$[M] = \begin{bmatrix} 1 & 0.874 & 0.385 & -0.801 \\ 0.678 & 0.961 & 0.850 & -0.001 \\ 0.593 & 0.368 & 0.829 & -0.004 \\ 0.233 & 0.062 & 0.002 & 0.060 \end{bmatrix} \tag{160}$$

	Tissue	Absorption coefficient (u_a)	Scattering coefficient (u_s)
1	Goat fat	0.63	37.2
2	Goat liver	1.01	14.8
3	Normal tissue (phantom)	1.34	5.3
4	cancerous tissue (phantom)	0.92	7.5

Table.7.1 Absorption and scattering coefficient of normal and cancerous tissues at 632.8 nm wavelength [118].

For healthy tissues

$$[M]=\begin{bmatrix} 1 & 0.774 & 0.732 & -0.001 \\ 0.778 & 0.320 & 0.50 & -0.001 \\ 0.693 & 0.468 & 0.632 & -0.104 \\ 0.033 & 0.002 & 0.102 & 0.250 \end{bmatrix} \quad (161)$$

For malignant

$$[M]=\begin{bmatrix} 1 & 0.774 & 0.632 & -0.001 \\ 0.778 & 0.61 & 0.50 & -0.001 \\ 0.593 & 0.468 & 0.882 & -0.004 \\ 0.003 & 0.002 & 0.002 & 0.193 \end{bmatrix} \quad (162)$$

The 16 output polarization Mueller matrix elements can characterize and provides a fingerprint for different tissues. The elements M_{11} and M_{22}, which are the addition of the

orthogonal horizontal and vertical linear polarization cases, confirms that polarization imaging can be used to eliminate pigmentation aliasing and allows the observation of the underlying tissue structure. In addition, the differences in the details of the underlying tissue structure between the elements other than M_{11} and M_{22}, indicate that the retention of polarization information is also dependent on the system input and output polarization states [Fig.7.3]. The specific experiments reported in this study have concentrated on the measurement of the scattering matrix of biological particles. One of the major problems arising in this type of experiment is related to the extreme short sampling. In addition there is deficiency in our knowledge concerning which scattering matrix elements of biological particles are of fundamental interest.

Experiments in a turbid system are mainly concerned with finite particles. Therefore, characterization of complete population is of main interest. Fortunately, symmetry conditions, especially valid for an ensemble of particles measured in a system reduce the number of independent matrix. Particles in a medium are randomly oriented on passing the laser beam. Therefore ensemble averaging can be applied. The characteristics, implicit in a experiment, contribute positively to the light scattering depolarization measurements of biological particles. On the other hand, however, the complete optical equipment demands some experimental and theoretical adaptations, the sharply focused laser beam constrains the theoretical description of the interaction of a particle with the laser beam.

Furthermore a Mueller matrix model is proposed to describe the scattering matrix of breast tissues in the medium the output Mueller matrix of air, normal and malignant tissues are given in Eq 160, 161 and 162. The difference in the linear and circular output transmission provides detail information's about the tissues under investigation [Fig.7.4]. To investigate the possibility of application of a system to measure the sixteen relevant scattering matrix elements of biological particles system with exactly known scattering characteristics must be studied. It is obvious that the measurement of biological particles allows us to test the parameters of the adapted theory and the experimental setup. However, it is implicit in this test system of spheres that no major differentiation between M_{22} and M_{11} or M_{33} and M_{44} can be obtained. Therefore, the consistency of M_{22} and M_{11} was checked by additional measurement of the combinations.

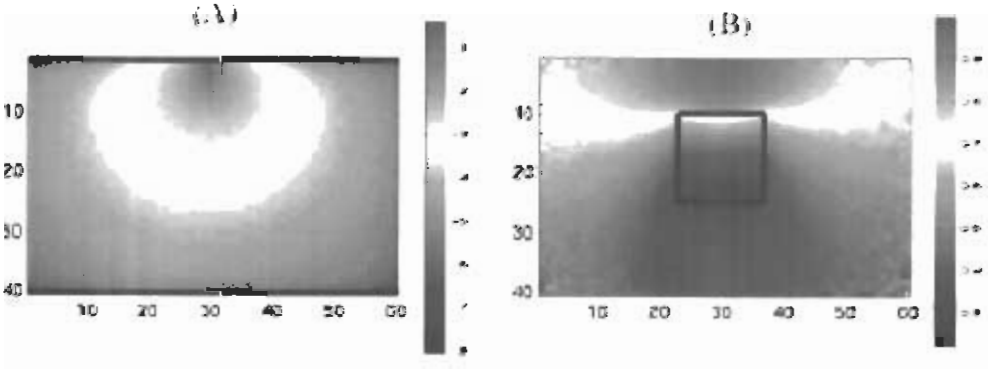

Figure 7.3. The transmitted output images at linearly polarized light for (A) normal and (B cancerous tissues.

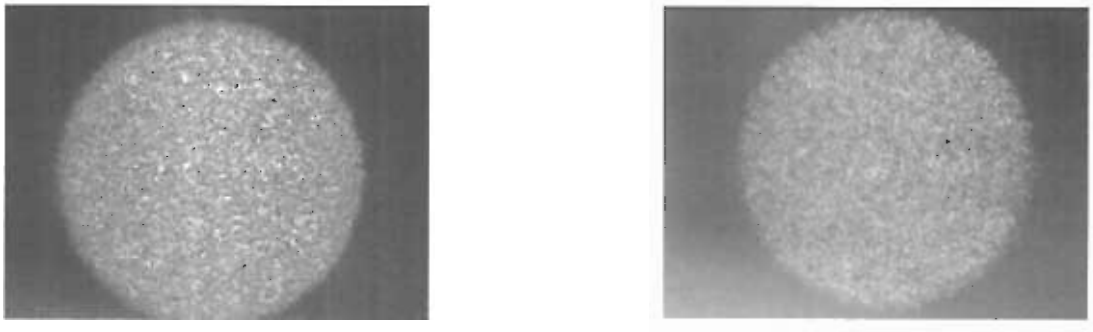

A B

Figure 7.4 the transmitted output images of turbid phantom for (A) a linearly polarized light and, (B) circular polarized light.

From these measurements M_{22} and M_{11} can be derived. No major differences in $M_{11}$and M_{22} were detected. Measurement of the M_{44} term was omitted since it requires a retarder analyzer. This would introduce inevitable complications especially for the measurement of the laser signal. The consistency of M_{33} =M_{44}in the directions of the beam was verified. To explore the extent to which the 16 scattering elements can be measured, a number of independent experiments were performed. It has been shown that theoretical study of this type of experiment requires implementation of the beam shape into Mie scattering functions. In addition large cone integration must be applied to account for the relatively large detector surfaces.

If tissue changes (e.g. tumors) in terms of its absorption or scattering properties to differ from surrounding (healthy) tissue, it should be possible to demonstrate this as a matrix elements. Although it is difficult to simulate actual conditions in corresponding phantom experiments, we can determine the sensitivity of such experiments. For this purpose various absorbers were placed in the middle of a 10 mm thick diluted milk solution and the measured transmission intensity was divided by the one of undiluted milk spectrum. It is logical that relative transmission values less then 1 indicate higher transmission by the phantom containing absorber, and vice versa. The wavelength dependency of the contrast correlates depends on the difference between the absorption characteristic of the object and its surrounding media. Clinical trials will be necessary to establish the correct wavelength for detecting pathological lesions with the highest possible contrast. The tissue specimens were directly illuminated in phantom. In contrast to the tissue-like media, the blood fraction can be identified by reduced transmittance at < 650 nm. The total transmission for the tissue thicknesses selected for these tests varied by more than two orders of magnitude.

7.1.3 Conclusion

In addition to tissue-like materials (water, vegetable oil, milk, and Intralipid), different types of animal tissue related to the female breast tissue in vitro have been investigated with the aim of correlating the dominant spectral features. Tissues that contain water are clearly distinguishable from fatty tissue on account of the absorption bands for water. The transmission differences are sufficiently clear to permit characterization of the human female breast.

The presented results establish the ability of the described Mueller matrix imaging system to precisely measure the 16 elements of a sample in either transmission or scattering modes. In the current configuration, it is clear that using 16 polarization images in the Mueller matrix reconstruction process is a trade off between maximizing accuracy a benefit of using an over determined system and acquisition time. Thus depending on the reconstruction process, it takes approximately 70 or 150 m to reconstruct the 16-EMM using 16 polarization images however, it should be noted that these times are not a direct reflection of the speed of either the electro-optic components or detector. Finally, the potential of the developed system for the detection of superficial cancerous lesions lies in its ability to remove pigmentation effects and to reject deeply scattered light at different depths, based on the incident and scattered polarizations within the tissue. These effects often mask the underlying superficial structures in laser tissue imaging. In addition, the ability to fully characterize the polarization properties of the sample under investigation can provide useful information in terms of the morphological structure differences present between normal and cancerous tissue. These changes can be used to help characterize and distinguish between tissue types. Furthermore, the ability to acquire such measurements in a minimal time frame gives promise for the future application of such a system to differentiate between normal, and cancerous tissue. Future studies will be directed at exploring the angular dependence of such measurements and in the development of algorithms to aid in the characterization and differentiation process.

7.2 The optical parameters measurement for skin tissue imaging and auto-florescence in vitro

From an optical point of view the outer most skin layers contain numerous structures by which penetrating radiation may be scattered as well as absorbed. The nature and strength of scattering and absorption may strongly influence the depth of penetration. We illuminated the chicken breast skin tissues with collimated radiation of 400-700 nm Nd-YAG pumped dye laser, and measured skin optical properties for dry and hydrated sample in vitro. Total reflected and transmitted intensities were recorded by which scattering, absorption and anisotropic factors of the sample. The in vitro optical parameters are higher then in vivo measurements. Our in vitro results are in agreements with other data available in literature [119]. Hydration of skin is found to influence its scattering properties. Skin autofurescence spectra were acquired under different excitation wavelength, from this spectrum the difference of tissues can analyzed.

7.2.1 Skin tissue imaging

To model tissues, the parameters involve in laser tissue interaction mechanism are important to measure. The values of absorption coefficient μ_a, scattering coefficient μ_s are normally obtained by measuring total reflectance R_{total} and total transmission T_{total} respectively

Several studies on the derivation of optical properties of skin samples from measurements with integrating sphere have been published [119]. The chicken breast skin sample was placed on the flat surface of the quartz hemisphere (radius 11 mm), the sample was covered with a circular diphagram of 1mm diameter, due to approximate match of the refractive index of the hemisphere and the sample, the light ray emerging from the skin sample passed through the skin-quartz interface without being refracted, impinged perpendicularly on the optics curved quartz-air interface. By using hemisphere as a sample carrier, we ensured that the angle at witch the light rays emerged remained approximately the same as the angle into which they were scattered in the intact skin. A collimated beam of monochromatic radiation illuminated the sample.

In order to investigate the influence of hydration on the scattering properties of the skin, two samples were hydrated overnight on a saline solution in covered dashes. The data were recorded at several wavelengths for perpendicular incident radiation, the sample was allowed to dry in room air and intensity is recorded.

The transmittance and reflectance data of the sample thickness 8mm in 400-700nm wavelength range with the step of 10nm were obtained using spectrophotometer to reconstruct the optical parameters, absorption coefficient, scattering coefficients and anisotropic factor. Various approaches have been used Kubelka -Munk theory, Diffusion approximation, Monte Carlo simulation and adding–doubling methods etc, for determination of reliable optical properties and need real geometry of the experiment and angular structure of radiation in the sample. Absorption and scattering coefficients were measured using total reflectance of the sample; anisotropic factor can be measured from independent measurements or empirical formula.

7.2.2 Experimental Results

The accuracy of determined absorption and scattering coefficients in all the discussed in vitro methods depends upon the accuracy of measured total reflectance and total transmission. The results of an experiment are in Table 7.2.

Author	Method	u_a $(mm)^{-1}$	u_s $(mm)^{-1}$	Anisotropy Factor"g"
Jacques et al	In Vitro	0.27	2.20	0.871
This work(dry sample)	In Vitro	0.19	2.38	0.834
This work(hydrated sample)	In Vitro	0.13	2.48	0.827

Table 7.2 Optical properties of chicken breast tissues at 400-700nm obtained by R_{total} and T_{total}.

Measurements of reflectance and transmittance were performed using a detector and Nd-YAG laser with detector. The zero transmittance (T_0) was measured by placing chopper between beam and entrance port of the integrating sphere. The 100% transmittance (T_{100}) was determined by placing an empty mass in the sample beam. Sample transmittance and reflectance is measured through detector. The experiment was repeated for hydrated and dry sample of skin, several times. The measurements were made over the 400-700 nm wavelength region. The R_t and T_t was computed using the relation,

$$R_t=(R_s - R_0)/(R_{100}-R_0)$$
$$T_t= (T_s-T_0) / (T_{100}-T_0). \quad (163)$$

The exact description of photon propagation is governed by the radiative transport equation, but it cannot be solved exactly, except for few special cases. Bears' law is a simple model that yields reasonable results in media when absorption dominates scattering. However most biological tissues are highly scattering and Bears' law is not applicable at many wavelengths.

In our experiment the optical parameters, μ_a, μ_s and g are summarized for several wavelength, placing the sample in integrating sphere the Absorption and scattering profile for hydrated and dry samples were obtained at several wavelengths, represented in Fig 8.5, 8.6. It is found that as a result of dry skin scattering is reduced. The amount of reduction does not depend strongly on wavelength but on hydration and other factors also, the hydrated sample look turbid and dry as opaque and thin. The general impression from our measurements is of a forward oriented scattering mechanism. Scattering occurs both at surface and throughout the skin medium. The reduce scattering of hydrated and dry sample is maximum at 470nm (Fig.7.6), as the melanin content show scattering at 470nm. On comparing our result to S. L. Jacques et al. [119], it becomes clear that in our sample scattering is less. The decrease in scattering and absorption, due to surface or volume scattering reduction cannot be separated, volume scattering in Fig 7.6, present in hydrated sample disappear in dry sample. When the optics of full thickness skin are being modeled, dermis scattering is the most important, as the penetrating radiation is quickly diffused. It is still just an approximation of the true solution. A more extensive theory would require

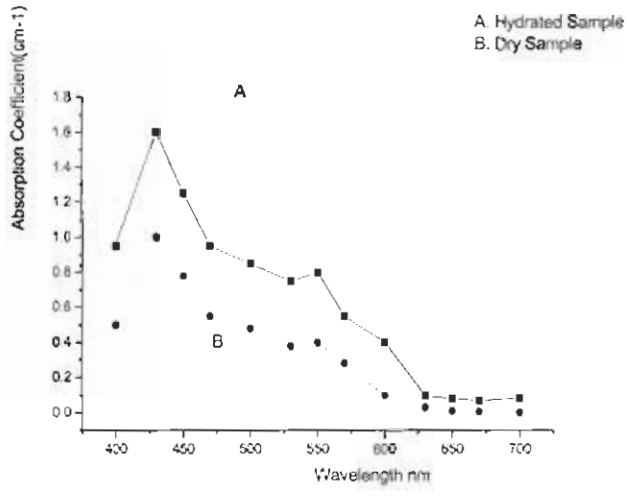

Figure 7.5 The absorption spectra of chicken breast skin tissue with detector.

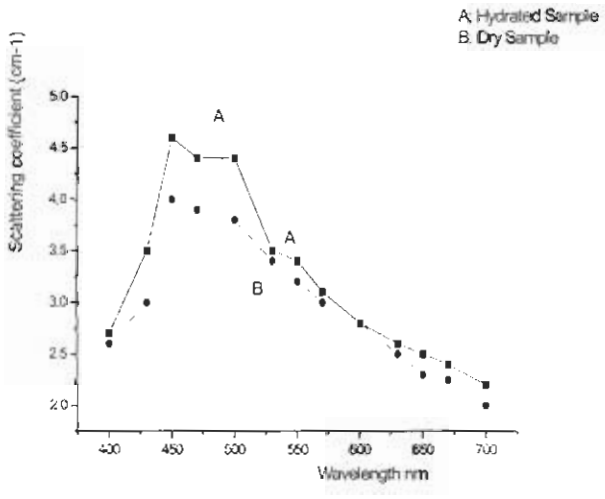

Figure 7.6 The scattering spectra of chicken breast skin tissue, with detector

for sophisticated numerical model for computation. This cannot be performed very accurately because of the large biological variations.

7.2.3 Discussion

The experimental found values for u_a and u_s are influenced slightly by melanin content of epidermis. Therefore small absorption coefficient cannot be determined accurately, as the sum of R_{total} and T_{total} is close to 01. Moreover loss of light within the sample holder may contribute to an increase in the absorption coefficient of tissue. Monte Carlo simulation in good agreement with those measured by Z.Song et al. [121].

Absorption measurement evidences a large variation from tissue to tissue of the absorption coefficient value ranging from < 02 to 20 cm^{-1}. This fact is easily explainable due to different blood contents, which still remain in the sliced samples. Different samples have verity in absorption coefficients. However integrating sphere in cavity measurements makes it possible to estimate reasonably the absorption coefficient of sample with a large scattering coefficient. Scattering measurements shows non-isotropic pattern. The anisotropic g factor value are some what higher then those reported (0.81), under the hypothesis that cell and there internal structure can be approximated by spherical particles and that the main contribution to scattering is due to the cell envelope. The difference between the measured values of u_a and u_s is due to measuring, calculation techniques and sample handling etc.

The measurements from integrating sphere is not straight forwarded, several studies on accuracy of measuring with integrating sphere shows that errors may be due to that the light which leaves the sample re-enter the tissue sample after reflectance. Measurements of total transmission depend on reflectance properties. One of the reasons of difference in results taken by Jacques et al. [119], by our calculations, is that they heated the sample which changes the scattering properties of the tissue. Scattering is almost doubles when the sample is heated. The value of g started to decrease slightly at less then 500nm and greater then 650nm (Fig. 7.9). Reflective index was taken as 1.4 for turbid medium and 1 for surrounding. We consider the rectangular shape of detector and the different values of μ_a and μ_s can be used to obtain the same intensity ratios at detector.

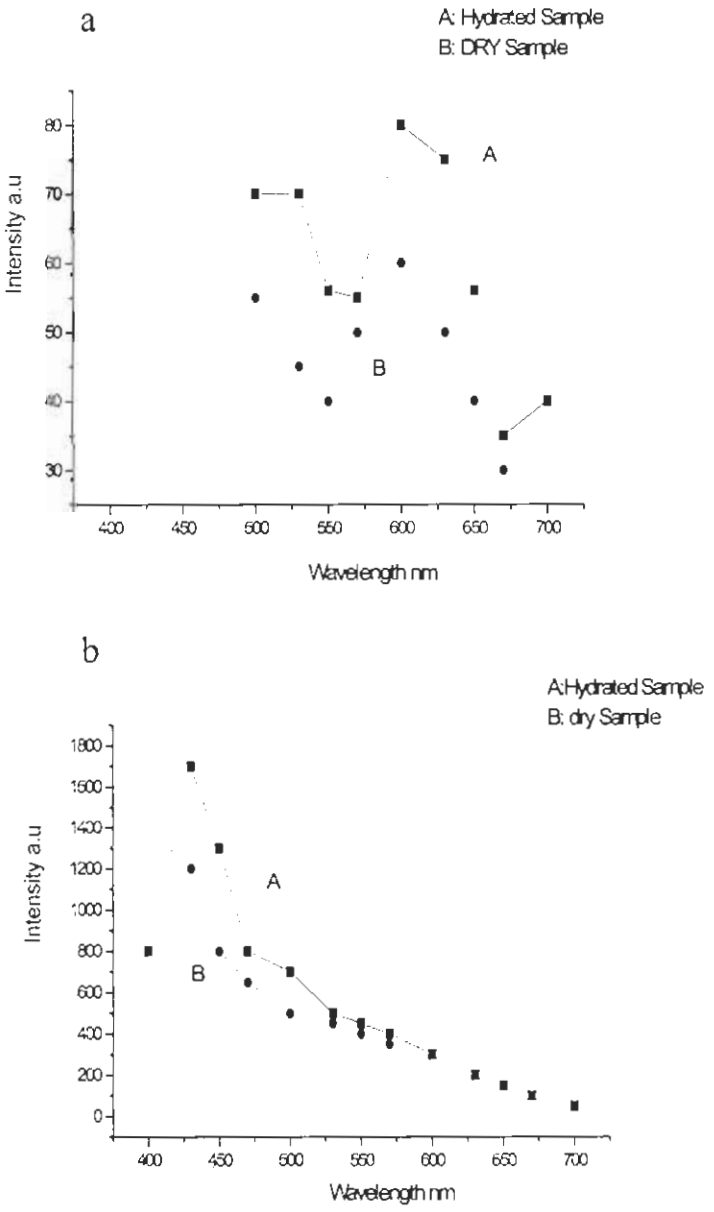

Figure 7.7 Auto fluorescence of chicken breast skin tissue for hydrated and dry sample. (a) Non heated. (b) Heated.

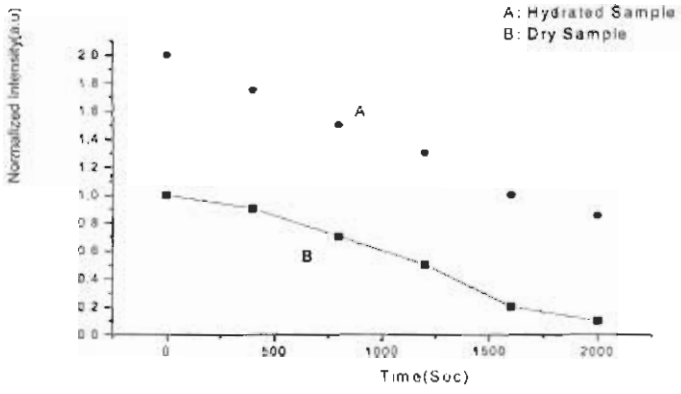

Figure 7.8. Transmitted intensity verses time behavior of hydrated and dry sample.

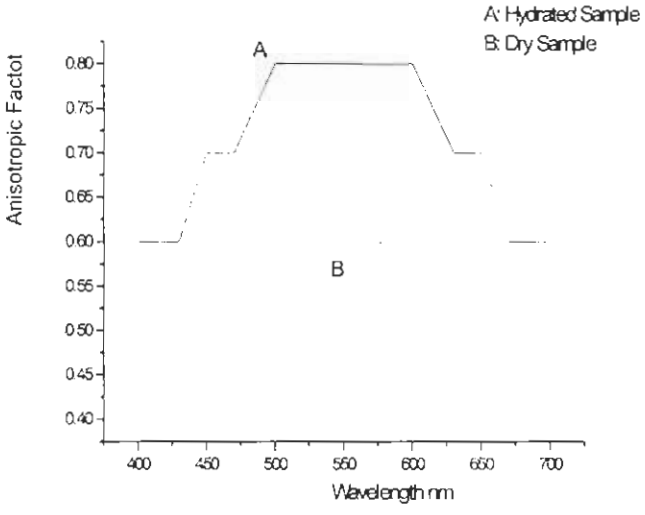

Figure 7.9 Anisotropic factor "g" as a function of wavelength.

In Fig.7.7-auto fluorescence data is taken from 400-700 nm excitation wavelengths and present the curve average of our several experiments. The data is similar to whole skin in vitro autofluroscence, its maximum at 420nm for dry and hydrated simple and maximum at 450nm wavelength. Florescence responsible for emission in this range may be proteins and NADH. Although the protein absorption region is located at shorter wavelength, NADH considerably presents in upper epidermis layer. In Fig.7.7 (b) we noted small maximum at 510nm region.

For the whole skin in vitro and 442nm excitation of skin strong peak was observed at 632nm, this peak is distributed to natural flurorapher in the sample. The spectra of dry skin is taken in dark at room temp, during first 24 hrs fluorescent intensity decreases by 07% and after four days to 70%, but at shorter wavelength rate of degradation is higher. The optical properties verses time behavior of the skin tissues is shown in fig.8.8. It concluded that intensity should be measured for skin in vitro not later then one day after sampling. The moisture effect should be considered for intensity measurements in Fig.8.9 the anisotropic factor g is shown as the function of wavelength and maximum at 500 to 650nm.

7.2.4. Conclusion

The method of our in vitro optical parameter measurement is not suitable to in vivo, but it gives important information for skin tissue modeling. Our experimental data and the investigations were performed at 400-700nm provides useful information for tissue imaging. It is reasonable to assume that the scattering coefficient is slightly dependent on wavelength in the visible range. This is not true for absorption coefficient, since tissue blood content and specific absorbing pigments play the main role in determining tissue characteristic. This fact should be kept in consideration while performing the evaluation of light flux distribution in depth. More efforts, therefore be made to determined more precisely the absorption and scattering coefficients and how they are related to other tissue contents. Analysis of autofluresence spectra of skin sample is suggested as a mean for skin status diagnostic and monitoring. The optical property of chicken skin tissue is different for different tissues. The variation in coefficients most likely was due to sample preparations and prolonged freezing time, which leads to cell rapture.

7.3 Development of glucose monitoring system with Mueller matrix polarimetry

The polarimetric glucose monitoring with polarized laser light of diabetic patients is the noninvasive method and is the topic of resent interest. We have investigated the interaction of polarized light with optically active turbid glucose water to aqueous humor for in vitro glucose monitoring. The interior part of the eye contains birefringent scattering medium for glucose measurement. In this work Mueller matrix polarimetric technique for simultaneous extraction of rotating linear and circular polarized light is theoretically discussed and experimentally implemented. This method requires calculation of Mueller matrix for different orientation of polarized light through turbid sample. Our research provides a model for in vitro and base for in vivo eye glucose corneal birefringence measurement with polarized laser to check the diabetic level of the patent.

7.3.1 Glucose measurement through polarimeter

Diabetes mellitus is the major leading cause of death. The primary defect in diabetes mellitus is a lack of insulin production [122, 124]. Insulin is hormone that regulates the transport of glucose from the blood stream into fat and muscle tissue, where glucose is utilized as an energy source. The insulin deficiency in diabetes leads to hyperglycemia and the inability to utilize glucose as a source of energy [125, 126]. Insulin replacement therapies are commonly prescribed in the treatment of diabetes mellitus [127, 128]. Diabetic patients regulate their insulin dosing by monitoring blood glucose levels. Long-term hyperglycernic states have been shown to accelerate the evolution of the complications associated with diabetes. Therefore, with tight control of blood glucose concatenations, the complications associated with diabetes mellitus can be minimized [129-130]. Unfortunately, many diabetics do not monitor their blood glucose concentrations at recommended frequencies. Lack of compliance in blood glucose monitoring is due partly to the inconvenience, pain, and tediousness of current home monitoring techniques. Patients who fail to maintain hyperglycemia suffer higher rates of morbidity and mortality caused by the associated complications of diabetes mellitus [131].

Due to the increased risk of infection whenever the blood-skin barrier is broken, a noninvasive blood glucose monitor would be ideal [132]. A sensitive polarimeter was designed to measure glucose concentrations within the aqueous humor of the eye the proposed glucose sensor is noninvasive and produces no medical waste. Finally, the polarimeter would not require a blood sample, thus reducing the risk of infection. The non-invasive detection of blood glucose levels in humans is an ambitious goal for managing diabetes. Diabetes can lead to severe complications over time. These can include blindness, renal and cardiovascular diseases, peripheral neuropathy associated with limb [133]. The proposed model is primarily based upon the measurement of the glucose concentration in the aqueous humor using polarimetry [134]. Test sites being explored include eye, fingertips, cuticle, finger web, forearm and ear lobe. However, many hurdles remain before these products reach the commercial market place. Glucose concentration in the aqueous humor closely mimics glucose levels in the blood [135]. Polarimetric techniques use the property of glucose as an optically active analyte that rotates the plane of polarization of incident linearly polarized light. The first documented use of polarized light to determine sugar concentration dates back to the late 1800s, where it was used for monitoring industrial sugar production processes. However, it is only in the last two decades that the use of polarized light has been applied to the physiological measurement of glucose. In 1982 March et al. were the first to propose the use of polarimetry to indirectly estimate blood glucose levels via the aqueous humor of the eye. They found in order to measure mille degree sensitive rotations due to glucose at physiological levels a very sensitive and stable polarimeter is required, in the past decade considerable work has been done in the development of such a polarimeter

In general, photons propagating in turbid media have their incident direction, phase, and polarization randomized by multiple scattering. Mueller matrix polarimetric technique provides simple analytical model for noninvasive glucose sensor. It is an experimental polarization birefringent measurement system.

A beam of light is composed of electromagnetic waves oscillating perpendicular to direction of light propagation. The polarizer and retarder rotate the polarization plane of light as it propagates through the sample. The plane of polarization may either be rotated

clockwise or counter-clockwise. The equation which relates optical rotation to a medium specific rotation is given by equation [135],

$$[\alpha]^{T}{}_{\lambda,pH} = \frac{\alpha}{LC} \tag{164}$$

where α is the specific rotation of an optically active compound in degrees on specific temperature T and PH of the system, wavelength λ, the optical path length L in dm, and the sample concentration C in grams of mass per ml of solution. The relationship in term of wavelength for specific rotation is given by Drude's equation [135],

$$[\alpha]^{T}{}_{\lambda,pH} = \frac{k_0}{\lambda^2 - \lambda_0{}^2} \tag{165}$$

Equation (2) is an approximation of Drude's equation and is valid only outside the absorption region for the molecule of interest. The optical instrument used to measure rotation due to an optically active sample in polarimetric system have the main components of polarizer, quarter wave plate, sample cell, a second polarizer known as the analyzer, a detector and CCD camera [Fig 3.2].

As the beam passes through the sample, the plane of polarization will rotate according to the concentration of sample and the path length of container. If an optically active sample is introduced into the system, the intensity of transmitted light will be proportional to the amount of rotation in polarization due to the sample. If the optical properties of a substance are same in all the directions regardless of its orientation, the substance is said to be isotropic. In many crystalline structures and some organic substances the optical properties are not the same in all directions and they have more than one index of refraction, these materials are known as anisotropic. Birefringence is a property of anisotropic substances in which two orthogonally oriented different refractive indices of light exist, the ordinary refractive index, (along the slow axis) and extraordinary refractive index (along the fast axis). This difference in the speed of propagation between the x and y polarized components induces a phase difference, depending on the magnitude of the components and the relative phase retardance. We can see different states varying from linear to circular light.

M_{11}=HH+HV+VH+VV	M_{12}=HH+HV-VH-VV	M_{13}=PH+PV-MH-MV	M_{14}=RH+RV-LH-LV
M_{21}=HH-HV+VH-VV	M_{22}=HH-HV-VH+VV	M_{23}=PH-PV-MH+MV	M_{24}= RH-RV-LH+LV
M_{31}=HP-+HM+VP-VM	M_{32}=HP-HM-VP+VM	M_{33}=PP-PM-MP+MM	M_{34}= RP-RM-LP+LM
M_{41}=HR-HL+VR-VL	M_{42}=HR-HL-VR+VL	M_{43}=PR-PL-MR+ML	M_{44}= RR-RL-LR+LL

Table 7.3. Calculation of the Mueller matrix images. The notation is as follows: the first term represents the input polarization state, while the second term represents the output polarization state. The states are defined as: H for horizontal, V for vertical, P for+45°, M for -45°, R for right circular, and L for left circular.

Constituent	Concentration (mg/dl)	Constituent	Concentration(mg/dl)
Glucose	51	Phosphorus	04
Protein	150	HCO_3	20
Urea Nitrogen	12	Sodium	140
Magnesium	1.5	Potassium	3.5
Calcium	04	Chloride	100

Table.7.4 Constituents of the aqueous humor solution

7.3.2 Results and discussion

A total of eight experiments were conducted with 632.8 nm He-Ne laser using a hyperglycemic concentration range for both the glucose-doped water and aqueous humor

mediums. The solution concentrations are illuminated to determine the model. Fig.7.10 shows the results of the measured glucose concentration in water solution. The experimental results of the mixture of glucose with ascorbic acid are shown in Fig 7.11. The rotational accuracy needed to perform these experiments can be calculated through experimental setup shown in Fig. 3.2 using the specific rotation, path length, and concentration. Therefore, for our system, the minimal rotational accuracy needed for normal blood glucose concentrations is $\alpha = 0.5*100*44.8/100 = 22.4m\deg$. The predicted glucose concentration was evaluated for actual concentration without a posterior retarder and polarizer in the optical train [see Fig.7.12]. The average glucose concentration in this model is 4.5 mg/dl and less than 10 mg/dl, which means the accuracy is less then 0.5 comparable to the work of Goetz. The Fig.7.13 shows the output intensity in volts for the given solutions concentration. The decrease in the intensity of aqueous humor solution is due to its birefrengent behavior. In this measurement we have used only the linear light (as our laser source is linear polarized). In water dissolved glucose solution the depolarization and intensity decrease varies gradually with change of glucose concentration. This process was repeated for several times for same composition.

The Mueller matrix 2D images [see Fig.7.14] of glucose concentration taken for aqueous humor solution by polarimetric setup and the resultant matrix of table 7.6 provide comprehensive details about the sample. The M_{11} element of the matrix shows the direct intensity pattern and the characteristic of the illuminating light. The other matrix is the results of linear and circular polarization output. These images and matrix were acquired through 49 orientations measurement given in table.7.3 of the polarized optics. Mueller matrix M_{22}, M_{33} and M_{44} are unitary and represent the horizontal, vertical, $\pm 45^0$, L-circular and R-circular polarization. Only looking to the diagonal matrix of the Mueller train, one can guess about the material concentration. These images along with matrix for normal glucose concentration can be taken as a model for polarimetric glucose sensor, and compared to other samples.

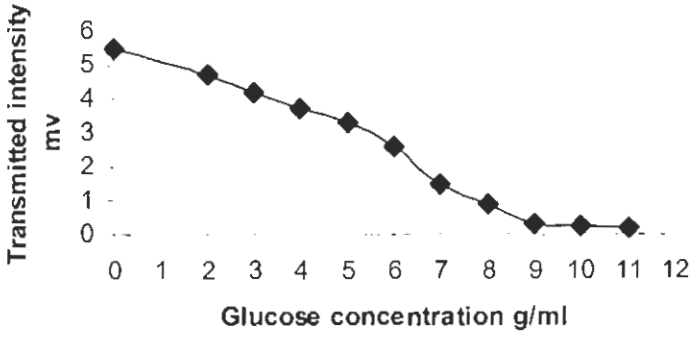

Figure 7.10 The output laser intensity verses glucose concentration for water glucose solution.

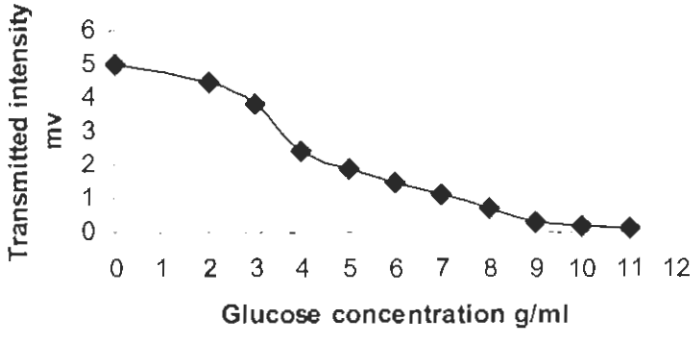

Figure 7.11 The output laser intensity verses glucose concentration for aqueous humor solution.

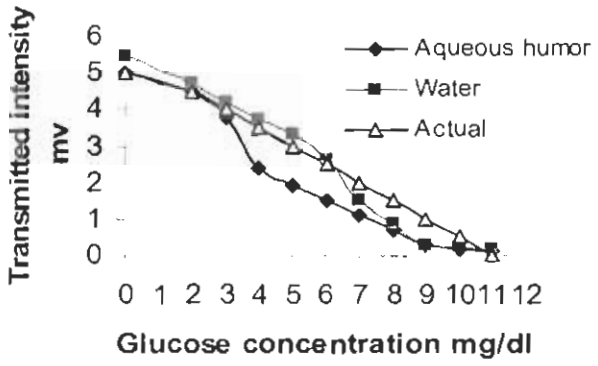

Figure 7.12 Predicted versus actual glucose concentration for water mixed and glucose doped aqueous humor experiment.

Figure 7.13 The out put intensity of the sample at a linear polarizer

The results of this investigation with polarimetric system for glucose concentrations from ascorbic acid and albumin are measured. In this study, the effect of ascorbic acid and

albumin alone at physiologic concentrations was indeed minimal compared to that of hyperglycemic glucose in the aqueous humor of the eye. Furthermore, since ascorbic acid, albumin, and other confounders in the aqueous humor are countra-rotatory, the effect of their combination at physiologic concentrations was even less. It can be assumed that material in the sample will also possess unique optical rotation spectra. A complete study of the optical rotation of the medium found in the aqueous humor is not readily available and therefore needs to be performed. Based on the work presented here and using the new equipment, the optical rotation of molecules in the aqueous humor will be established

If the albumin was undergoing any type of conformational changes, then the voltage out of the polarimeter would also fluctuate. Further, naturally occurring small fluid movements in the test cell would also affect the position of the protein molecules in the solution. These changes could cause the system to drift since the conformational variations and fluid movements of the solution occur as random events throughout the solution. Although a nonlinear analysis might be appropriate for the in vitro system that may be affected by conformational changes, these changes are not expected to occur in vivo due to the association constants of the molecules naturally occurring in the aqueous humor. Therefore, the analysis for this work focused on the use of a polarized model, which should be more appropriate for the final system. Moreover, with more optimized equipment the polarization analysis could likely be developed for glucose sensor. Lasers demonstrated an increase in the rotation observed when ascorbic acid was added to the glucose concentrations and a decrease in the observed rotation with albumin was added to the glucose concentrations.

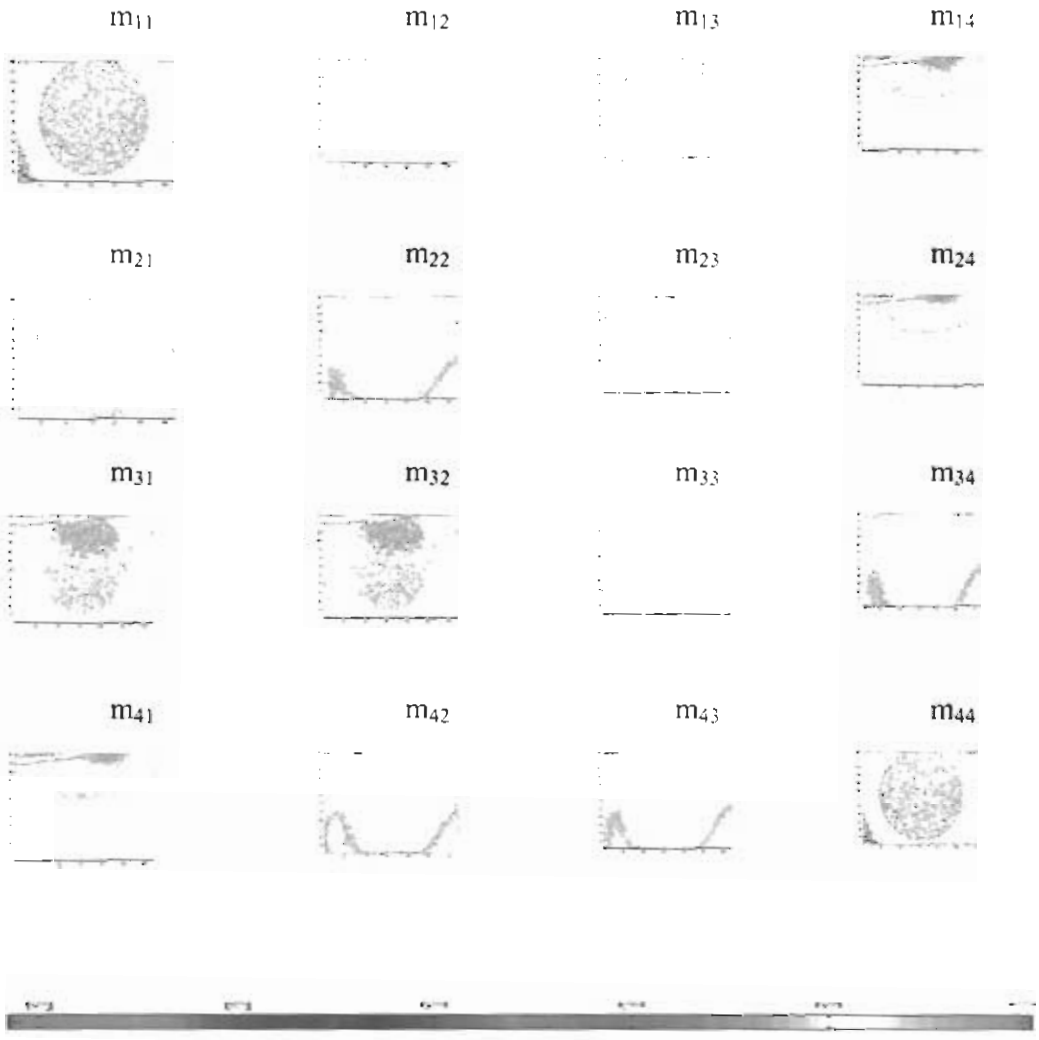

Figure 7.14 The two dimensional images of 16 Mueller matrix transmitted intensity elements for aqueous humor.

m_{11}	m_{12}	m_{13}	m_{14}
1.012	0.501	-0.254	0.059
m_{21}	m_{22}	m_{23}	m_{24}
0.582	0.651	0.831	0.061
m_{31}	m_{32}	m_{33}	m_{34}
0.385	0.324	0.519	0.321
m_{41}	m_{42}	m_{43}	m_{44}
0.0653	0.325	-0.136	0.139

Table 7.5 The Mueller matrix data for transmitted polarized laser beam from aqueous humor glucose solution.

In general, scattering and absorption that are wavelength dependent could cause both an intensity variation and depolarization of the light. As the conformation of the protein

7.3.3 Conclusion

The presented results demonstrate the ability of the polarimeter to accurately measure glucose concentrations in both water and aqueous humor mediums. This research represents an important step toward the development of a noninvasive glucose sensor which may eventually be capable of detecting glucose levels in the aqueous humor of the eye. Polarimeter is the simplest method for glucose sensing system and its development for in vivo measurement provides a home base glucose sensor in easy way. Mueller matrix provides a fingerprint of the solution and detected analysis for glucose aqueous humor solution.

Chapter 8

Summary

We have developed a Mueller matrix polarimeter for characterization of turbid medium and biological tissues in vitro, using polarized light. The comprehensive matrix analysis for different samples provides detail information about optical properties of medium.

the 1st and 2nd chapter contains the essential background material related to polarization optics and light absorption, transmission, scattering and a review of the field of optical imaging, a introduction to Stokes, Jones and Mueller matrix optical calculus that is needed to understand the latter chapters. The review mainly concentrates on the analysis methods adopted in Mueller matrix imaging polarimetric setup. The 3rd chapter describes the material and methods adopted during the research, the polarimetric characteristics, experimental setup, error analysis and precaution needed for accurate results through Mueller matrix polarimeter

In 4th chapter the turbid medium is characterized by stokes vector polarimetry, the principal motive behind the development of optical Stokes vector polarimetry, which is cost-effective compared to time-resolved and frequency-domain techniques, is to provide a safe and effective method of detecting and specifying diseases in the soft-tissue structures. The applications of Stokes vector polarimetric system to tissue-phantoms and biological tissues show that the present technique could be employed to detect structural changes. This technique is sensitive to detect changes in absorption coefficient and the size of the particles of the medium. Due to its simplicity and versatility, this may prove to be an ideal system for structural analysis of turbid sample and soft tissues. Optical parameters quantify the medium and tissue changes, and imaging could further provide data on variability of tissue composition below the skin over an entire organ. The Stokes Mueller polarization images of transmitted intensity along with degree of polarization provides fingerprint of the turbid medium. Careful analysis of images and degree of polarization, one can differentiate the scatterer in term of its concentration, size, shape and orientation .The results are related

to polarized light propagation, and these densely packed images are likely to exhibit scattering and, therefore polarization effects. The linear polarization preservation is dominant over circular due to scatterer density rather then size of the particle in medium. We have seen that linearly and circularly polarized light propagates differently for turbid samples. Further, we have demonstrated that Stokes vector imaging by polarized light preferable to imaging with un-polarized light. Finally, we have indicated the structural features in turbid medium that influence the degree of polarization and the importance of these structures on polarized light propagation. We have demonstrated high-precision, low-noise polarimetric measurements in turbid media using LCVR Stokes polarimetric detection. The technique allows the polarized intensity measurements necessary to determine Stokes parameters in small interval of time i.e., less than 20 second.. The surviving polarization fractions in turbid suspensions have been measured in the forward direction and are in reasonable agreement with literature. The measurements of optical rotation in turbid suspensions demonstrate the possibility of determining polarization change in a highly scattering and depolarizing medium made of intralipid. Measurements of optical rotation that is due to turbid scattering phantom solutions when the depolarization is has higher values in highly birefringent solutions when intensities are transmitted over large areas, this is supported by literature [119].

In 5th chapter, the polarization properties of light scattered from a scattering medium have been investigated. It has been shown that the degree of polarization is sensitive to the optical properties of the turbid medium and this offers a potential tool for characterizing the medium. Calculation of the 16 element of the output Mueller matrix shows that theoretically only seven elements of backscattered light are independent and remaining nine can be calculated through symmetry relation The introduction of the Mueller-matrix concept for the scattered light provides detailed information about scattering media. Because the description of the optical characteristics with the Mueller matrix is complete, any information about particle size, refractive index, particle shape etc. has to be found in the Mueller matrix by careful analysis of the matrix elements. If some information about the medium cannot be extracted from the various matrix elements, this information cannot be extracted from any other additional scattering measurements. However, further information may be gained, for example, by measuring the diffuse transmittance, the

diffuse back reflectance at different incident and observation angles, or time-dependent polarization effects.

The polarization properties of scattering, depolarization, and absorption of optical active medium, nitrobenzene experimentally calculated trough Mueller matrix technique. We showed that the optical field passing through bulk nitrobenzene could be described by superposition of: (a) a non-scattered dc field, which is polarized and follows Kerr effect, (b) scattered un-polarized field, which doesn't follow Kerr effect, and (c) an absorbed field, which directly depends upon strength of applied electric field. Using the corresponding deterministic and stochastic Jones matrices, we have derived a simplified Mueller matrix representation in which only eight coefficients are required to describe the scattering, depolarizing, and absorption in bulk nitrobenzene. Using Stokes vectors, we are then able to calculate and simulate the transmitted optical intensity for light passing through our device in terms of eight corresponding coefficients.

By placing our nitrobenzene device (having parallel-plate electrode geometry) between a pair of polarizer, we perform relatively simple experimental measurements to solve for the unknown coefficients. As we vary the electric potential across the nitrobenzene device, we generate a dataset describing the coefficients of scattering, depolarization, absorption, and electro-optic phase response as functions of the applied electric field. Our characterization shows distinctly different electro-optic responses for weak, medium, and strong electric-field strengths. Therefore, for accurate simulation of changes in phase (or index of refraction) resulting from large electric field gradients, we used a higher order electro-optic model.

Although nitrobenzene has anisotropic scattering, to reduce the number of unknowns in our Mueller matrix, we have made assumptions to make the model simpler to solve. This can be justified on the basis of the similarity between the measured intensities for the various polarized, depolarized, and absorbed components. Using the experimental data we have compared the intensities of the two orthogonal polarized components (A, B) and have found that the average difference is negligibly small (almost less than 5%). Similarly we have compared the intensities of cross-coupled depolarization coefficients (U_3, U_4) and found that the average difference is less than 1% with maximum difference of 2%. Therefore within a less than 5% average error we can use the semi-isotropic scattering to

simplify our Mueller matrix and have only five unknown coefficients (A, $U_{|}$, $U\perp$, I_{Λ}, and $\Delta\varphi$). At last we applied our characterization study to computer aided device simulations and saw that the simulated graphs are matching to the experimental graphs within error range of 5% which could be further reduced by increasing the order of curve fitting.

In 6th chapter, We describe the Mueller matrix polarization discrimination (MMPD) technique for characterization of highly scattering media through laser beam. In our experiments, the scattering regime was adjusted to be at the incipient transition between single and multiple scattering. From an experimental standpoint the scattering is most challenging and on the other hand, it is rich in information content because the low-order scattering events are responsible for non-trivial polarization features. Our results demonstrate that the Mueller matrix components satisfy symmetry relations. These measurements provide detailed information about the changes in the magnitude and sign of Mueller matrix components. This should offer more insight and could lead to novel procedures for characterizing scattering phenomena. We discuss the entire experimental measured Mueller polarized matrix in detail for extracting information about the structure, size, and shape of the scattering particles. This has the potential of characterization of turbid sample for their optical properties through polarized laser radiations. The capability to measure polarization properties of multiply scattered light in vitro is exciting in that it yields several experimental observables which can be used to study and characterize turbid systems in vivo. Furthermore, the ability to acquire such measurements in a short time gives promise for the future application of such a system to differentiate between biological tissue in case of cancer and other malignant tissues.

The presented results establish the ability of the described Mueller matrix imaging system to precisely measure within a 97% accuracy, the 16 elements of a sample in either transmission, reflection, or backscattering modes. In the current configuration, it is clear that using 16 polarization images in the Mueller matrix reconstruction process is a trade off between maximizing accuracy a benefit of using an over determined system and acquisition time. Thus depending on the reconstruction process, it takes less time to reconstruct the 16 element of Mueller matrix using either the 16 polarization images, respectively, however, it should be noted that these times are not a direct reflection of the speed of either the optical components or detector. The distance in the probing light

beam has the effect of increasing the retardation errors, which are extremely wavelength dependent, therefore, resulting in noticeable errors in the circular polarization containing matrix elements. Going to an incoherent, coherence scrambled laser source, or using a narrower pass band filter could help compensate for this error.

Finally, the potential of the developed system for the detection of superficial cancerous lesions lies in its ability to remove pigmentation effects and to reject deeply backscattered light at different depths, based on the incident and backscattered polarizations within the tissue. These effects often mask the underlying superficial structures in laser tissue imaging. In addition, the ability to fully characterize the polarization properties of the sample under investigation can provide useful information in terms of the morphological structure differences present between normal and cancerous tissue. These changes can be used to help characterize and distinguish between tissue types. Furthermore, the ability to acquire such measurements in a minimal time frame gives promise for the future application of such a system to differentiate between normal, benign, and cancerous tissue. Future studies will be directed at exploring the angular dependence of such measurements and in the development of algorithms to aid in the characterization and differentiation process.

In 7^{th} chapter, laser transmission, absorption, and scattering technique for photon migration in human breast tissues phantom with Mueller matrix polarimetry have been investigated. Polarized laser transmission, including depolarization of wave applied to biological tissues provide a comprehensive frame work and simple way for diagnostic and treatment of skin lesion. He-Ne Laser (λ =632.8 nm) imaging system is described for non invasive and non radioactive clinical procedure. The system generates 16 out put Mueller matrices for characterization of tissues. This matrix along with optical images can characterize the normal and malignant tissues for diagnostic as will as treatment procedures of breast cancer. Although the in vitro measurements are smaller then in vivo, but this research work provides a base for designing quick model of polarized laser tissues culturing and imaging. The method of our in vitro optical parameter measurement is not suitable to in vivo, but it gives important information for skin tissue modeling. Our experimental data and the investigations were performed at 400-700nm (visible & near IR) provides useful information for tissue imaging. It is reasonable to assume that the scattering coefficient is

slightly dependent on wavelength in the visible range. This is not true for absorption coefficient, since tissue blood content and specific absorbing pigments play the main role in determining tissue characteristic. This fact should be kept in consideration while performing the evaluation of light flux distribution in depth. More efforts, therefore be made to determined more precisely the absorption and scattering coefficients and how they are related to blood flow contents. Analysis of autofluresence spectra of skin sample is suggested as a mean for skin diagnostic and monitoring. The optical property of chicken skin tissue is different for different tissues. The variation in coefficients most likely was due to biological variation, preparations of sample and prolonged freezing time, which leads to cell rapture.

The presented results demonstrate the ability of the polarimeter to accurately measure glucose concentrations in both water and aqueous humor mediums. This research represents an important step toward the development of a noninvasive glucose sensor which may eventually be capable of detecting glucose levels in the aqueous humor of the eye. Polarimeter is the simplest method for glucose sensing system and its development for in vivo measurement provides a home base glucose sensor in easy way. Mueller matrix provides a fingerprint of the solution and detected analysis for glucose aqueous humor solution. Our research provides a model for in vitro and base for in vivo eye glucose corneal birefringence measurement with polarized laser to check the diabetic level of the patent.

Future studies will be directed at exploring the angular dependence of such measurements and in the development of algorithms to aid in the characterization and differentiation process. The in vivo Mueller matrix polarimetry is essential for clinical diagnostic procedures. The extension of this in vitro technique for in vivo measurement will be the future research.

AFTERWORD

I regret that I have not been able to give a in vivo Mueller matrix polarimetric images in this thesis. Many aspects such as rigorous sampling and model comparison are still missing. The priors are most probably still too simple for real in vivo polarimetric imaging with polarized light. But I believe that my work at least has set a first step towards that goal.

And I also stress that I am not suggesting that Mueller matrix modeling is a fleshed out framework for Optical characterization. I am proposing that this technique raises many open questions that might be worthy of consideration by the clinical community. If one is willing to combine both fields then I sincerely believe that true progress can be made.

Although, in my opinion, the Mueller matrix polarimetry for tissue optics is a major step forward toward bio-material characterization, especially malignant tissues and turbid medium.

REFERENCES

[1] R. R. Alfano, Advances in Optical Imaging and Photon Migration, Proc. OSA, 21 (1994).

[2] R. L. Barbour and H. L. Graber, Diagnostic imaging with light, and beyond, Proc. 19th International conference-IEEE, 2735-2740, (1997).

[3] J. C. Hebden, S. R. Arridge, and D. T. Delpy, Optical imaging in medicine: I. experimental techniques, Phys. Med. Biol., 42, 825-840 (1997).

[4] N. S. Kopeika, A System Engineering Approach to Imaging. SPIE. Optical Engineering Press, Bellingham, Washington, USA (1998).

[5] M. P. Rowe, E. N. Pugh, J. S. Tyo, and N. Engheta, Polarization difference imaging: a biologically inspired technique for observation through scattering media, Opt. Lett., 20, 608-610 (1995).

[6] S. L. Jacques, J. C. Ramella, and K. Lee, Imaging skin pathology with polarized light, J. Biomed. Opt., 7, 329-340 (2002).

[7] S. G. Demos and R. R. Alfano, Optical polarization imaging, App. Opt., 36, 150-155 (1997).

[8] I. Freund, Correlation imaging through multiply scattering media, Phy. Lett., 147, 502-506 (1990).

[9] I. Freund, Image reconstruction through multiple scattering media, Opt. Comm., 86, 216-227(1991).

[10] S. P. Morgan, M. P. Knong, and M. G. Somekh, Effects of polarization state and scatterer concentration on optical imaging through scattering media, App. Opt., 36, 1560-1565 (1997).

[11] H. Horinaka, K. Hashimoto, K. Wada, T. Umeda, and Y. Cho, Optical imaging in highly scattering media by extraction of photons preserving initial polarization, Proc. SPIE, 2873, 54-57 (1996).

[12] P. Chang, J. Walker, K. Hopcraft, B. Ablitt, and E. Jakeman, Polarization discrimination for active imaging in scattering media, Opt. Comm., 159, 1-6 (1999).

[13] E. P. Zege, A. P. Ivanov, and I. L. Katsev, Image transfer through a scattering medium. Berlin Heidelberg: Springer-Verlag, 145 (1991).

[14] S. P. Morgan, M. P. Khong, and M. G. Somekh, Polarization imaging through scattering media, Proc. SPIE, 2626, 265-272 (1995).

[15] V. Dobschuetz , P. Biberthaler , T. Mussack, S. Langer, K. Messmer, and T. Hoffmann, Noninvasive in vivo assessment of the pancreatic microcirculation: orthogonal polarization spectral imaging, Opt. Express, 26, 139-43 (2003).

[16] C. Cote, I. A. Vitkin, Balanced detection for low noise precision polarimetric measurements of optically active multiply scattering tissue phantoms, J. Biomed. Opt. 9, 213-220 (2004).

[17] A. Clarke, and C. Eberhardt, Microscopy techniques for materials science, University of Leeds, UK (2002).

[18] A. C. Kak and M. Slaney, Principles of computerized tomographic imaging. IEEE Press New York (1988).

[19] L.-H. Wang, S. L. Jacques, and X. Zhao, Continuous-wave ultrasonic modulation of scattered laser light to image objects in turbid media, Opt. Lett. 20, 629-631 (1995).

[20] F. A. Duck. Physical properties of tissue, Academic Press, New York, 320–328 (1990).

[21] S. P. Morgan, and I. M. Stockford, Surface-reflection elimination in polarization imaging of superficial tissue, Opt Lett. 28, 114-116 (2003).

[22] S. L. Jacques, J. R. Roman, and K. Lee, Imaging superficial tissues with polarized light, Lasers Surg Med. 26, 119-129 (2000).

[23] I. L. Maywood, Anatomy of the Skin, Loyola University Health System, (2003).

[24] American Cancer Society, Skin Cancer Facts & Figures 2004, American Cancer Society, Pub. No. 5008 (2004).

[25] Y. Liu, Y. Kim, X. Li, and V. Backman, Investigation of depth selectivity of polarization gating for tissue characterization, Opt. Exp., 13, 601-611 (2005).

[26] Y. Kasuya, T. Michino, T. Yamamoto, S. Dohi, Cerebral oxygen saturation and hemoglobin index under separate brain perfusion American Cancer Society, Pub. No. 5009 (2004).

[27] M. Fukuda, K. Dobashi, T. Hirose, Y. Kurihara, T. Okugi, T. Omori, I. Sakai, J. Urakawa, and M. Washio Polarimetry of short-pulse gamma rays produced through inverse Compton scattering of circularly polarized laser beams, Phys Rev Lett. 91, 1648-1653 (2003).

[28] B. E. Bouma, J. Tearney , Handbook of Optical Coherence Tomography, university of Hawai, USA(2002)

[29] A. Stanworth and E. J. Naylor, The polarization optics of the isolated cornea, Brit. J. Ophtha, 34, 201-211 (1950).

[30] S. Firdous and M. Ikram, Characterization of turbid medium through diffusely scattering polarized light and matrix calculus-II, Proc. IEEE, pp 115-123, International Networking and Communications Conference, 11-13 June, Lahore University of Management Sciences, 2004.

[31] D. C. Pereda, J. D. Arce, R. Rentmeesters, Characterization of depolarizing optical media by means of the entropy factor: application to biological tissues, Appl Opt. 44, 58-65 (2005).

[32] W. S. Bickel, J.F. Davidson, D.R. Huffman, and R. Kilkson, Application of polarization effects in light scattering: a new biophysical tool," Proc. Natl. Acad. Sci. USA, 73, 488 (1976).

[33] J. F. Deboer, T. E. Milner, Review of polarization sensitive optical coherence tomography and stokes vector determination, J. Biomed. Opt. 7, 359-371 (2002).

[34] F. Moreno, F Gonzales, Light Scattering from Microstructures, Springer, New York (2000)

[35] J. D. E. Beynon and D. R. Lamb, Charge-coupled devices and their applications. McGraw- Hill London, UK (1980).

[36] M. Kerker, The scattering of light and other electromagnetic radiations, Academic press, New York (1969).

[37] J. S. Tyo, M. P. Rowe, E. N. Pugh, and N. Engheta, Target detection in optically scattering media by polarization difference imaging, App. Opt., 35, 1855-1870 (1996).

[38] M. Xu, R. R. Alfano, Random walk of polarized light in turbid media, Phys. Rev. Lett. 95, 213901 (2005).

[39] E. Hecht, Optics, 4th ed., New York: Addison Wesley, 2002.

[40] B. C. Wilson, M. S. Patterson, and S. T. Flock, Indirect versus direct techniques for the measurement of the optical properties of tissues. Photochem. Photobiol. 46, 601–608 (1987).

[41] Y. Y. Schechner, S. G. Narasimhan, and S. K. Nayar, Polarization-based vision through haze, App. Opt., 42, 511-525(2003).

[42] C. D. Malchoff, K. Shoukri, J. I. Landau, and J. M. Buchert, A novel non-invasive blood glucose monitor, Diabetes Care 25, 2268-2275 (2002).

[43] C. Brosseau, Fundamentals of polarized light-A statistical optics approach. John Wiley and Sons Inc, New York (1998).

[44] D. T. Joop, W. Hovenier, M. I. Mishchenko, Light Scattering by Nonspherical Particles: Theory, Measurements, and Applications, Elsevier, New York (2000).

[45] E. Collett, Polarized Light Fundamentals and Applications, Marcel Dekker, New York (1993).

[46] M. C. Pierce, J. Strasswimmer, B. H. Park, and J. F. Deboer, Birefringence measurement in human skin using polarization-sensitive optical coherence tomography, J. Biomed. Opt. 9, 287-291 (2004).

[47] I. J. Hodgkinson, Q. W. Hong, Birefringent thin films and polarizing elements, World Scientific, Oxford (2002).

[48] V. Tuchin, Tissue Optics, Light scattering methods and instrument for medical diagnosis, Bellingham, SPIE Press, New York (2000).

[49] H. Jiang, N. V. Iftimia, Y. Xu, J. A. Eggert, L. L. Fajardo, and K. L. Klove, Near-infrared optical imaging of the breast with model-based reconstruction, Academic Radiology, 9, 186-194 (2002).

[50] H. C. Van de Hulst, Light scattering by small particles, Dover, New York (1981).

[51] S. L. Jacques and J.C. Ramella, Propagation of polarized light beams through biological tissues, Proc. SPIE , 3914, 345-349 (2000).

[52] B. B. Das, K. K. Yoo, and R. R. Alfano, Ultrafast time-gated imaging in thick tissues: a step towards optical mammography, Opt. Lett. 18, 092-1094 (1993).

[53] R. Hema, Imaging through turbid media,Curr. Science, 76, 1334-1340 (1999).

[54] H. Horinaka, K. Hashimoto, K. Wada, and Y. Cho, Extraction of quasi straight-forward propagating photons from diffused light transmission through a scattering medium by polarization modulation, Opt. Lett, 20, 1501-1503 (1995).

[55] O. Rampado, P. Isoardi, R. Ropolo, Quantitative assessment of computed radiography quality control parameters, Phys. Med Biol., 51, 1577-1593 (2006).

[56] P. C. Jackson, P. H. Stevens, J. H. Smith, P. N. Wells, The development of a system for transillumination computed tomography Br. J. Radiol., 60, 375–380 (1983).

[57] B. D. Cameron, The Application of Polarized Light to Biomedical Diagnostics and Monitoring, Ph.D. Dissertation, Texas A&M University, College Station, TX (2000).

[58] S. Firdous and M. Ikram, Transmission and scattering matrix of polarization imaging for biological turbid medium, Proc. SPIE, 5867, 25-35(2005).

[59] O. Emile, F. Bretenaker, and A. L. Floch, Rotating polarization imaging in turbidmedia, Opy. Lett., 21, 1706-1708 (1996).

[60] H. Mueller, The foundation of optics, J. Opt. Soc. Am.38, 468-478 (1948).

[61] S. William,. A. Bickel, and M. Wilbur, Stokes vector, Mueller matrices, and polarized scattered light .Am. J.Phys.53, 468-478 (1985).

[62] J. C. Hebden and D. T. Delpy, Diagnostic imaging with light, The British Journal of Radiology, 70, S206-S214 (1997).

[63] V. Rossum and T. M. Nieuwenhuizen, Multiple scattering of classical waves: microscopy mesoscopy and diffusion, Rev. Modern Phys., 71, 103-108 (1999).

[64] J. S. Baba, J. R .Chung, A. H. DeLaughter, B. D. Cameron, and G. L. Cote′, Development and calibration of an automated Mueller matrix polarization imaging system, J. Biomed. Opt. 7, 341–349 (2002).

[65] S. Firdous and M. Ikram, Imaging of biological tissues with optical coherence tomography system using Jones-Mueller calculus, Proc. SPIE, 5861, 237-244 (2005).

[66] E. Wolf, Optics in terms of observable quantities, Cimento 12, 884-888 (1954).

[67] W. A. Shurcliff, Polarized Light: Production and Use, Oxford university press, London (1980).

[68] G. G. Stokes, On the composition and resolution of streams polarized light from different sources, Trans. Cambridge Phill. Soc. 9, 399-416 (1852).

[69] F. M. Caimi, A review of recent underwater imaging methods and advancements, in Coastal Ocean: Prospects for the 21st Century, Proc., IEEE, 1, 69-71 (1996).

[70] R. A. Chipman, Polarimetry, Chap. 22 in the Handbook of Optics, Vol. II, McGraw-Hill, New York (1995).

[71] J. L. Pezzantini and R. A. Chipman, Mueller matrix imaging polarimetry, Opt. Engg, 34, 1558-1562 (1995).

[72] E.Ardeshir, R. Guran,, Electromagnetic Wave Interactions, World Scientific, Oxford (1996).

[73] M. Born, and E. Wolf, Principles of Optics: Electromagnetic Theory of Propagation, Interference and Diffraction of Light, Cambridge University Press (2003).

[74] M. I. Mishchenko and J. W. Hovenier, Depolarization of light scattered by randomly oriented nonspherical particles, Opt. Lett. 20, 1356–1358 (1995).

[75] G. Bohren and D. Hoffman, Absorption and scattering of light by small particles, Wiley, New York (1983).

[76] C. S. Johnson, D. A.Gabriel, Laser Light Scattering, Courier Dover Publications (1994).

[77] R. Srinivasan, and M. Singh, Laser backscattering and transillumination imaging of human tissues and their equivalent phantoms. IEEE Trans. Biomed. Eng., 50, 724–730 (2003).

[78] J. M. Schmitt, A. H. Gandjbakhche, and R. F. Bonner, Use of polarized light to discriminate short-path photons in a multiply scattering medium, Appl. Opt. 31, 6535–6546 (1992).

[79] M. P. Albada and A. Lagendijk, Observation of weak localization of light in a random medium, Phys. Rev. Lett. 55, 2692–2695 (1985).

[80] S. L. Jacques, J. C. Ramella-Roman, and K. Lee, Imaging skin pathology with polarized light, J. Biomed. Opt. 7, 329–340 (2002).

[81] S. Firdous and M. Ikram, Polarized Laser Beam Scattering through Turbid Medium for Application in Tissue Imaging, Science Asia, 31,167-172 (2005).

[82] S. A.Kartazayeva, Xiaohui Ni, R. R. Alfano, Backscattering Target Detection in a Turbid Medium by use of Circularly and Linearly Polarized Light, Opt. Lett., 30, 1168-73 (2005).

[83] M. Juan, A. Bueno, Polarimetry using liquid-crystal variable retarders: theory and calibration, J. Opt. A: Pure Appl. Opt. 2, 216–222 (2000)

[84] S. Firdous, K. Hassan, and M. Ikram, Modeling of electro-optic devices for scattering and absorption of polarized light with Muller Matrix, Proceeding of International Symposium on Photonics in Measurement, pp 285-306, Institute of Optics Technology, 23-24 June, Frankfurt, Germany, 2004.

[85] S. T Flock, S. L Jacques, B. C. Wilson, W. M Star, M. C van Gemert, Optical Properties of Intralipid: A phantom medium for light propagation studies, Lasers in Surgery and Medicine 12, 510-519 (1992).

[86] R. A. Chipman, Polarimetry Handbook of Optics 2nd edn, Vol 2, (New York, McGraw-Hill) ch 22 (1995).

[87] C. C. Yang, W. Chia, C. K. Lee, C. W. Lu, M. T. Tsai, C. Yang, and Y. W. Kiang, Comparisons of the transmitted signals of time, aperture, and angle gating in biological tissues and a phantom, Optics Express, 12, 1157-1168 (2004).

[88] J. N. Damask, Polarization Optics In Telecommunications, Springer, New York (2004).

[89] A. H. Hielscher, A. A. Eick et al,. Diffuse backscattering Mueller matrix of highly scattering media, Opt. Exp. 1, 441-443(1997).

[90] S. L. Jacques, Introduction to Biomedical Optics, Acadamic Inc, London (2001).

[91] A. Gerrard, Introduction to Matrix Methods in Optics, Courier Dover Publications (1994).

[92] A. Clarke and C. Eberhardt, Microscopy techniques for materials science, University of Leeds, UK (2002).

[93] P. E. Sahmes, P. C. Sun, Y. Fainman Modeling of scattering and depolarizing electro-optic devices. II. Device simulation, Appl. Opt. 37, 3726-3734 (1998).

beam using optics calculus, Proceeding of World Conference on 21st Century Mathematics, pp 52-67, March 17-20, School of Mathematical Sciences, G. C. University, Lahore, 2004.

[97] R. M. A. Azzaro and N. M. Bashara, "Ellipsometry and Polarized Light, North-Holland, Amsterdam (1987).

[98] S. Jiao, W. Yu, G. Stoica and L. V. Wang, Contrast mechanisms in polarization sensitive Mueller matrix optical coherence topography and applications in burn imaging, Appl. Opt. 42, 5191-5197(2003).

[99] F. Jaillon, and H. S. Jalmes, Description and time reduction of a Monte Carlo code to simulate propagation of polarized light through scattering media, Appl. Opt. 42, 3290-3296(2003).

[100] D. M Anderson, and R.Barakat, Necessary and sufficient conditions for a Mueller matrix to derivable from Jones matrix, J. Opt. Soc. Am. A, 11, 2305-2319 (1994).

[101] J. S. Baba, The Use of Polarized Light for Biomedical Applications, Ph.D. Dissertation, Texas A&M University, College Station, TX 77843, (2003).

[102] A. K. Ishimaru, Wave Propagation and Scattering in Random Media, Academic Press, San Diego, Calif., (1978).

[103] K. Kim, L. Mandel, and E. Wolf, Relationship between Jones and Mueller matrices for random media, J. Opt. Soc. Am. A 4, 433-437 (1987).

[104] W. A. Shurcliff, Polarized Light, Haward University press, Chap. 5(1994).

[105] C. F. Bohren and D. R. Huffman, Absorption and Scattering of Light by Small Particles, Wiley, New York (1983).

[106] K. Hassan, Development of an optical modulator using kerr cell and characterization of nitrobenzene, M.Phil thesis, 2004.

[107] S. Firdous, K. Hassan, and M. Ikram, Formulation of Mueller Matrix and Modeling of depolarizing and scattering of nitrobenzene in a Kerr Cell, Appl. Opt. 44 (7),1171-1177 (2005).

[108] S. G. Demos and R. R. Alfano, Deep subsurface imaging in tissues using spectral and polarization filtering Appl. Opt. 36, 150 (1997).

[109] S. Firdous and M. Ikram, Mueller matrix imaging polarimetry for the characterization of turbid medium, Annals of Bio-med. Res. Education, 5, 55-60 (2005).

[110] F. Delplancke, Automated high-speed Mueller matrix scatterometer, Appl. Opt. 36, 5388–5395 (1997).

[111] A. Torricelli, A. Pifferi,, P. Taroni, E. Giambattistelli, and R. Cubbedu, In vivo optical characterization of human tissues from 610 to 1100 nm by time-resolved reflectance spectroscopy, Phys. Med. Biol., 46, 2227–2237 (2001).

[112] D. S. Kilger, J. W. Lewis, and C. E. Randall, Polarized Light in Optics and Spectroscopy, Academic, San Diego, CA (1990).

[113] D. H. Goldstein, Mueller matrix dual-rotating retarder polarimeter, Appl. Opt. 31, 6676-6683 (1992).

[114] P. A. Williams, A. H. Rose, and C. M. Wang, Rotating-polarizer polarimeter for accurate retardance measurement, Appl. Opt. 36, 6466-6472 (1997).

[115] J. Li, G. Yao, and L. V. Wang, Degree of polarization in laser speckles from turbid media; implication in tissue optics, J. Biomed. Opt. 7, 307-312 (2004).

[116] M. j. Rakovic, G. W. Kittawar, M. Mehrubeoglu, B.D.Cameron, L. V. Wang, S.Resteger, and G.L.Cote., Light backscattering polarization pattern from turbid media:theory and experiment, Appl. Opt.38, 3399-3408 (1999)

[117] L.Jacques, and R.J.Ramella, Propagation of polarized light beams through biological tissues, Proc.SPIE, 3914, 345-352 (2000)

[118] R. Srinivasan, D. Kumar and M. Singh, Optical characterization and imaging of biological tissues, Curr. Science, 87, 218-228 (2004).

[119] S.L.Jacques, M.Ostemeyer, L.V.Wang and D.Stephens, Polarized light transmittion through skin using video reflectometry: toward optical tomography of superficial tissue layers, Proc.SPIE, 2671, 199-210(1996).

[120] J.Q. Lu, X.H. Hu, Modeling of Light Scattering in Biological Systems, invited Chapter in Recent Research Developments in Optics, vol. 2 (2002)

[121] Z. Song, K. Dong, X. H. Hu, and J. Q. Lu, Monte Carlo Simulation of Converging Laser Beams Propagating in Biological Tissues, Appl. Opt., 38, 2944-2949 (1999)

[122] S. Firdous and M. Ikram, and M. Faisal, Measurements of the optical properties of Breast tissues in vitro using Mueller matrix polarimetry, Int. J. Cancer Res. 1, 29-35(2005).

[123] R. R. Ansari, S. Bockle, L. Rovati, New optical scheme for a polarimetric based glucose sensor, J. Biomed. Opt., 9, 103–115 (2004).

[124] S. Bockle, L. Rovati, and R. R. Ansari, Polarimetric glucose sensing using the Brewster-reflection off the eye lens: theoretical analysis, Proc. SPIE 4624, 160–164 (2002).

[125] B. D. Cameron, W. G. Harshal, B. Satheesan, and G. L. Cote, The use of polarized laser light through the eye for noninvasive glucose monitoring, Diabetes Technol. Therap., 1, 135-143 (1999).

[126] D. W. Foster, Diabetes mellits in Harrison, Principles of Intrnal medicine, McGraw-Hili, New York, 1739-1758 (1991).

[127] B. D. Cameron, H. W. Gorde, and G. L. Cote, Development of an optical polarimeter system for in vivo glucose monitoring, Proc. SPIE, 3599, 43–49 (1999).

[128] S. Pelizzari, L. Rovati, and C. De Angelis, Rotating polarizer and rotating retarder plate polarimeters: comparison of performances, Proc. SPIE 4285, 235–243 (2001).

[129] S. Firdous and M. Ikram, Polarized Mueller Matrix Analytical Model for Glucose Measurement in Vitro, Turk. J. Med. Sci., 35, 145-159 (2005).

[130] W. T. Driskill, Diabetes continues to be the nation's fourth leading cause of death, Health Educator, 12, (1996).

[131] B. Rabinovitch,, W. F. March, and R. L. Adams, Nonivasive glucose monitoring of the aqueous humor of the eye. Part I. Measurement of very small optical rotations, Diabetes Care, 5, 254-258 (1982).

[132] C. A. Browne and F. W. Zerban, Physical and Chemical Methods of Sugar Analysis, New York, London: Chapman & Hill, (1941).

[133] R. J. McNichols and G. L. Cote', Optical glucose sensing in biological fluids: an overview, J. Biomed. Opt. 5, 5–16 (2000).

[134] R. W. Knighton and X. Huang, Linear birefringence of the central human cornea, Invest. Ophthalmol. Visual Sci., 43, 82–86 (2002).

[135] D. C. Klonoff, Noninvasive blood glucose monitoring, Clinical Diabetes, 16, 43-45(1998).